CARL
VON
OSSIETZKY
universität OLDENBURG

Influence of presence of a heteroatom source on the synthesis of layered silicates - ilerite, magadiite and kenyaite.

Von der Fakultät für Mathematik und Naturwissenschaften

der Carl von Ossietzky Universität Oldenburg zur Erlangung des Grades und Titels eines

Doctor rerum naturalium

(Dr. rer. nat.)

Angenommene Dissertation

Von Herrn Wojciech Andrzej Supronowicz

Geboren am 22.05.1983 in Sosnowiec (Polen)

Gutachter: Prof. Dr. Frank Rößner

                    Carl von Ossietzky Universität Oldenburg

Zweitgutachter: Prof. Dr. Wilhelm Schwieger

                    Friedrich-Alexander-Universität Erlangen-Nürnberg

Tag der Disputation: 15. April 2011

For my Wife,

Parents and Grandparents.

Acknowledgement

First of all, I wish to thanks my supervisor Prof. Dr. Dr. h.c. Frank Rößner for giving me the opportunity to work in his group, where I had the possibility to develop myself both at the professional and personal levels. I have especially appreciated the enthusiasm he had shown in my work, the time spent in fruitful discussions, and the freedom received during these years.

Prof. Dr. Wilhelm Schwieger and Jimmi Ofili (University Erlangen-Nuremberg) for the stimulating discussions and introduction to low angle XRD.

Philipp Adryan and Oliver Meyer for the help provided when I started to work on this intriguing topic.

Robert Henkel for all the great parties, all the CD´s with great music and help.

Stefan Schoenen for his hospitality, help in the laboratory and repairing my old car.

Kerstin Esser and Olesya Fomenko for their help and friendship during the last years.

Renate Kort and Mikhail Meilikhov fort the SEM and MAS NMR measurements.

Finally, the German Academic Exchange service (DAAD) for financial support and CWK Bad Koestritz (Germany) for donation of chemicals.

Abstract

In this thesis the hydrothermal syntheses of layered silicate structures – ilerite, magadiite and kenyaite - were conducted in presence of heteroatom source - $SnCl_4*5H_2O$ or $Al(O-i-Pr)_3$. The main aim of the study was to investigate the influence of the above mentioned compounds on the resulting material as well as the possibility of isomorphous replacement of silicon by tin atoms. Properties of the resulting samples were studied with use of different characterization methods, e.g. X-ray diffraction (XRD), scanning electron microscopy (SEM), temperature-programmed reduction (TPR), and diffuse reflectance infrared fourier transform (DRIFT) spectroscopy. Catalytic properties were studied in the decomposition of 2-methyl-3-butyn-2-ol (MBOH). For comparison, non-modified, impregnated by SnO_2, as well as aluminium-containing samples, were made and characterized with use of the same methods like for the Sn-modified samples.

It has been found that the presence of the heteroatom source in the ilerite synthesis mixture redirects the synthesis towards magadiite structure even when the synthesis was conducted in the presence of ilerite seeds. Dissimilar to ilerite syntheses, no redirecting effect was observed in the case of magadiite and kenyaite syntheses. The synthesis methods applied to the tin modified materials were unsuitable for introduction of aluminum.

Applied characterization methods, indicate the presence of metal oxide species only on the surface of the ilerite crystals. There is no straight evidence on existence of pillars between the layers in all samples.

Split of the Q_3 signal in ^{29}Si MAS NMR made for the tin-modified magadiite, as well as the red-ox properties of the tin-containing samples, indicate the presence of –OSn bonded to SiO_4 tetrahedra. Therefore, the obtained data seems to confirm that the silicon atoms in the layered silicates can be isomorphously substitution similar like these in zeolites.

Abstract

In dieser Arbeit wird die hydrothermale Synthese von Schichtsilikat Strukturen - Ilerite, Magadiit und Kenyait - in Anwesenheit einer Heteroatomquelle (SnCl$_4$ * 5H$_2$O oder Al(Oi-Pr)$_3$) behandelt. Das Hauptziel der Studie war den Einfluss der oben genannten Verbindungen auf das entstehende Material und auch die Möglichkeit des isomorphen Ersatzes von Silizium durch Zinn-Atomen zu untersuchen. Die Eigenschaften der resultierenden Proben wurden unter Einsatz verschiedener Methoden wie zum Beispiel Röntgenbeugung (XRD), Rasterelektronenmikroskopie (SEM), Temperatur-Reduktion (TPR) und diffuse Reflexion Fouriertransformationsinfrarotspektroskopie (DRIFT) charakterisiert. Katalytische Eigenschaften wurden bei der Zersetzung von 2-Methyl-3-Butin-2-ol (MBOH) untersucht. Zum Vergleich wurden nicht-modifizierte, mit SnO$_2$ getränkte, sowie Aluminium-haltige Proben hergestellt und charakterisiert unter Verwendung der gleichen Methoden wie für die Sn-modifizierten Proben.

Es wurde festgestellt, dass die Anwesenheit der Heteroatomquelle in der Ilerite Synthesemischung die Synthese zur Magadiit Struktur leitet auch wenn die Synthese in Gegenwart von Ilerite-Impfkristallen durchgeführt wurde. Anders als bei der Synthese von Ilerite wurde keine vergleichbare Wirkung im Falle von Magadiit und Kenyait Synthesen beobachtet. Angewandte Synthesemethoden zu Zinn modifizierten Materialien erwiesen sich als ungeeignet für die Einführung von Aluminium.

Verwendete Charakterisierungsmethoden Methoden zur zeigen das Vorhandensein von Metalloxid-Arten ausschließlich auf der Oberfläche der Ilerite Kristalle. In allen Proben gibt es keine Beweise für die Existens von „pillars" zwischen den Schichten.

Ein entsprechender Split des Q$_3$-Signals in ^{29}Si-MAS-NMR Messungen für Zinn-modifizierten Magadiit sowie dessen Redox-Eigenschaften deuten auf das Vorhandensein von OSn gebundenen SiO$_2$- Tetraedern hin. Demzufolge scheinen die erhaltenen Daten zu bestätigen, dass die Silizium-Atome in den Schichtsilikaten substituiert werden können.

Content

1. Introduction

Production of many thousands of products requires a presence of a catalyst somewhere in the production chain. In fact, in many cases the final product could not be commercialized, if the production cost were not significantly lowered by use of proper catalyst. A tight relation can be made between an occurrence of new catalysts and introduction to the market of new products. Although we often do not recognize it, catalysis has often direct impact on our everyday life level. We can only guess how our world would look like without fertilizers produced with use of ammonia, which production process involves iron-based catalyst.

The history of modern catalysis starts almost 120 years ago when BASF started the first catalytic process – the synthesis of sulphuric acid by the contact process. A few years later (1908) Fritz Haber has discovered the synthesis of ammonia from nitrogen and hydrogen. The industry process was; however, based on catalyst found by Alwin Mittasch in 1910. Mittasch and his colleagues have tested more than 3000 differently compounded and doped samples of iron oxide before finding a suitable catalyst.

One of very important stepping stones was the first synthesis and industrial application of zeolites. The first efforts to synthesize zeolites can be dated around 1862 [1]. However, first successful synthesis of a zeolite, which did not have a natural counterpart, was made by Barrer in 1948 [1]. In 1962, Barrer and Denny reported the first zeolite synthesis with structure-directing agent named also as template. This discovery has opened a route to synthesis of various porous materials. It was soon realized that through changes of synthesis parameters one can control properties of the resulting material. Furthermore, it is possible to design a suitable catalyst to particular process. Although, we are just starting to understand the mechanism of zeolite formation [2,3] the whole research process involve much less random steps then work of Mittasch.

However, one must be aware that all materials have their limitations that can not be overcome by their synthesis parameters modification. Application of zeolites is limited by small radii of their pores. Therefore, material with similar properties to the three-dimensional silicates; however, characterized by presence of larger pores is needed. Moreover, it should be relatively easy modified with use of similar techniques like in the case of zeolites.

Within the present work layered hydrous sodium silicates (named here as layered silicates), which pore radius can be adjusted by the introduction of different sized pillars, are

presented as such an alternative. Similar like in the case of zeolites, synthesis in hydrothermal conditions is the most popular way to obtain layered silicates. Although the exactly synthesis mechanism is still unknown numerous reports confirm significant influence of different synthesis parameters, e.g. temperature, time of crystallization, and composition of synthesis mixture on the properties of the resulting materials [4]. The above mentioned parameters play an important role also in synthesis of various molecular sieves. The similarities between the synthesis procedures, structures of silica layers and frameworks of zeolites [5], as well as successful introduction of aluminium and boron into silica layers [6,7] seems to suggest that it is possible to synthesize layered silicates derivatives with properties similar to those of zeolite-like materials.

2. Literature part

2.1. Silicates

Silicates are natural occurring chemical compounds containing silicon, oxygen and one or more metal ions, e.g. aluminum, barium, calcium, magnesium, potassium, sodium or zirconium. Together with silicon oxide they are building approximately 90% of the lithosphere [8]. Depending from conditions during their formation, they can occur in many various geological and chemical forms. Silicates can be found in most of common rock-forming minerals such as quartz, mica or, recently popular because of its health hazardous properties – asbestos. They are also essential ingredient of sedimentary rocks, e.g. clays, schist and sandstones.

2.1.1. Structure and classification of silicates

The first classification of silicates, based on the silicic acid theory of the constitution of the silicates was made already in 1811 [9]. According to it, there are four groups of silicates: ortho-, meta-, di-, or trisilicates - named according to the acid from which they are theoretically derived. Nowadays they are also classified according to their crystalline structure.

The main building blocks of all silicates are SiO_4 tetrahedra, which are connected to each other by corners (Figure 2.1). Depending from the number of the corners, which are connected to other tetrahedra, different structures can be made. The above mentioned structures can be also used as the basis for classification of various minerals.

Orthosilicates

Orthosilicates are built from separated SiO_4 tetrahedral units. Oxygen atoms are coordinately bound to a metal atom and depending from the coordination number of the metal, different crystallographic structures are created e.g. Zn_2SiO_4, where zinc is tetrahedrally surrounded by four oxygen atoms; or Mg_2SiO_4, where magnesium is octahedrally surrounded by six atoms of oxygen [8].
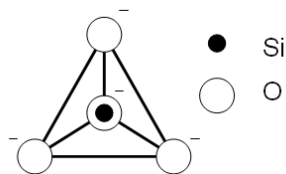
Figure 2.1: *Scheme of SiO_4 tetrahedra.*

Pyrosilicates

Pyrosilicates (Figure 2.2) are the simplest and in the same time, very rare silicate ions, where two SiO_4 are bonded together by one oxygen atom, e.g. $Sc_2(Si_2O_7)$ [8].
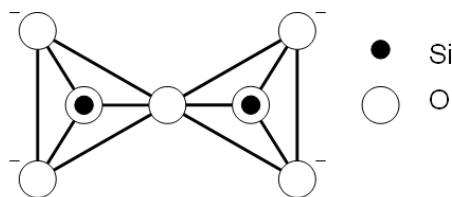
Figure 2.2: *Scheme of $Si_2O_7^{6-}$ ion.*

Cyclosilicates (the ring stuctures)

If a SiO_4 tetrahedron is connected to two others by two different corners, a ring structure can be created (Figure 2.3). Such arrangement was detected in many minerals,

e.g. $Be_3Al_2(Si_6O_{18})$, where Si_6O_{18} units are above each other and are creating channels accessible for small gas molecules [8].
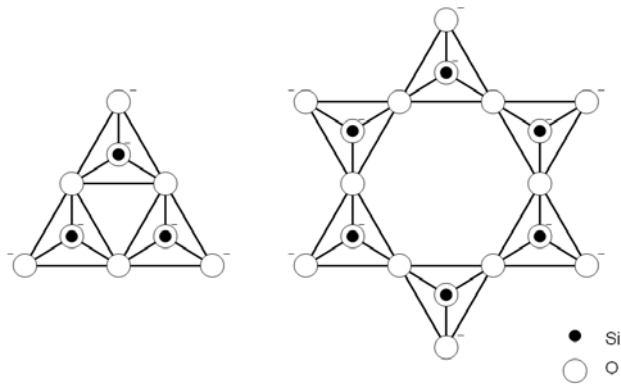
Figure 2.3: *Scheme of $Si_3O_9^{6-}$ ion and $Si_8O_{18}^{12-}$ ion.*

Pyroxene
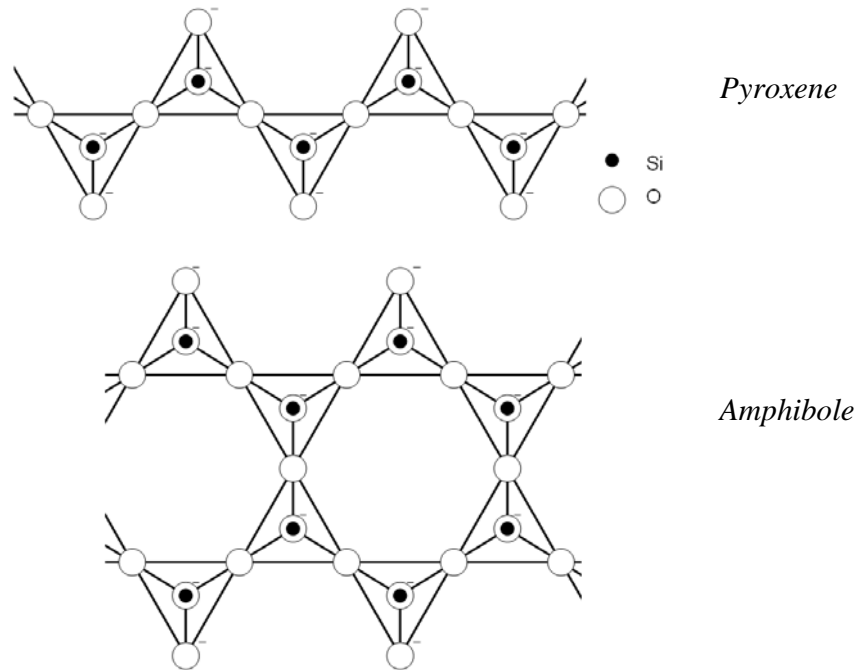
Amphibole

Figure 2.4: *Scheme of pyroxene and amphibole type chains.*

Inosilicates

Other structures, created by SiO_4 tetrahedra connected to two others, are chains. Besides the simplest one, two other types can be found in nature (Figure 2.4): pyroxenes, which are single chains found in the minerals such as $LiAl(SiO_3)_2$ and amphiboles, which are double chains found in tremolite and krokidolit [8].

Layered silicates

After sharing three oxygen atoms with other tetrahedra, infinitive two-dimensional layered structures are created (Figure 2.5). Each layer is weakly bonded to another via cations or oxides, which are positioned between the silica layers, e.g. $Mg_3(OH)_2(Si_4O_{10})$ or $Al_2(OH)_4(SiO_5)$ [8].
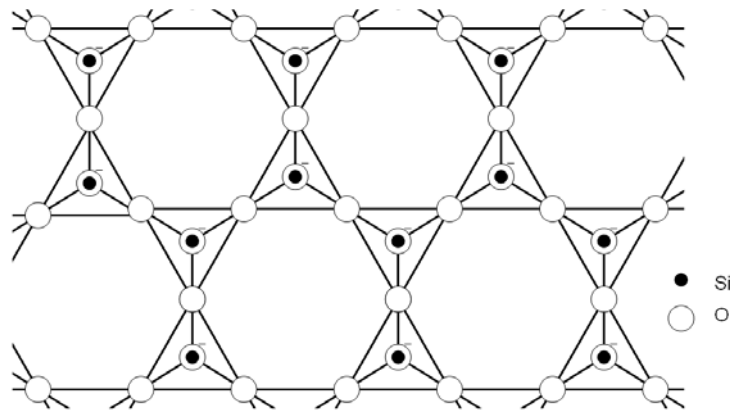
Figure 2.5: *Scheme of ($Si_2O_5)_n^{2n-}$ layer.*

Three-dimensional silicates

From sharing four oxygen atoms with four different tetrahedra a three-dimensional structure is created, e.g. quartz [8]. Very common derivatives of such silicates metallosilicates are minerals, in which part of silicon atoms were isomorphously substituted with usually four-coordinated metal [8]. Examples of such materials, with

great importance to chemical industry, are porous aluminosilicates – zeolites [1]. Isomorphic substitution of Si^{4+} by Al^{3+} requires presence of an additional, extra-framework cation that is compensating a negative charge created by AlO_4^-. Moreover, because the number of SiO_4 tetrahedra connected to each other can differ, the tetrahedra can create different building units (SBU – secondary building units). They are building bricks of variety of open, porous zeolitic structures, e.g. faujasite (Figure 2.6). Porosity and the possibility of introduction of various metal cations into the extra-framework positions are the main reasons of their significant industrial success.
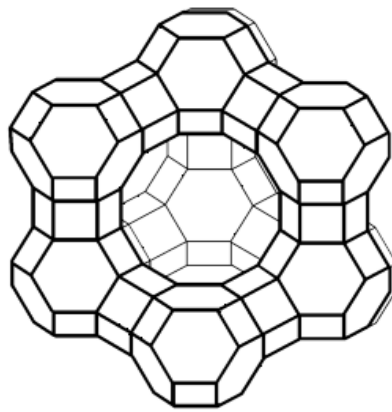
Figure 2.6: *Zeolite Y structure, Faujasite (FAU).*

2.1.2. Layered silicates

Layered silicates were first discovered by H.P. Eugster in 1967 at Lake Magadie in Kenya [11]. Their occurrence in nature is related to existence of an alkaline carbonate-rich hydrogeochemical environment, in which there is a high concentration of dissolved silica as well as necessary temperature and pressure, required to form the above mentioned materials. Their relatively ease of transformation into chert, makes their occurrence very rare [12].

2.1.2.1. Natural layered silicates

There are several types of layered silicates, which are described in literature - magadiite, kenyaite, kanemite, makatit, and silhydrite. The first two - magadiite and kenyaite - are the most common forms and, due to the character of present work, only those two will be described in detail.

Magadiite

Magadiite was first discovered in pleistocene sediments from Magadi Lake (Kenya) by Eugster in 1967 [10]. One of the richest sites was discovered later in the Chad basin. It occurs as a plastic, white paste that is changing irreversibly into much harder white powder after drying. In nature, magadiite crystals exist usually as a massive microstructure or very thin sheet-like crystals belonging to the monoclinic system. Contrary to the natural one, synthetic magadiite (Figure 2.7) consist of rosette-like shaped crystals, which are the result of transition from the palissadic/massive to the spherulitic microstructure [11] (Figure 2.8).
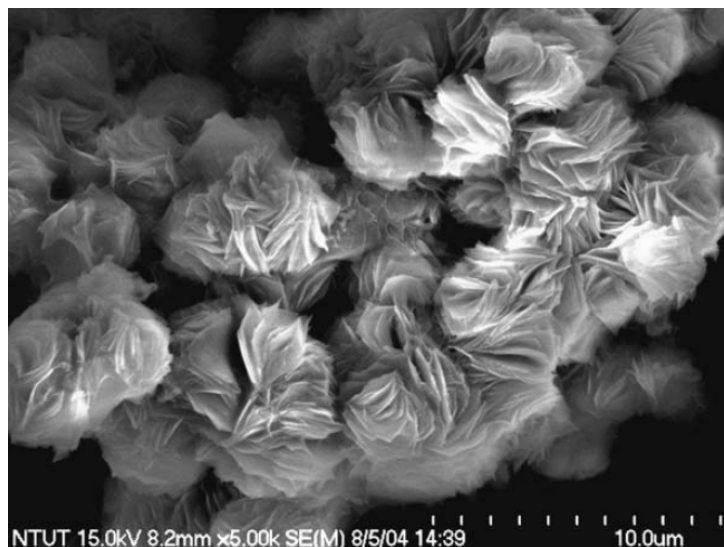
Figure 2.7: *Magadiite crystals [12]*
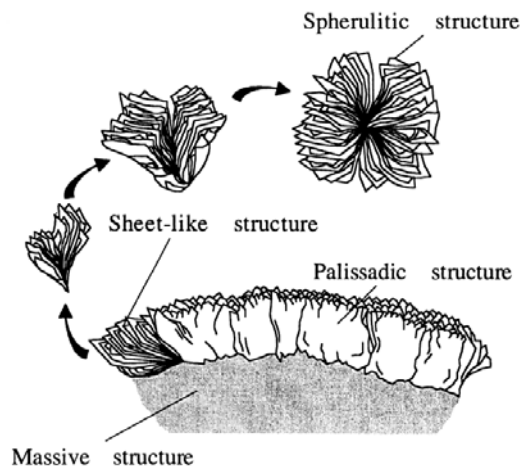
Figure 2.8: *Proposed model of transition from palissadic/massive to spherulitic microstructure [11].*

In comparison to zeolites, the crystallinity of the layered silicates is often inferior, thus; information given by powder diffraction are restricted to d values in the range 2 – 1,5 Å. Due to poor resolution of diffraction patterns, structures of two-dimensional silicates are often still under discussion [13, 14]. One of the first complete structure analysis of mentioned above material, with use of NMR, XRD and TG/DTA methods, was described by Schwieger et al. [15-19].
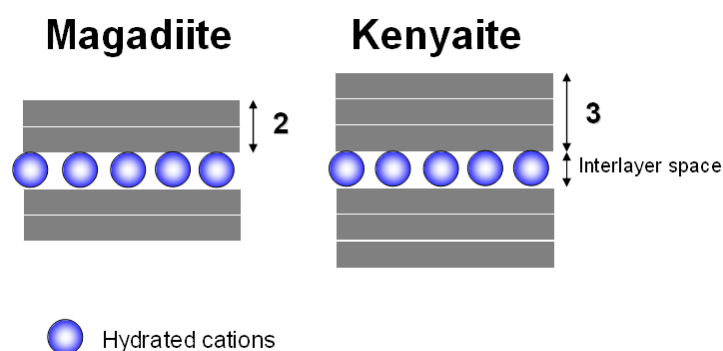
Figure 2.9: *Schematic structure of magadiite and kenyaite.*

Magadiite is a material that consists of two-dimensionally silicate layers, separated by interlayer space. Its schematic diagram can bee seen on Figure 2.9. Each silica layer is build by two sheets of SiO_4 tetrahedra [20] (Figure 2.9). One of the first approaches to resolve its structure, based on [28]Si MAS NMR spectra results, was proposed by Schwieger et al. [15-18]. Two signals - Q^3 - OSi(OSi≡)$_3$ and Q^4 - Si(OSi≡)$_4$ -were observed and the ratio between them was calculated. To interpret the resulting Q^3/Q^4 ratio, it has been assumed that the two magadiite silica layers can be treated as one thick layer consisting of three silica sheets (Figure 2.10). After adjustment of the crystallographic coordinates, it can be seen that Schwieger's experimental results stay with good agreement with the theoretical data (Figure 2.11) [21].
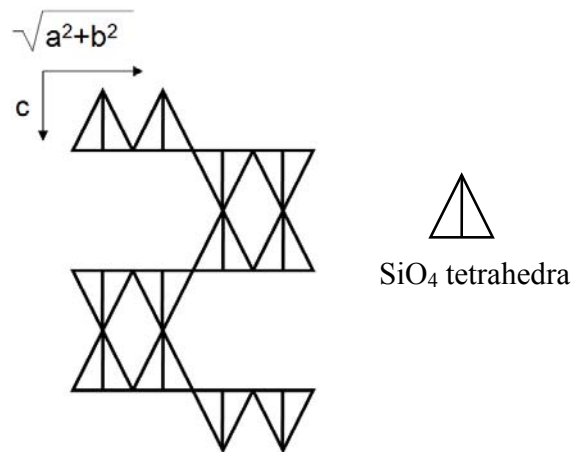
Figure 2.10: *Model structure of magadiite silica layers proposed by Brandt et al. [17].*

Between the silica layers are hydrated cation layers. The water from the hydratation shell can be reversibly removed what leads to decrease of the distance (basal spacing) between the silica layers [18, 22].
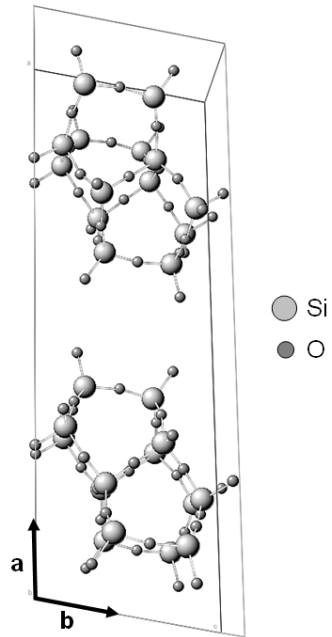
Figure 2.11: *Hypothetical model structure of magadiite silica layers proposed by Garces et al. [21].*

Kenyaite
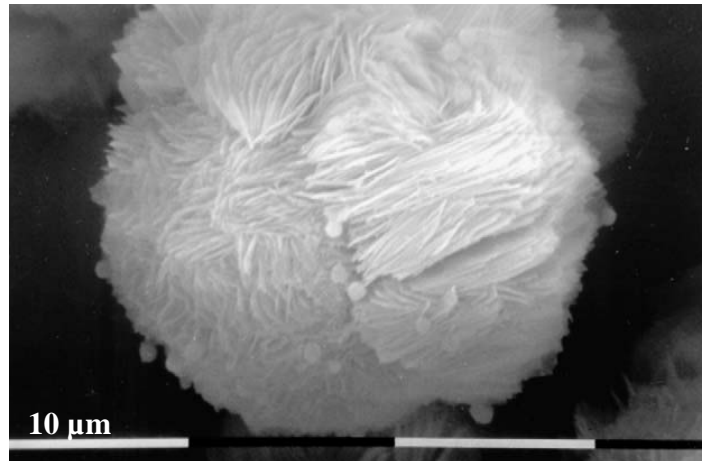
Figure 2.12: *Kenyaite crystal [23].*

Kenyaite is forming at the center of the magadiite concretions or in the form of nodules inside the layers of magadiite [11]. There are no reports concerning its existence in the form of beds. Although the transformation of the magadiite structure into kenyaite in the laboratory conditions is well described in the literature [24], there are no confirmed proofs that similar process occurred in nature [11].
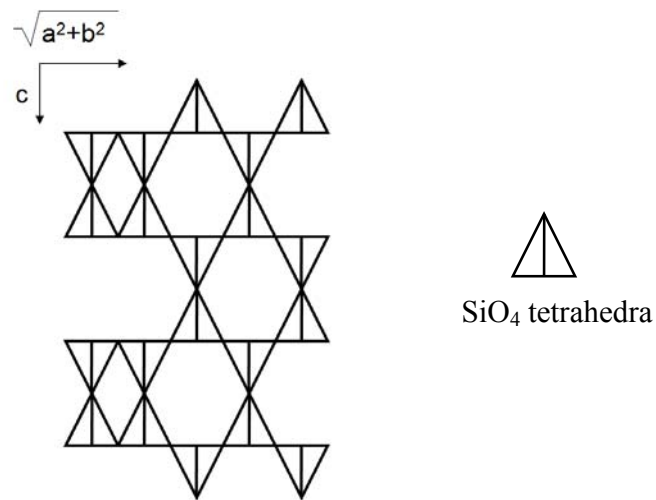
Figure 2.13: *Model structure of kenyaite silica layers proposed by Brandt et al. [17].*

Likewise that of magadiite, the structure of kenyaite is often discussed. Kenyaite is composed from silica and hydrated cations layers; however, each silica layer is build from three silica sheets, instead of two as in the case of magadiite (Figure 2.9). Also for this material, one of the first experimental approaches to resolve its structure was done by Schwieger at al. [17]. Similar experiments and assumptions, likewise those made for magadiite structure, were made. The study concluded that silica layer consist of four silica sheets/monolayers (Figure 2.13). The above mentioned results stay in good agreement with later experiments made by Almond et al. [20] (Figure 2.14).
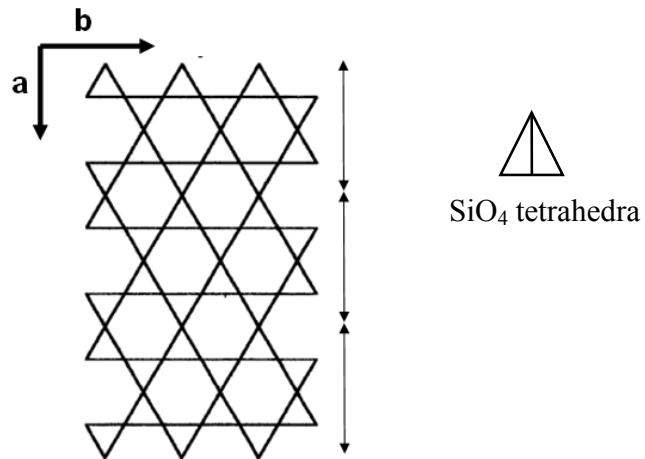
Figure 2.14: *Model structure of kenyaite silica layers proposed by Almond et al. [20].*

2.1.2.2. Synthetic layered silicates
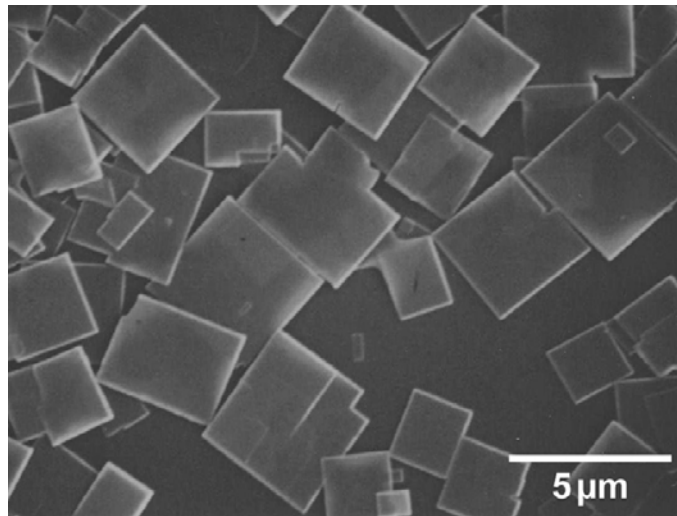
Figure 2.15: *Ilerite crystals [25].*

The first layered silicate was synthesized by Iler in 1964 [26]. It is not only the simplest one from the above mentioned, but also the only one that does not occur in the natural environment. The synthetic material was named by Wolf and Schwieger in 1979 [27] as ilerite; however, different authors are using also other names such as octosilicate

[15] or RUB-18 [14, 28]. Contrary to magadiite and kenyaite, typical ilerite crystals are plate-like shaped [25] (Figure 2.15).

Ilerite, similar like the above mentioned materials, consist of silica and hydrated cations layers. However, the silica layer is build by only one sheet of SiO_4 tetrahedra. One of the first experimental approaches to resolve its structure was done by Schwieger at al. [15]. After similar experiments and assumptions, which were made for the magadiite and kenyaite structures, it has been concluded that its composition correspond to $SiO_2/Na_2O = 8$ [15]. Consequently, the material was named as octosilicate (Figure 2.16).
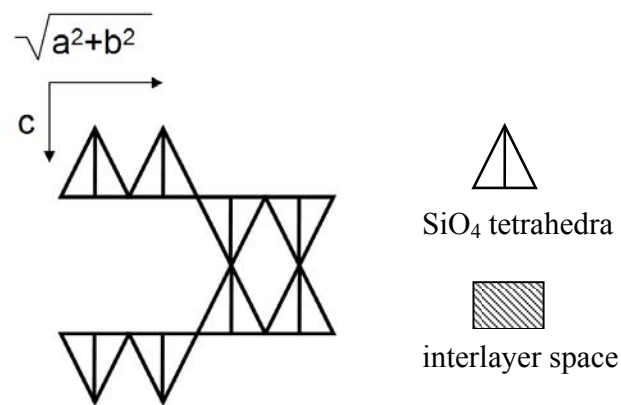
Figure 2.16: M*odel structure of ilerite silica layer proposed by Schwieger et al. [17].*

Different conclusions were made by Vortmann et al. and Borowski et al. [13, 14]. On the basis of XRD and NMR experiments, it has been concluded that the model proposed by Schwieger et al. is wrong and new model should be used (Figure 2.17).

Still lasting discussion about correctness of the proposed layered silicates' structures reflects how complex and complicated those materials are. Thus, one should use particular structure model with caution.
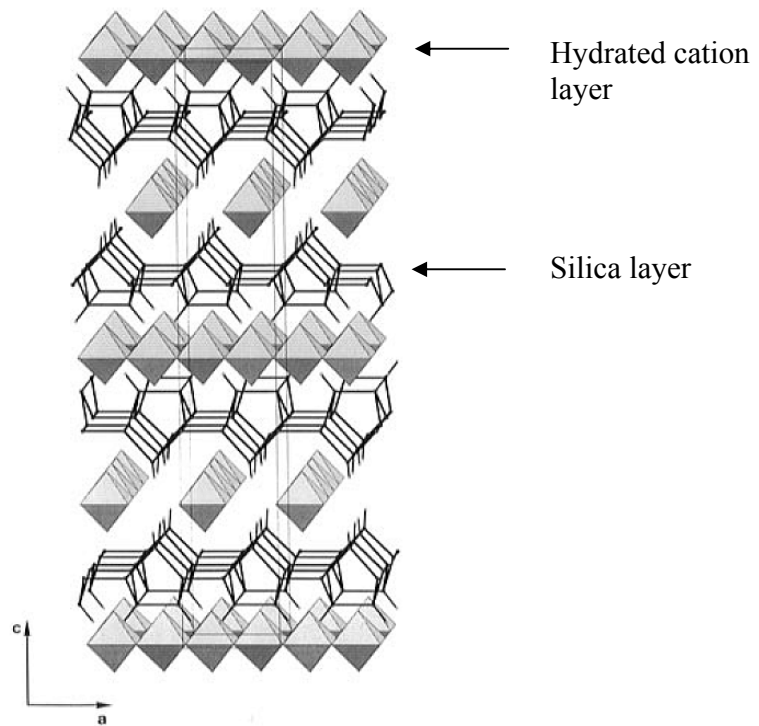
Figure 2.17: M*odel structure of ilerite silica layers proposed by* Vortmann et al. and Borowski et al. [13, 14].

2.2. Properties and possible applications

Properties

Layered silicates (particularly ilerite, magadiite and kenyaite) are solid materials, commonly used in laboratories in a form of a white powder. The above mentioned materials are characterized by relatively small surface area (usually not exceeding 100 m^2/g [4, 29], and presence of ultramicropores between silica layers and interlayer cations, which are smaller than 20 Å. Thus, can not be detected in adsorption measurements with use of nitrogen and a BET method [4, 22]. Although nitrogen is able to penetrate pores to some extend, the nitrogen molecules are trapped between the layers and are not desorbed at 77 K. Each material distinguishes itself by characteristic basal spacing distance (Table 2.1) [20].

Table 2.1: *Basal spacing distance for different layered silicates.*

layered silicate	ilerite	magadiite	kenyaite
basal spacing (Å)	11.0	15.6	20.0

During heating desorption of water from the crystal surface, followed by destruction of the hydratation shell, occurs. The above described process is fully reversible. However, if exposed to temperature higher than 973 K, the dehydroxylated structure is collapsing and recrystallizes to quartz [22].

Layered silicates are stable in solutions with high pH, however, if exposed on a long term work of condensed basic solution, they are dissolving. They are also dissolving in HF and hot $HClO_3$.

The interlayer cations can be exchanged in the ion-exchange process. Therefore, layered silicates are considered as high capacity ion exchangers [20]. Furthermore, there is relatively large flexibility of radii and charge of the above mentioned cations. Numerous publications confirm successful exchange of interlayer cations by small H^+ cations [13-22, 27-29], various oxides, and organic compounds (paragraph 2.4). After

introduction of new cations into the interlayer space, the basal spacing is adjusting according to the size of the introduced cations. As a result, new micro- or even mesopores can be created. Consequently, big interlayer cations can be treated as pillars between the silica layers [30, 31, 36].

Possible applications

Due to relatively ease of exchanging the interlayer cations, layered silicates are anticipated to be useful ion exchangers and, similar like zeolites, catalyst supports [23] (see also paragraph 2.4). After introduction of active compounds into the interlayer space or into the silica layers, the above mentioned materials could be use as catalyst for various reactions (see also paragraph 2.4). Depending from the nature of introduced compound or cation, they can be used also as sensors [28]. Layered silicates are also efficient adsorbents [28].

It is possible to form a bond between silica layers and polymers and consequently, obtain a nanocomposite material [12].

2.3. Synthesis of layered silicates

Natural layered silicates are formed in an alkali environment (usually provided by presence of sodium carbonates), in which there is a high concentration of dissolved silica. High pressure and temperature are necessary as well. Similar conditions are used in laboratories.

```
┌─────────────────────────────────────┐
│  Source of silica + deionized water  │
└─────────────────────────────────────┘
                   +
┌─────────────────────────────────────┐
│  Source of alkali + deionized water  │
└─────────────────────────────────────┘
                   │
                   ↓
                Mixing
                   │
                   ↓
         ┌──────────────────┐
         │  Crystallization  │
         └──────────────────┘
                   │
                   ↓
         ┌──────────────────┐
         │  Washing, drying  │
         └──────────────────┘
```
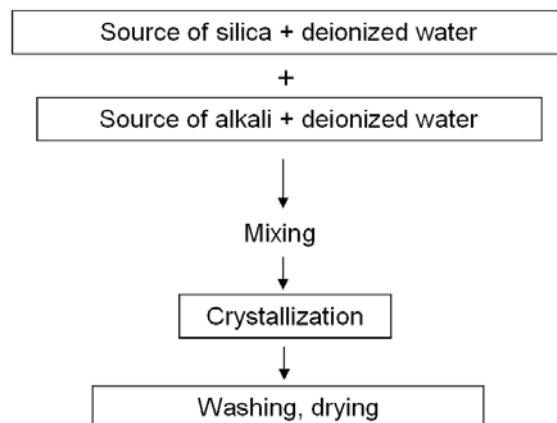
Scheme 2.1: *General synthesis procedure used in syntheses of layered silicates.*

Generally, synthesis of layered silicates (particularly ilerite, magadiite and kenyaite) is conducted in a few steps (Scheme 2.1), which combine mixing of silica and alkali source in an aqueous solution and crystallization. By changing the synthesis mixture composition, different structures can be synthesized [12, 24, 27]. However, synthesis mixture composition does not have so significant influence i.e. the temperature of the synthesis [25]. All syntheses are made in hydrothermal (autogenous pressure) and static conditions [12, 24, 27].

There are no complete models of the crystallization process of layered silicates. Few attempts to clarify the above mentioned process were made [32] (Figure 2.18), however none of it is giving the complete overview [28].

Similar as in the case of zeolite syntheses, particular layered structure can be obtained in different conditions as well as with different synthesis mixture compositions. Influence of applied synthesis parameters on the character of the resulting material was widely studied by various authors [4].
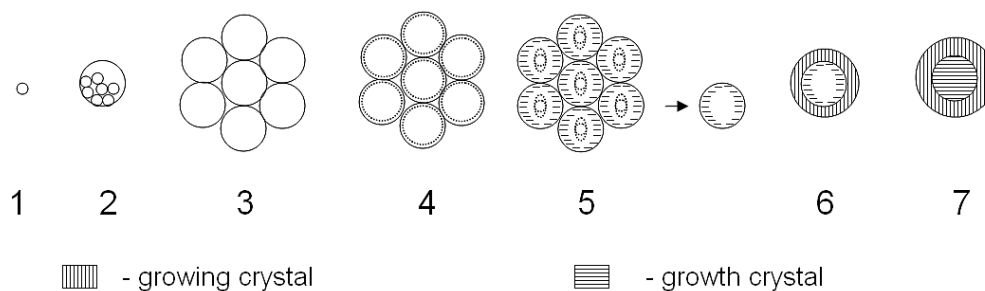
Figure 2.18: *Model of the crystallization process proposed by Schwieger et al.[32] 1 - small gel particles, 2 – agglomerates of small gel particles, 3 – gelation (homogeneous hydrogel), 4 – building of the first crystal seeds, 5 – beginning of the crystallization, 6 – growth of the crystals, 7 – end of the process.*

2.3.1. Modification of synthesis parameters

Source of silica

Similar as in the case of zeolites, various source of silica can be used. They should be also in a reactive state. Most commonly used silica source are: fumed silica [33, 34], colloidal silica [35, 36], sodium silicate (water glass) [25, 12] and silica gel [24, 28]. Contrary to the above mentioned authors, who have synthesized layered silicates in hydrothermal conditions, Crone et al. [37] have used solid sodium metasilicate, Na_2SiO_3, and SiO_2 in the form of a xerogel in synthesis of ilerite and magadiite. All substrates (all in solid state) were milled and calcined in various temperatures.

Apart from work of Feng et al. [33], where syntheses in presence of templates are described, there are no reports confirming influence of a silica source on a structure of resulting material.

Source of alkali

Contrary to syntheses of zeolites [38], influence of different hydroxides on synthesis of layered silicates was not well studied. Although there are reports concerning use of lithium and potassium, most authors are using sodium hydroxide as primary source of alkali [4].

Kwon et al. [39], Fletcher and Bibby [34] are describing syntheses of magadiite and kenyaite from solutions, in which part of alkali source, similar like in nature, is Na_2CO_3. Sodium carbonate is reported to enhance the syntheses of the above mentioned materials; thus, besides NaOH, it is commonly used as alkali and sodium co-source. If added to an ilerite synthesis mixture, Na_2CO_3 redirects the synthesis towards magadiite and kenyaite structures [34, 39]; therefore, the only alkali source in ilerite syntheses is NaOH. The exactly mechanism of this process remains unknown.

Synthesis mixture composition

Numerous authors [12, 24, 27, 39] reported influence of the SiO_2/alkali and H_2O/alkali ratios on the structure and purity of the obtained material. Increase of the SiO_2/alkali, as well as the H_2O/alkali ratios, leads to formation of kenyaite. However, if compared to the crystallization time and temperature [25], synthesis mixture composition occurs as the moderate synthesis modification factor.

Crystallization temperature

With increasing temperature, the time of crystallization is significantly shortened. Due to higher activation energy of seed formation and the longer crystal growth periods for materials with higher Si/Na ratio, the above mentioned effect is stronger for high-alkali silicates [4]. Furthermore, the resulting material is much faster recrystallizing into more stable one according to the following sequence of phase transformation: ilerite $\rightarrow$ magadiite $\rightarrow$ kenyaite $\rightarrow$ quartz [40]. Moreover, by changing the crystallization

temperature different structures from the same synthesis mixture can be obtained [12, 24, 39, 40].

Schwieger and Lagaly [4] are reporting that layered silicates can not be synthesized in hydrothermal conditions above certain temperatures: 120°C for ilerite, 200°C for magadiite, and 240°C for kenyaite. However, by appropriate change of other synthesis conditions the above mentioned temperatures can be shifted.

Crystallization time

Like in nature, synthetic layered silicates are crystallizing according to the following sequence of phase transformation: amorphous material $\rightarrow$ ilerite $\rightarrow$ magadiite $\rightarrow$ kenyaite $\rightarrow$ quartz [40]. Therefore, an increase of crystallization time, besides increase of crystal size, leads to recrystallization of synthesized material. Similar like the crystallization temperature, the crystallization time has significant influence on type and purity of the synthesized material [12].

Presence of a structure directing agent (template)

Contrary to zeolites, only occasional attempts of use of templates have been described. Triethanolamine was tested in layered silicates syntheses; however, an effect was detected only for makatite [4]. Feng and Balkus [33] are reporting successful use of poly(ethylene glycol) – PEG as the template. Conducted syntheses lead to crystalline products, whereas syntheses made without PEG lead only to amorphous products. Influence of silica source, as well as changed sequence of phase transformation (from magadiite $\rightarrow$ kenyaite to kenyaite $\rightarrow$ magadiite), was described. It has been concluded that reported changes are closely related to template - reagents interactions. Unfortunately, calcination of the template leads to more than 90% loss of crystallinity.

Presence of crystal seeds

Iwasaki et al. [25] is describing the seeding effect on crystal growth of ilerite. Similar as in the case of zeolites, significant decrease of the crystallization time, as well as increase of the synthesis yield, was observed already when synthesis mixture mass to seed ratio equaled 0.0001 [25].

2.4. Modification of layered silicates

Layered silicates can be easily modified using various methods and techniques. Due to the structure and the properties of the silica layers, layered silicates can be considered as material similar to zeolites. Thus, by describing and systemizing those distinctive modification possibilities, it is suitable to use the same classification such as those used for three-dimensional silicates.

Post synthesis modifications

Most popular and in the same time the simplest method to adjust the properties of layered silicates is an ion exchange of the interlayer cations. Introduction of new cations, characterized by larger radius than those being exchanged, leads to swelling of the structure. The intercalated cations act as pillars between the silica layers. The distance between the silica layers is increasing [31, 36, 41, 42, 43] and as a result, micro and/or mesopores are created. Such modified material with accessible active "pillars" could be used as a catalyst.

Activity of metal (Cu, Zn) - pillared ilerite in direct synthesis of dimethyl ether from synthesis gas - was reported by Ahn et al. [41]. Kim et al. [36] is reporting on successful ion exchange of sodium cations with tantalum oxide in ilerite. After intercalation, the precursor - $Ta(OC_2H_5)_5$ - was calcinated to form metaloxides pillars. Afterwards, Ta-ilerite was loaded with platinum and palladium oxides. Material was active and stable in the vapor phase Beckmann rearrangements of cyclohexanone oxime.

Similar approach was described by Schwieger et al. [31] where ilerite sodium cations were exchanged with $Pt(NH_3)_4^{2+}$ followed by calcination of such modified layered material. In such manner, highly loaded with Pt nanoparticles (up to 20 wt%) ilerite was prepared. Its bifunctional character was examined and described by Kuhlmann et al. [42]. Schwieger et al. [43] describes similar experiments made with use of the magadiite material. In this case, even higher platinum load was achieved (22.2 wt%). Moreover, the structure of the silica layers was not affected, which indicates the stability of the mentioned host - matrix system.

Properties of another layered silicate - metal nanocomposite were described by Ozawa et al. [44, 45], who have successfully prepared Ag- and ZnO-magadiite nanocoposite, containing well dispersed Ag and ZnO single crystalline particles, with size between 3-5 nm (Figure 2.19). Kalvachev et al. [23] describes activity of a cobalt-containing kenyaite in complete hexane oxidation. Also here, after intercalation of the precursor –$Co(OH)_2$, stability of host - matrix system was reported.
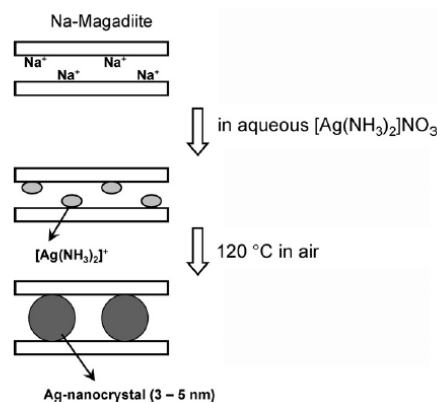
Figure 2.19: *Proposed model of synthesis of layerd silicate – metal nanocomposite [45].*

In each the above described example, an inorganic precursor was introduced into the interlayer space. However, also organic compounds can be relatively easily intercalated. Mentioned approach is often used in synthesis of micro- and mesoporous structures from layered materials.

Selvam et al. [45] is describing a synthesis of impurities free, highly crystalline zeolite BEA from kanemite with a template (tetraethylammonium) in its interlayer space.

After heating at 413 K kanemite recrystallized to BEA zeolite with large intercrystalline voids. Moreover, the yield of the recrystallization was higher then that of a hydrothermal synthesis. After intercalation of acetic acid into ilerite, Ikeda et al.[28] has synthesized zeolite RWR.

Detailed studies over recrystallization of various structures (ilerite, magadiite and kenyaite), containing various templates, were made by Feng and Balkus Jr. [46], who have successfully synthesized silicalite-1 under variety of conditions. The study concluded that its degree of crystallinity, morphology and crystal size strongly depend from reaction parameters such as the type of the layered silicate, the recrystallization time and the recrystallization temperature. Furthermore, layered silicates showed higher reactivity than fumed silica used in similar syntheses.

Possibility of an ion-exchange of the sodium cations with bulky organic compounds was also used to synthesize microporous layered organic-inorganic hybrids. Such intercalation is considered as a promising route to obtain materials that physical and chemical properties can be designed and controlled [48]. Work of Ishii et al. [49] where ilerite was alkoxysilylated with p-aminotrimethoxysilane, can be given as the example. The resulting material is characterized by presence of micropores; therefore, it could be used as adsorbent. Wang et al. [49] is successfully using chemically stable siloxane surfaces of magadiite to form an organic-inorganic nanocomposite, containing n-hexadecyl trimethyl-ammonium bromide (CTAB). Such organic derivative is reported to have the capability for further accommodation of organic molecules thanks to its organophilicity. Similar aim has the work of Park et al. [50], who has modified magadiite by interlamellar silylation with octyl triethoxysilane. The same author is also describing modification of kenyaite with use of 3-aminopropyltriethoxysilane [51] (Figure 2.20) to create active amine groups attached to the surface of H-kenyaite. Guo et al. [52] has intercalated photoactive molecules as azobenzene into interlayer space of magadiite. Ion-exchange of the sodium cations with active organic molecules in ilerite was also described by Royer et al. [53]. Resulting material, containing cetyltrimethylammonium cations, was tested for use as a sorbent for the Reactive Black 5 textile dye removal.
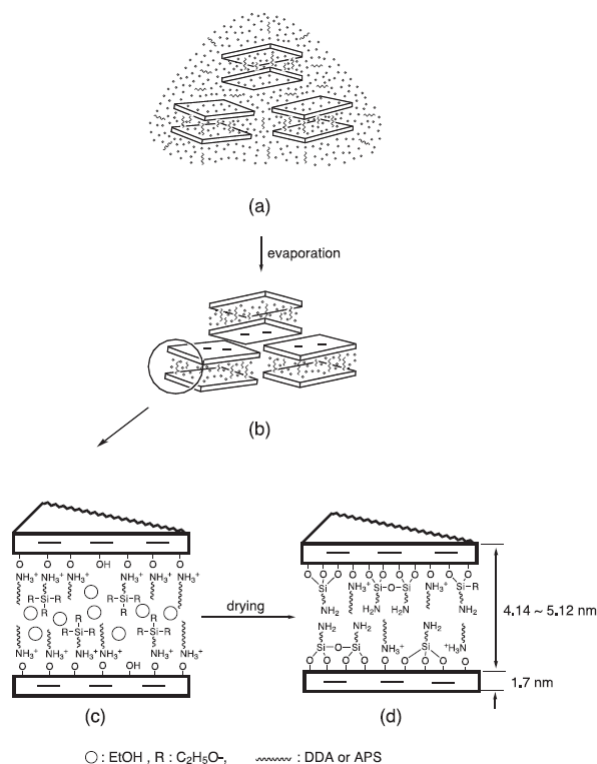
Figure 2.20: *Schematic representation of the intercalation and silylation of dodecylamine (DDA) and 3-aminopropyltriethoxysilane (APS) of H-kenyaite [51].*

Incorporation of a heteroatom

The above mentioned examples are showing the variety of interlayer space modifications, whereas the silica layer remains unmodified. However, various authors are comparing properties of layered silicates to those of zeolites [5, 14, 54].

One of the main zeolites´ attributes is relatively ease to isomorphously exchange their framework atoms. Various authors are reporting successful incorporation of various species characterized by different cation size and charge e.g. Cr, Ga, Fe, Ti, B, V, Cu [55-58]. The resulting material is usually showing analogous structure as that of known zeolite. The heteroatoms are usually introduced into zeolitic structures upon hydrothermal synthesis. In such a way new families of materials such as aluminum phosphates [59], metallosilicates [55-58] and metallogermanates [60, 61] were obtained.

Due to certain similarities between zeolitic frameworks and structures of layer silicates, one can assume that silica layers will have analogues properties such as those of zeolite.

Basing on the MAS-NMR spectroscopy experiments made for ilerite, Borbély et al. [6] has proved that it is possible to ismorphously substitute silicon with aluminium atoms in the silica layers. Schwieger et al. [7] has done also experiments on possibility as well as on consequences of ismorphous substitution of silicon. Contrary to work of Borbély et al. [6] boron has been chosen as the heteroatom. Furthermore, the experiments were done on more stable layered structure - magadiite. The study concluded that the presence of the heteroatom source in the synthesis mixture retards the crystallization and changes the product sequence in the crystallization process, which is similar like those observed by Feng and Balkus [33]. Significant influence of presence of the heteroatom source on the final product of the crystallization was also reported by Cheng et al. [62]. It has been observed that kenyaite synthesis is redirected towards zeolite MCM-22 already when Al/Si ratio in the synthesis mixture equals 0.02.

Pal-Borbely et al. [63, 64] is describing syntheses of aluminium-containing magadiite, which was later recrystallized into MFI, MEL ferrierite. Mihalyi et al. [65] and Fudala et al. [66-68] are also using the magadiite structure with framework aluminium as a precursor of zeolitic and mesoporous structures. Fudala [68] is even introducing MCM-41 pillars into the interlayer space of Al-magadiite. Unfortunately, the mentioned authors focus mostly on the characteristic of zeolites and/or mesoporous materials, whereas description of aluminium-containing layered structures is neglected. Complex characterization of Al-magadiite was done by Superti et al. [5]. Two different synthesis methods were used to synthesize Al-magadiite – direct method (standard hydrothermal synthesis in presence of an Al source) and Aluminium-Induced Crystallization Method, in which part of the aluminium is added to the synthesis mixture during the crystallization process. Conducted variable-temperature XRD analysis clearly indicated that the resulting material is as stable as the unmodified magadiite and it exhibit the same morphology. Moreover, likewise zeolites, additional negative charge on the framework/silica layer, coming from the AlO_4 tetrahedra, was detected (FTIR measurements of adsorbed CO). In conclusions, the authors are pointing on very interesting properties of such modified magadiite and its possible catalytic applications.

Similar properties and possible applications of silica-pillared aluminum-containing kanemite were reported by Toriya et al. [54]. The above mentioned material has been found to have large specific surface areas and large micropores. Also here, new acid sites were formed by the incorporation of Al atoms into silicate sheets.

Successful incorporation of heteroatoms into the silica layers and numerous similarities between zeolites and the silica layers could lead to an assumption that incorporation of other transition metals, similar as in the case of metalosilicates, could be possible as well.

2.5. Catalytic activity of tin

Due to the character of the hereby presented work, the description of tin properties will be tightened to few examples of its catalytic activity in porous materials.

Mal et al. [69] reported successful synthesis of stannosilicate Sn-MFI and its activity in phenol hydroxylation. Moreover, activity of the above mentioned material was comparable to that of Ti-MFI. In another work, Mal et al. [70, 71] is describing activity of Sn-silicalite-1 in liquid phase hydroxylation of phenol in presence of dilute H_2O_2. Activity of molecular sieves, containing framework tin, in liquid phase hydroxylation of phenol was also described by Boronat et al. [72].

Corma et al. [74] described a beta zeolite, containing framework tin. The catalyst showed good stereoselectivity and activity (even after it has been several times recycled) in Meervein-Pendorv-Verley reduction. Furthermore, Sn-Beta is water resistant what make it an attractive alternative to the commercially used catalysts.

Activity of Sn-Beta in other redox reactions, e.g. Baeyer-Villiger reaction and cyclisation of citronellal to isopulegol was reported also by Boronat et al. [74]. Also here the considerable stability of the catalyst was reported. Moreover, the process of the production of δ-decalatone, in which Sn-Beta is used, is being scaled up by Takasago company.

Numerous reports also confirm activity of silica based, Sn-containing mesoporous materials such as Sn-MCM-41, Sn-MCM-48, Sn-HMS, and Sn-SBA-15 in various reactions, e.g. epoxidation of norborne [75], Mukaiyama-type aldol condensation [76], transesterification [77], synthesis of poly(L-lactic acid) [78], acylation of aromatics and heteroaromatics [79] or selective oxidative dehydrogenation of cyclohexane [73].

Alarcón et al. [80] is describing kenyaite material, modified by tin-containing pillars, that is active in nopol synthesis. However, although catalyst exhibit 94% selectivity to nopol, conversion of the substrate drops to around 20% after 4th recycling. One could speculate that conversion decrease would be smaller, if Sn was introduced into the silica layers.

3. Aim of the work

Silicon based porous materials, *i.e.* zeolites or zeolite-like materials are proved to be very successful catalysts, supports, or ion-exchangers [58]. Their framework is built by silicon tetrahedras, which part of them can be isomorphically substituted by tetrahedras consisting heteroatom, *i.e.* Al, Ti, Sn. Introduced heteroatom tetrahedras usually significantly change the properties of the resulting material either by creating additional acid/basic sites or red-ox active sites.

One of the best-known examples of such modification is titanosilicalite (TS-1), with isolated transition metal ions introduced into framework position [81], which was proved to be efficient catalyst for mild oxidation reactions. However, small radii of its pores significantly limited its applications in oxidation of bulky organic compounds. Consequently, material with similar properties to three-dimensional silicates, which can be modified through the use of isomorphic substitution, is needed.

Answer for such a need could be layered silicates. Their advantage, compared with the microporous, three-dimensional structure of zeolites, consists in the option to adjust the distance between the silica layers. Therefore, bulky organic molecules could access eventual active centers located in the layers. This could allow their application in liquid phase oxidation reactions.

Superti et al. [5] is pointing on very interesting properties of such modified magadiite and its possible catalytic applications. Similarities between zeolitic framework and silica layers of layered silicates along with successful incorporation of aluminum and boron heteroatoms into silica layers [6,7], leads to an assumption that incorporation of other transition metals could be possible as well. Such materials could be used as efficient catalysts, thus a complete study of synthesis methods and their properties is required.

After considering the activity of tin-containing catalyst in various processes (paragraph 2.5), one can assume that isomorphously tin-substituted layered silicates

would exhibit similar activity such as those mentioned in the paragraph 2.5. Incorporation of tin atoms into the silica layers could result in the material that could be later pillared and used as a catalyst. First step of such investigation will be an attempt to replace isomorphously part of the silicon by tin atoms. Therefore, the aim of the present work was to investigate the influence of presence of the heteroatom source (particularly – $SnCl_4*5H_2O$) on the synthesis of layered silicates. Some samples, in which silicon atoms were partially substituted by aluminum, were synthesized as well; however, they were used mostly as a comparison for tin-containing samples.

4. Experimental part

4.1. Synthesis

The sodium forms (Na-forms) of the un- and tin-modified samples with the structures of ilerite, magadiite or kenyaite were synthesized. All the above mentioned samples described within the present work were synthesized in the hydrothermal conditions. In the case of all the syntheses the same reactants were used:

- colloidal silica Köstrosol 0730 (CWK Bad Koestritz, 30% m/m SiO_2 in H_2O) – as a source of silicon atoms,
- sodium hydroxide (Merck, 98%) - as a source of sodium cations and OH groups,
- sodium carbonate (Riedel-de Haen, 99%) – as a co-source of sodium cations and the source of carbonate anions,
- tin(IV) chloride pentahydrate (Riedel-de Haen, 98%) – as a tin heteroatom source,
- aluminium isopropoxide (Fluka, 99%) - as an aluminium heteroatom source.

Comparison of the composition of synthesis mixtures and main parameters for different types of syntheses are listened in Table 4.1.

4.1.1. Ilerite synthesis

In order to synthesize a material with the ilerite structure, two general synthesis procedures were used – procedure I1 and procedure I2. The synthesis procedure I1 (Scheme 4.1), similar to that described by Borbely et al. [6], consisted of mixing a colloidal silica with a deionized water for 15 min. and adding a mixture containing heteroatom source and NaOH dissolved in a deionized water. After mixing, a dense gel was formed immediately (pH~14). The molar ratio of the reactants in the pre-synthesis

mixture is – x*M : 4SiO$_2$: (y*x+1)Na$_2$O : 30H$_2$O, where y = 4 or 6 - similar to that described in the work of Borbely et al. [6]. After 45 min. of stirring, the gel was placed in a teflon-lined stainless autoclave. Crystallization took place at 373 K in static conditions for 3 and 4 weeks, respectively. The synthesized solid material was washed and dried at 323 K. The resulting samples were named according to the ratios of heteroatom to silicon atoms in the synthesis mixture – xM / Si, where M = Al, Sn and x = molar ratio of M. Unmodified ilerite (no heteroatom or ion exchange modification) was decoded as Na-ilerite.

Table 4.1 *Composition and synthesis details of different structures.*

	ilerite	magadiite	kenyaite
unit cell composition	xM:Na$_2$O:(8-x)SiO$_2$:9H$_2$O	xM:Na$_2$O:(14-x)SiO$_2$:9H$_2$O	xM:Na$_2$O:(22-x)SiO$_2$:10H$_2$O
synthesis composition	xM:(6*x+2)NaOH: 4SiO$_2$:30H$_2$O	xM:7SiO$_2$:(6*x+0.33) NaOH:0.66Na$_2$CO$_3$:100H$_2$O	xM:1SiO$_2$:(6*x+0.33) NaOH:0.66Na$_2$CO$_3$:20H$_2$O
silica layers	1	2	3
synthesis temperature (K)	393	423	443
drying temperature (K)	323	353	353
max. Sn/Si in synthesis mixture	0.00125	0.01500	0.04500
max. Sn/Si in sample	0.00112	0.01920	0.06300

M = Al, Sn; x = molar ratio of M.
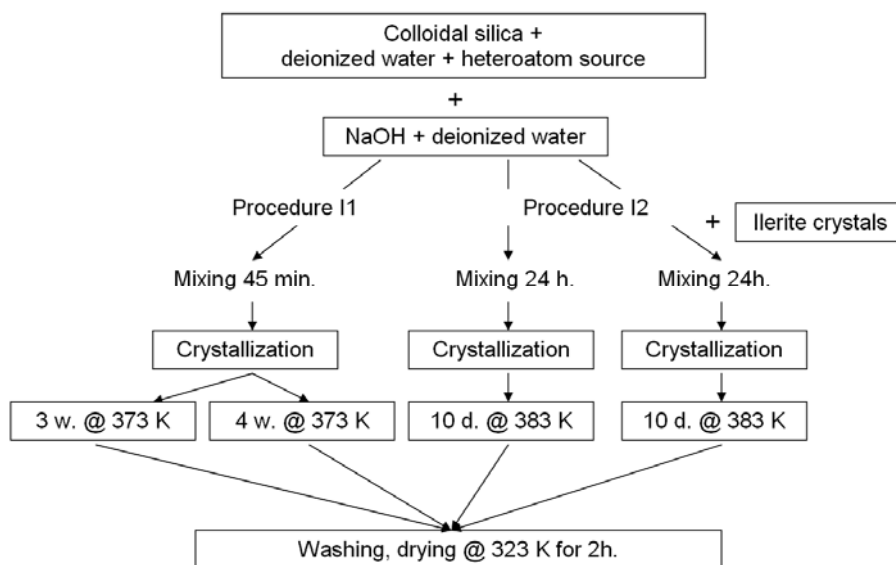
Scheme 4.1: *Different ilerite synthesis procedures. w-weeks, d-days*

Procedure I2 was adapted from Kim et al. [36] (Scheme 4.1). It differs from the procedure I1 both in the mixing time of starting gel (24 h), in the temperature and in crystallization time (383 K, 10 days). For comparison reasons, the molar ratio of reactants was adjusted to the same value as in the procedure I1.

To check the influence of crystallization time on the synthesis, samples crystallized for 15 days at 383 K were also synthesized. Similar like described by Iwasaki et al. [25] - some syntheses were modified with the use of 0.1g of ilerite seeds (particularly in samples with $0.00125 \leq x \leq 0.00250$) to enhance the efficiency of the syntheses. The ilerite seeds were taken from the Na-ilerite sample.

4.1.2. Magadiite synthesis

Magadiite samples were synthesized according to the procedure M1, which is similar to that proposed by Wang et al. [12] (Scheme 4.2). In standard syntheses, colloidal silica was mixed with a heteroatom source - tin(IV) chloride pentahydrate or aluminium isopropoxide - and dissolved in water. Afterwards, NaOH and Na_2CO_3 were

added in small portions. After mixing all substrates, a dense gel was formed immediately (pH~12.5). No additional NaOH, to establish the pH value, was added before or after the formation of gel. The mixture was vigorous stirred for 1h and sealed in a teflon-lined stainless autoclave. The molar ratio of the reactants in the synthesis mixture was – x*M : $7SiO_2$: $(y*x+0.33)NaOH$: $0.66Na_2CO_3$: $100H_2O$ where y = 4 or 6 for Al- or Sn-samples, respectively. Crystallization took place at autogenous pressure at 423 K for 48 h under static conditions. Afterwards, solid samples were washed and dried at 353 K. The synthesized magadiite samples were named according to the ratios of heteroatom to silicon atoms in the synthesis mixture – xM / Si, where M = Sn, Al and x = molar ratio of M. Unmodified magadiite (no heteroatom or ion exchange modification) was decoded as Na-magadiite.

As has been reported by various authors, the magadiite synthesis can be enhanced by the addition of a sodium carbonate as a sodium co-source [34]. One could not exclude the precipitation of aluminium(III)- or tin(IV)carbonate salts during the synthesis. Thus, to check the influence of carbonate ions on the number of incorporated heteroatom and on crystallinity of the resulting samples, syntheses with NaOH as the only sodium source were made as well.

The influence of crystallization time on the synthesis was checked by prolonging it from 48 h to 72 h.

In an attempt to enhance the synthesis efficiency, syntheses with addition of 0.1 g of magadiite seeds (coming from Na-magadiite sample) were performed.
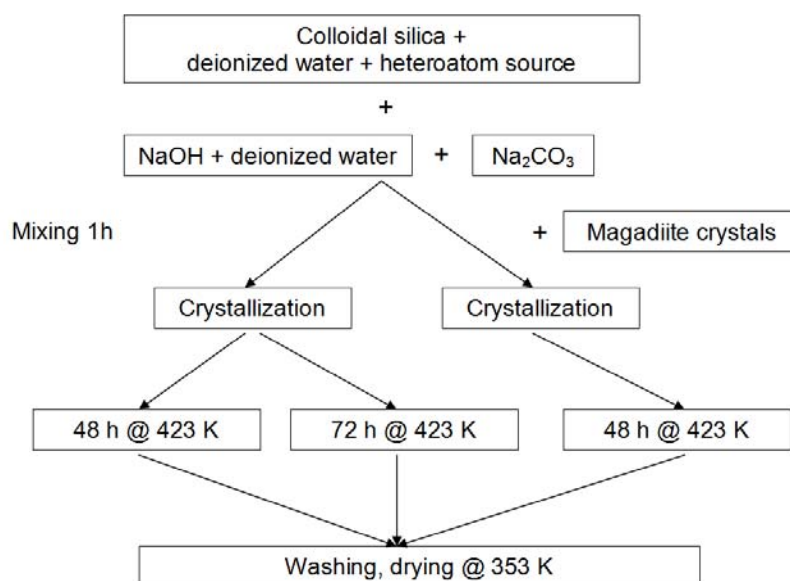
Scheme 4.2: *Applied magadiite synthesis procedure. h-hours*

4.1.3. Kenyaite synthesis

Kenyaite samples were synthesized according to the synthesis procedure K1, which was adapted from Kwon et al. [39] (Scheme 4.3). In the standard syntheses, colloidal silica was mixed with the tin or aluminium heteroatom source and dissolved in water. Afterwards, NaOH and Na_2CO_3 were added in small portions. After mixing all substrates, a dense gel was formed immediately (pH~12.5). The mixture was vigorous stirred for 1h and sealed in a teflon-lined stainless autoclave. Synthesis composition was as follows – $xM : 1SiO_2 : (6*x+0.33)NaOH : 0.66Na_2CO_3 : 20H_2O$ where y = 6 or 4 for Sn- or Al- samples, respectively. The crystallization took place at autogenous pressure at 443 K for 72 h under static conditions. Afterwards, solid samples were washed and dried at 353 K. The resulting samples were named according to ratios of heteroatom to silicon atoms in the synthesis mixture – xM / Si, where M = Sn, Al and x = molar ratio of M. Unmodified kenyaite (no heteroatom or ion exchange modification) was decoded as Na-kenyaite.
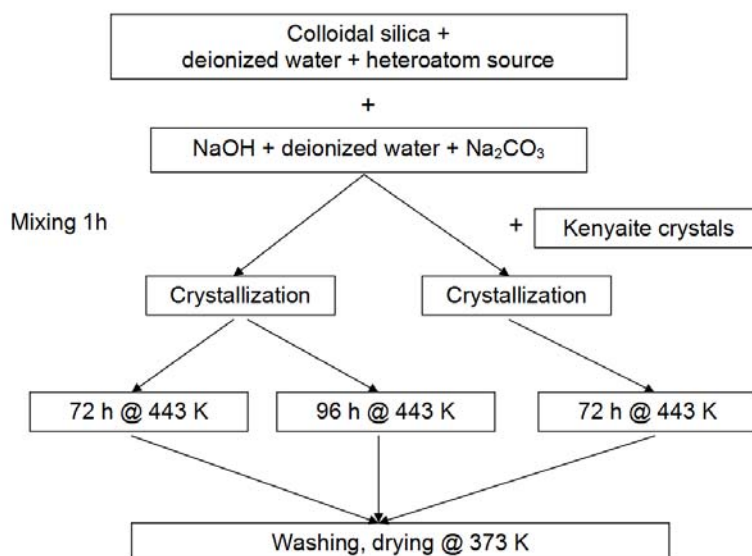
Scheme 4.3: *Applied kenyaite synthesis procedure. h-hours*

As has been reported by various authors, kenyaite synthesis can be enhanced by the addition of sodium carbonate as a sodium co-source [34]; therefore, likewise in the syntheses of the magadiite samples, sodium carbonate was added to the kenyaite synthesis mixture.

The influence of crystallization time on the synthesis was checked by prolonging it from 72 h to 96 h.

In an attempt to enhance the synthesis efficiency, syntheses with addition of 0.1 g of kenyaite seeds (coming from Na-kenyaite sample) were performed.

4.1.4. Post-synthesis modification of layered silicate samples

All samples were modified by ion exchange with the intention of obtaining their H-forms. 2 g of a sample was added to 40 mL of deionized water. The pH was adjusted to pH = 2 by adding 0.1 M HCl dropwise. After 24h of stirring the H-form of material was

washed, filtered and dried for 2 h at 323 K, 353 K or 373 K for the ilerite, magadiite or kenyaite samples, respectively.

For comparison, unmodified samples with bulky SnO_2 on the surface of the layered silicate crystals were made. To obtain them 2 g of Na-ilerite, Na-magadiite and Na-kenyaite, respectively, was mixed for 2 h with 20 mL deionized water containing dissolved $SnCl_4*5H_2O$. Amount of salt was adjusted so, that the Sn/Si ratio in the resulting material would be equal to the highest Sn/Si ratio used in the synthesis mixture for the particular structure (Table 4.1). After mixing, water was evaporated and the solid material was heated at 383 K for 4h to obtain SnO_2. The resulting samples where decoded as SnO_2 / Na-ilerite and SnO_2 / Na-magadiite, respectively. An exception to this rule is SnO_2 / H-kenyaite, which will be explained in paragraph 5.1.

4.2. Characterization methods and equipment

X-ray powder diffractography (XRD)

X-ray powder diffractography was used to estimate the type of crystallographic structure as well as crystallinity of the synthesized samples. Within the present work XRD patterns were recorded on two types of X-ray diffractometers - Stoe STADI P (equipped with Cu- X-ray lamp with 0,154 nm wavelength ($K_{\alpha 1}$)) for samples coming from the ilerite syntheses and Philips X'Pert (equipped with Cu- X-ray lamp with 0,154 nm wavelength ($K_{\alpha 1}$)) for samples coming from the magadiite and kenyaite syntheses. In order to estimate the amount of an amorphous material in the synthesized samples, no background noises reduction was applied to the recorded XRD patterns. The area of characteristic reflexes was counted to estimate the relative crystallinity of the samples.

Scanning Electron Microscopy (SEM)

Topography of crystals of the synthesized samples was studied with the use of the Scanning Electron Microscopy technique. Within the present work two different

microscopes were used: FEI QUANTA 200 3D for ilerite and magadiite samples, and Hitachi S-3200N for kenyaite samples.

Nitrogen adsorption

Textural properties of the samples were determined by analysis of the isotherms of adsorption of nitrogen. Measurements were done on an Autosorb-1 Quantachrome at T = 77 K. Prior to the adsorption the samples were evacuated at 573 K for 3 h. The Brunauer-Emmett-Teller method (BET) was used for determination of the surface areas.

Thermal analysis

Differential Thermal Analysis and Thermal Gravimetry Analysis (DTA/TG) were used for the study of the thermal behaviour of synthesized samples. Analyses were made on a TGA/SDTA 851^e-Mettler-Toledo GMBH. During the test, samples were heated to 1273 K (heating rate: 10 K/min) in nitrogen environment.

Elemental analysis

Total amount of tin in synthesized samples was analyzed by the Inductively Coupled Plasma Atomic Emission Spectroscopy (ICP-AES). Analysis was carried out on a Thermo Scientific – iCAP 6000 series and conducted after dissolving 100 mg of the sample in 500 mg HF.

Infrared spectroscopy (IR)

Infrared spectroscopy was used to study characteristic vibrations of the framework. IR spectra were recorded using a Bruker EQIUNOX 55 equipped with a Diffuse Reflection Attachment unit and a Harricks high temperature dome. Spectra were recorded in different temperatures – room temperature (RT), 373 K, 473 K, 573 K, 673 K. Prior to each measurement, at the temperature higher than RT, samples were heated

for 1 h at the particular temperature under a constant nitrogen flow (50 mL/min). The samples were diluted with a diamond powder (1:4) to improve the reflection at low wave numbers.

^{29}Si *magic-angle spinning nuclear magnetic resonance (^{29}Si MAS NMR)*

Solid-state NMR spectra were measured with a Bruker DSX 400 MHz instrument under MAS conditions in 2.5 mm ZrO_2 rotors with a sample volume of 12 µL(rotation frequency 20kHz). The ^{29}Si-CP-NMR(79.460 MHz) were carried out with the pulse program CP4C.

Hydrogen temperature-programmed reduction (H_2-TPR)

The red-ox properties of the samples were determined in a modified AMI-100 unit (Raczek Analysentechnik). In the H_2-TPR test, 0.3 g of the sample (fraction 315-200 µm) was placed in a quartz u-pipe. During the pre-treatment procedure, sample was heated in argon stream (50 mL/min) to 573 K with the heating rate at 20 K/min. After 2h, the sample was cooled down to 373 K. The reduction measurement was conducted under flow of argon containing 7.5% of H_2 (50mL/min) by heating the sample up to 973 K (5 K/min). Hydrogen consumption was detected by a TCD detector.

Temperature-programmed ammonia desorption (NH_3 -TPD)

The acidity of the samples was determined in a modified AMI-100 unit (Raczek Analysentechnik). In the NH_3-TPD tests, 0.3 g of the sample (grain fraction 200-315 µm) was heated in helium stream (50 mL/min) to 573 K with the heating rate 20 K/min. After 2 h heating in 573 K, the sample was treated with NH_3 (25 mL/min) at 343 K for 30 min. The physically adsorbed ammonia was removed at 423 K in He (50 mL/min) for 2 hours. Desorption of the chemisorbed NH_3 was conducted in He (50 mL/min) in temperature range 423-973 K with the heating rate 10 K/min. The amount of desorbed ammonia was detected by a TCD detector.

Conversion of 2-methyl-3-butyn-2-ol (MBOH)

- Experimental apparatus

The experimental set-up consists of a feeding unit for the educt, a heatable catalyst containing reactor and an analysis unit. A valve unit, which combines a three line valve and a check valve, was used to control the type of flowing gases (nitrogen or synthetic air). The gas flow is controlled by a mass flow controller with a corresponding control unit (Bronkhorst Company). Due to the static nitrogen pressure, a constant flow of the MBOH/toluene mixture was realized. To control the mixture flow rate (0.02 mL/min), the MBOH/toluene reservoir was followed by a spiral thermostated capillary (~300 cm length and 1.5 mm diameter). The evaporator was first covered in a spiral way with heating bands, then wrapped with copper bands for equally heating and finally wrapped with an isolation material. After evaporation, the MBOH/n-hexane mixture proceeds then to a tubular reactor (7mm diameter) with catalyst placed in its isothermal section.
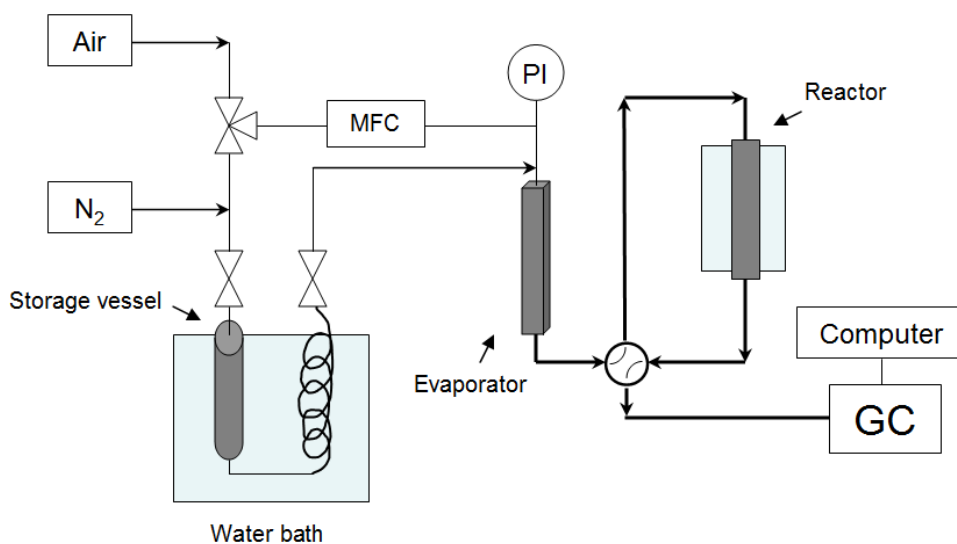
Scheme 4.1: *Apparatus used for the MBOH conversion.*

To insure a steady stream of the substrate over the solid catalyst, a bypass was installed to pass a stream of the MBOH/n-hexane mixture from a evaporator directly to a gas chromatograph. After establishing constant flow of the mentioned mixture, the stream was orientated to the top of the reactor via a four way valve.

- Experimental procedure

The conversion of 2-methyl-3-butyn-2-ol (MBOH) (Lancaster) mixed with toluene (Fluka) as an internal standard was carried out in a fixed-bed reactor, embedded in a computer controlled bench unit. The reaction mixture (95 vol. % of MBOH and 5 vol. % of toluene) was held in a storage vessel at constant temperature (287 K). Static nitrogen pressure was applied to realize a constant liquid flow to the evaporator (0.02 mL/min). The catalyst (0.2 g, fraction 200-315 μm) was placed in the centre of the tubular reactor and activated at 773 K first in synthetic air flow (7.4 mL/min) for 4 hours. Afterwards, air was replaced by a nitrogen (7.4 mL/min), which was passed through the catalyst bed also for 4 hours. The reaction was carried out at 393 K and its products were analyzed on-line by a gas chromatograph of HP 5890 Series II equipped with a capillary column (OPTIMA-WAX – 0.25μm ; 60m ∗0.25mm) and a FID detector.

.

5. Experimental data

5.1. X-Ray Powder Diffractography

5.1.1. Ilerite

As can be seen in Figure 5.1 Na-ilerite sample exhibit typical reflexes for this type of the structure - $2\theta \sim 8.0^o$; 18.6^o; 21.8^o; 25.6^o; 29.2^o (according to Vortmann et al. [14]). Both synthesis procedures I1 and I2 resulted in the formation of ilerite (Figure 5.1). The presence of additional diffraction reflexes after prolonging the synthesis time, especially that at $2\theta \sim 5.75^o$, indicates traces of the magadiite phase impurities (Figure 5.1 c).
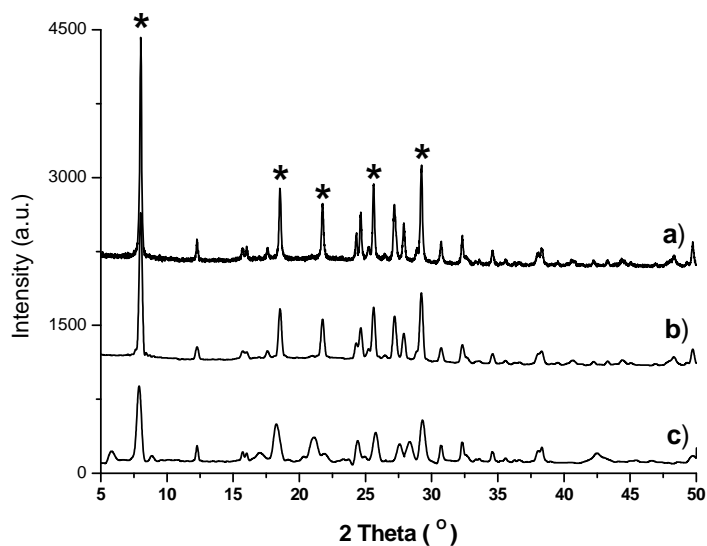
Figure. 5.1: *XRD patterns of unmodified Na-ilerite synthesized according to: a) procedure I2, b) procedure I1 – 3 weeks, c) procedure I1 – 4 weeks. * - typical reflexes for the ilerite structure*

The addition of the tin source to the pre-synthesis mixture results in an entire formation of the magadiite structure (Figure 5.2) - represented by characteristic reflexes at $2 \theta \sim 5.75$; 17.10; 26.00; 27.00; 28.00 [33]. Moreover, the samples with Sn/Si ratio higher than 0.0005 were amorphous. Crystalline material with higher tin loading (0.0005 < Sn/Si $\leq$ 0.00125) was detected only after adding an additional NaOH to the synthesis mixture with the intention of compensating the amount of the alkalinity needed for an in-situ formation of sodium hexahydroxo stannate(IV) from tin(IV) chloride pentahydrate during the synthesis. Also in this case magadiite phase was dominating (Figure 5.2).
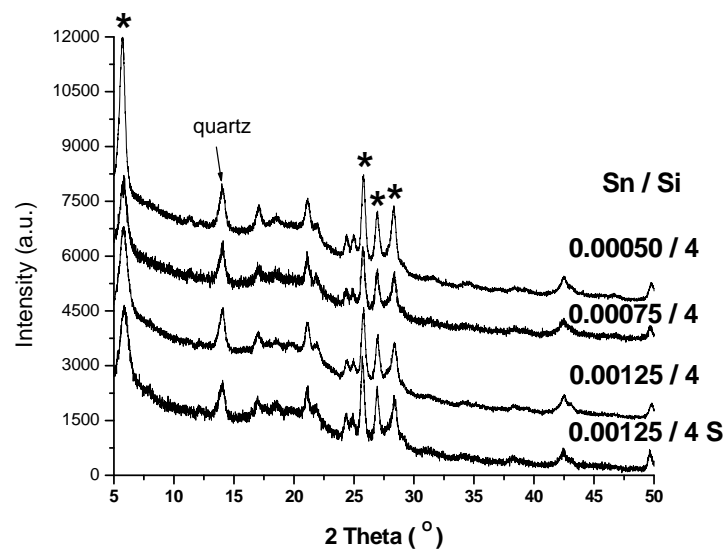
Figure 5.2: *XRD patterns of the various Na-forms of Sn-containing samples synthesized according to the procedure I2 with additional alkali. S –synthesis in the presence of ilerite seeds. * - typical reflexes for the magadiite structure*

Such a modification of synthesis procedure does not affect syntheses when aluminium isopropoxide was added. Typical magadiite structure reflexes have been found only for the sample with the lowest aluminium content (Figure 5.3 a). There were no crystallization products after 10 days in the synthesis mixtures for the samples with 0.0005 < Al/Si $\geq$ 0.0025 and Sn/Si > 0.00125. Therefore, crystallization time in the procedure I2 was prolonged to 15 days. The tin-containing samples obtained by this

modified method were containing high amounts of amorphous material (significant increase of baseline - Figure 5.4) and some magadiite phase. In the case of aluminium-modified samples (Figure 5.3), the magadiite structure was detected for the samples with 0.00125 Al/Si ratio. However, the samples with higher aluminium loading were amorphous.
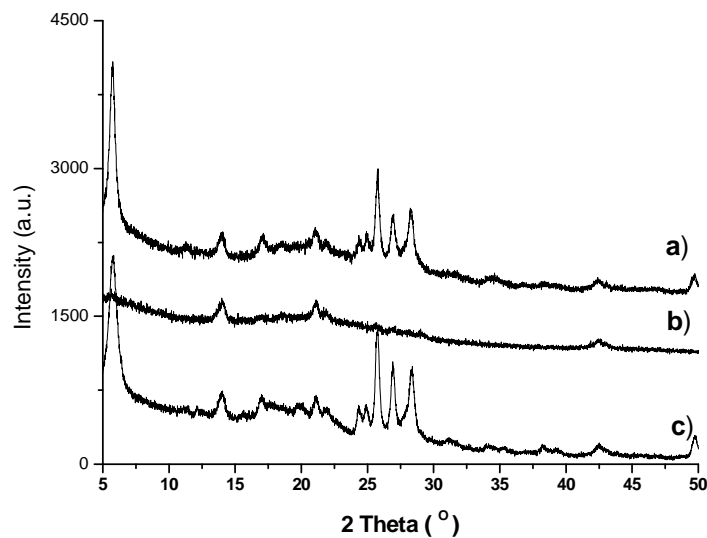
Figure 5.3: *XRD patterns of the Na-forms of the samples synthesized with additional alkali: a) 0.0005 Al/Si magadiite – procedure I2, b) 0.00125 Al/Si magadiite – procedure I2, c) 0.00125 Al/Si magadiite – procedure I2 (15 d. synthesis).*

Synthesis of crystalline samples with 0.0025 Sn/Si was possible only after addition of ilerite seeds to pre-synthesis mixture. As in the case of the above described modified crystalline samples, synthesis leads to magadiite as a dominating layered silicate phase. However, as can be seen in Figure 5.4, low intensity of the peaks and the high background indicates a very low degree of crystallinity and the presence of impurities of an amorphous phase. The increase of crystallization time to 15 days led to a significant formation of quartz (Figure 5.4 b), characterized by the diffraction reflex at $2\theta = 13.8^{\circ}$.

A similar influence of crystallization time was observed in the case of 0.025 Al/Si samples (Figure 5.4). Additional intensive reflex at $2\theta = 33.7^o$ indicates the presence of a Na_2CO_3 phase [83], most probably occluded in the amorphous silica. The prolonging of crystallization time to 15 days leads to mordenite [84, 85,] as the dominating phase in the sample.
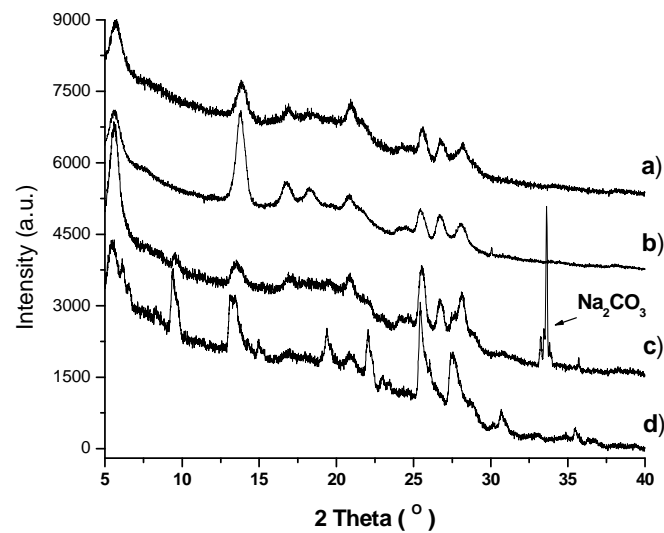
Figure 5.4: *XRD patterns of the Na-forms of the samples synthesized according to the procedure I2 with additional alkali and in the presence of ilerite seeds in the synthesis mixture: a) 0.0025 Sn/Si, b) 0.0025 Sn/Si- 15 d. synthesis, c) 0.0025 Al/Si, d) 0.0025 Al/Si- 15 d. synthesis.*

5.1.2. Magadiite

The XRD patterns of the magadiite samples coming from the magadiite syntheses are shown in Figures 5.5-5.9. Both synthesis ways (in or without the presence of CO_3^{2-} anions) lead to the magadiite structure characterized by $2\theta \sim 5.6^o$; 25.8^o; 26.9^o; 28.3^o [63] (Figure 5.5). Furthermore, no significant influence of carbonate anions, added to the

synthesis mixture, on crystallinity of the resulting samples has been found. Similar as in the case of ilerite syntheses, crystallinity of the magadiite material is decreasing with increasing tin content (Table 5.1). The above mentioned dependence can be particularly clearly seen in the example of the sample with the highest tin loading (0.071 Sn/Si – Figure 5.5), that was ~90% amorphous, with only traces of the magadiite phase. No significant influence of the applied synthesis procedure on crystallinity of the synthesized material was detected (Figure 5.5).
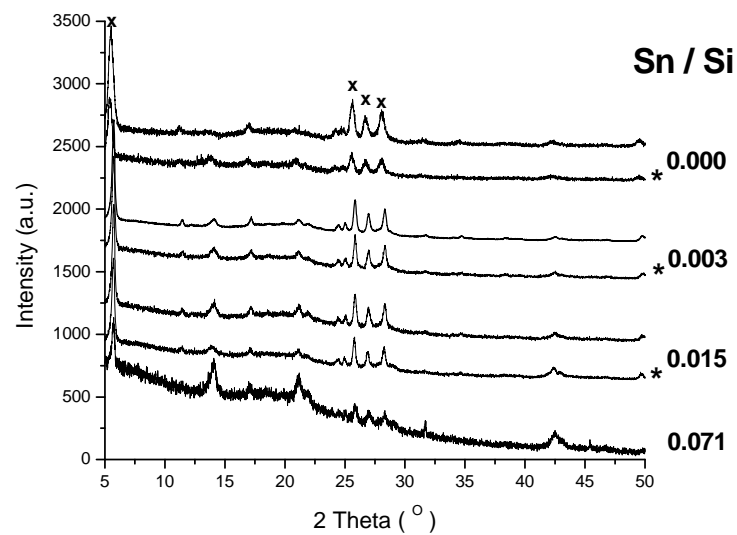
Figure 5.5: *XRD patterns of samples synthesized according to the procedure M1 with different tin loading. * -synthesis without Na_2CO_3 X- typical reflexes for the magadiite structure*
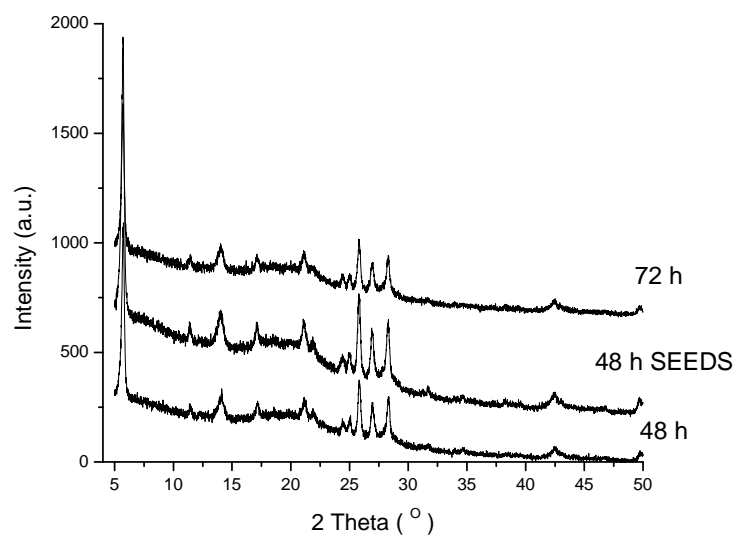
Figure 5.6: XRD profiles of 0.015 Sn / Si magadiite samples synthesized according to the procedure M1 in different time and in the presence of magadiite seeds.
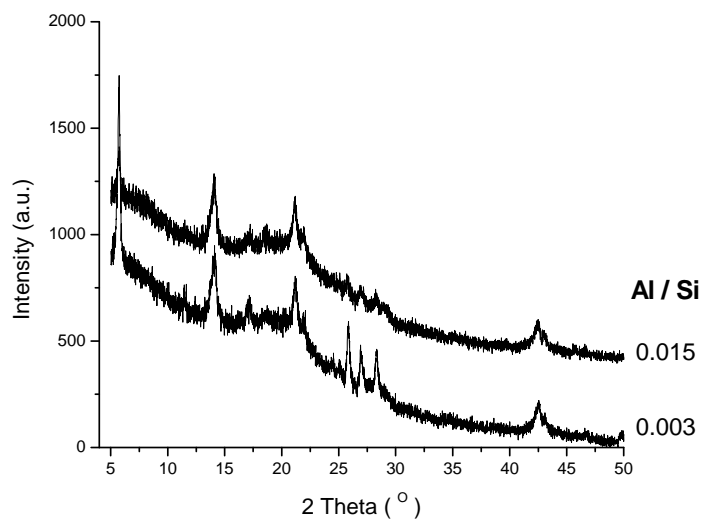
Figure 5.7: *XRD patterns of various Al-containing magadiite samples synthesized according to the procedure M1 in the presence of Na₂CO₃.*

Similar as in the case of ilerite syntheses, amount of incorporated aluminium is significant smaller than that of tin. Material with Al/Si ≥ 0.015 in the synthesis mixture is mostly amorphous (Figure 5.7). Therefore, also for the magadiite structure, there is a

negative influence of the charge of the heteroatom tetrahedra on crystallinity of the resulting magadiite samples.

Table 5.1: *Relative crystallinity of various Sn-magadiite synthesized according to the procedure M1 (calculated on the basis of the characteristic reflexes area).*

Sn / Si	Synthesis	Relative crystallinity (%)
0.000	standard	100
0.000	without Na_2CO_3	92
0.015	standard	72
0.015	without Na_2CO_3	74
0.015	3 days synthesis	71
0.015	synthesis in the presence of magadiite seeds	72
0.071	standard	11

Distance between the silica layers is indicated by the basal spacing reflex, which can be found for the magadiite structure at $2\theta = 5.6^{o}$. Similar position of this reflex for the different samples (Figure 5.8), leads to a conclusion that there are no tin-containing or any other pillars between the silica layers. Due to lower distance between the silica layers for the H-forms of un- and tin-modified samples, the above described reflex is noticeably shifted to $2\theta = 7.37^{o}$ (Figure 5.9). Moreover, there is no clear indication of the presence of other reflexes in low 2θ region; therefore, it can be concluded that there are no other cations then H^{+} between the silica layers and, as follows, ion exchange to H^{+} cations seems to be nearly complete.
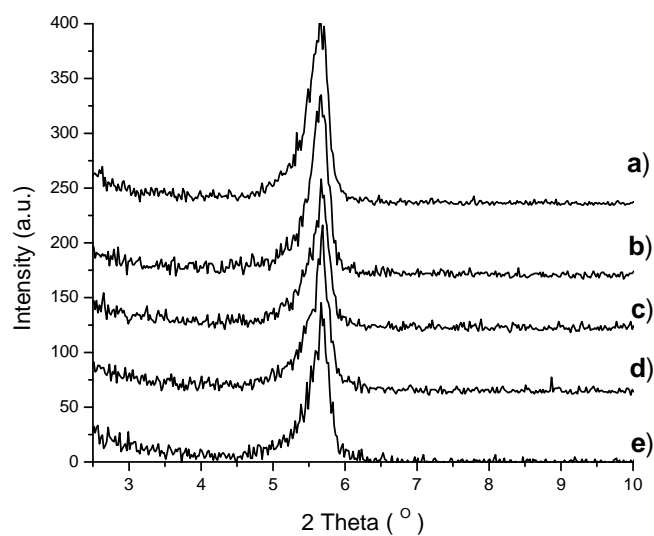
Figure 5.8: *Basal spacing reflexes of the Na-forms of various magadiite samples synthesized according to the procedure M1: a) 0.000 Sn/Si synthesized with Na_2CO_3, b) 0.015 Sn/Si synthesized without Na_2CO_3, c) 0.015 Sn/Si synthesized with Na_2CO_3, d) 0.015 Sn/Si synthesized with Na_2CO_3 in 72 h, e) 0.015 Sn/Si synthesized with Na_2CO_3 and with magadiite seeds.*
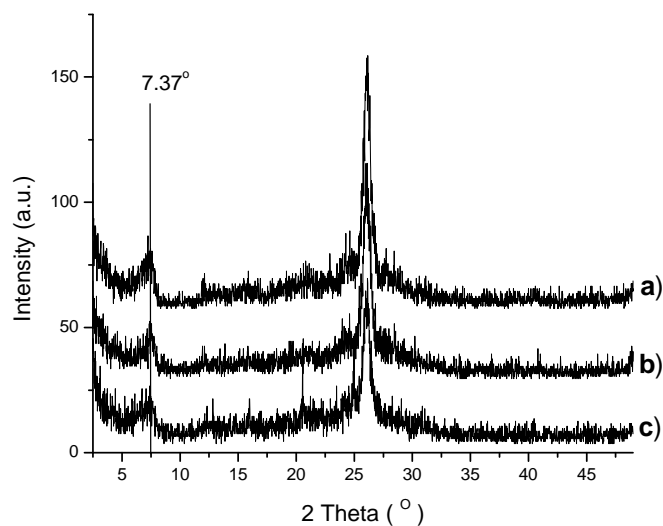
Figure 5.9: *XRD patterns of H-forms of various magadiite samples synthesized according to the procedure M1: a) 0.000 Sn/Si synthesized with Na_2CO_3, b) 0.015 Sn/Si synthesized without Na_2CO_3, c) 0.015 Sn/Si synthesized with Na_2CO_3.*

5.1.3. Kenyaite

XRD profiles of various kenyaite samples are shown in Figure 5.10-5.12. In all un- and tin-modified samples (Figure 5.10; 5.11), reflexes typically for the kenyaite structure have been found ($2\theta \sim 4.47^{\circ}$; 9°; 25.93°; 27.85° [39]). The Na-kenyaite sample synthesized in 96 h was less crystalline than that synthesized in 72 h (Table 5.2). Moreover, there are no shifts of reflex at $2\theta = 4.47^{\circ}$ for all Sn-modified samples (Figure 5.11). Therefore, like in the above paragraph, the presence of tin between the silica layers can be excluded.
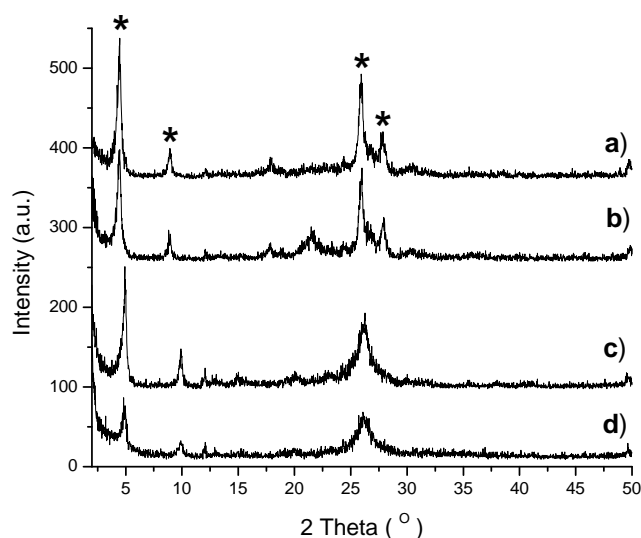
Figure 5.10: *XRD patterns of various kenyaite samples: a) Na-kenyaite 72h synthesis, b) Na-kenyaite 96h synthesis, c) H-kenyaite, d) SnO$_2$ / Na-kenyaite. * - typical reflexes for the kenyaite structure*

As can be seen in the example of H-kenyaite (Figure 5.10), reflex corresponding to the basal spacing in H-forms of the samples is shifted towards higher 2θ values (from 4.47° to 4.90°), which indicate decrease of the distance between the silica layers. Lack of presence of other reflexes in this 2θ region leads to similar conclusion likewise those for the magadiite samples, in which the distance between silica layers is unified. Therefore, on can assume that all Na^{+} cations were completely ion-exchanged to H^{+} (Figure 5.12).

Acquired data match closely to those reported in the literature [23, 39]. XRD profile of SnO$_2$ / kenyaite is very much alike that of H-kenyaite (Figure 5.10 c,d).
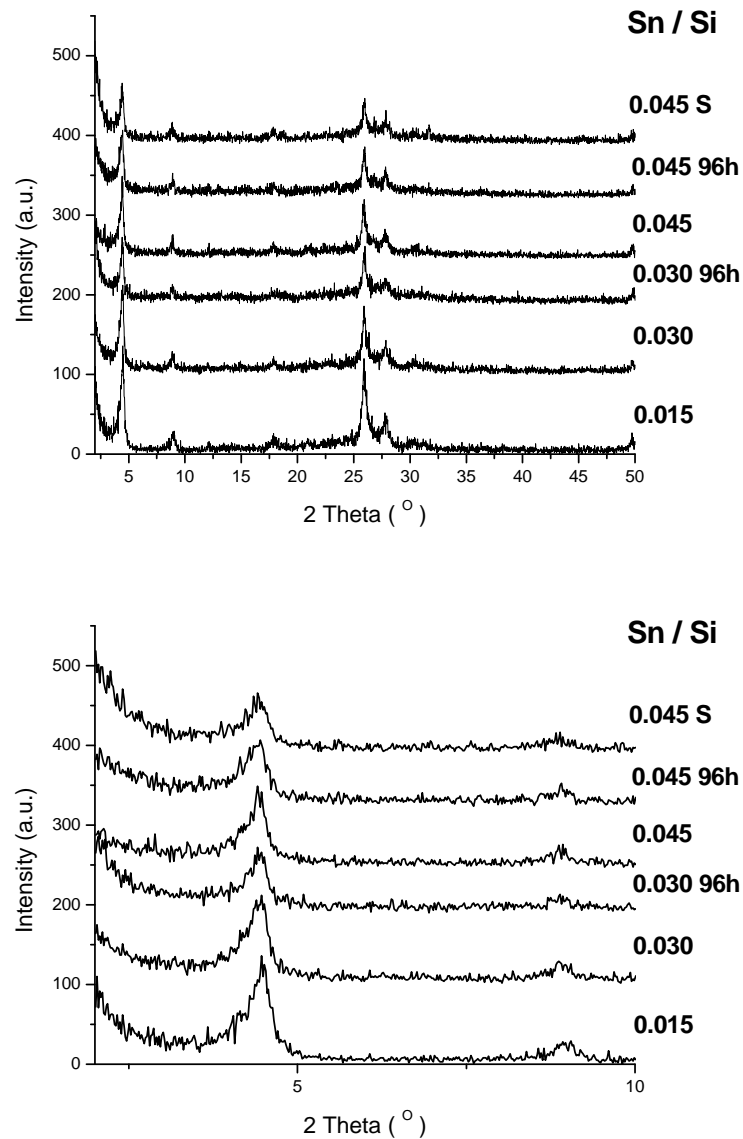
Figure 5.11: *XRD patterns of various Sn-kenyaite samples synthesized in 72h or 96h and their basal spacing reflexes. S - synthesis in the presence of kenyaite seeds*

Identical position of basal spacing reflex at $2\theta=4.90^{\circ}$ for the H-kenyaite and the SnO$_2$ / kenyaite sample indicates that there are both H-forms. It can be concluded, especially after considering the low pH value of used SnCl$_4$ *5H$_2$O solution, that besides

impregnation the ion-exchange process took place as well. Absence of other reflexes in low 2θ regions indicates that after impregnation there is no tin between the silica layers (Figure 5.10). Therefore, the above mentioned sample was decoded as SnO_2 / H-kenyaite.
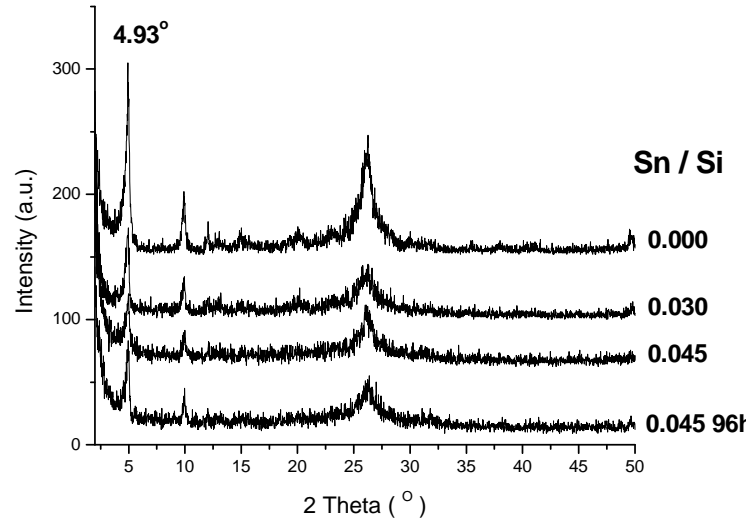
Figure 5.12: *XRD profiles of H-forms of various kenyaite samples synthesized according to the procedure K1.*

Table 5.2: *Relative crystallinity of various kenyaite samples (calculated on the basis of the characteristic reflexes area).*

Sn / Si	Synthesis	Relative crystallinity (%)
0.000	standard	100
0.000	4 days	92
0.015	standard	89
0.030	standard	72
0.030	4 days	51
0.045	standard	63
0.045	4 days	51
0.045	synthesis in the presence of kenyaite seeds	49

Similar like for ilerite and magadiite, crystallinity of the tin-substituted samples is decreasing with increasing tin content (Figure 5.11 and Table 5.2). Prolonging the time of the crystallization does not have any significant influence on crystallinity of the resulting

Sn-kenyaite samples. The samples synthesized in the presence of kenyaite seeds were slightly less crystalline than those synthesized without them.

5.1.4. Summary

Incorporation of a heteroatom into the silica layers will always lead to tensions or defects caused by the differences in crystallographic radii. Theoretically, substitution of a silicon atom should cause fewer tensions in material with only one silica sheet, e.g. ilerite; thus, higher stability of such modified ilerite can be expected. However, ilerite synthesis in the presence of the heteroatom source is leading to formation of the magadiite phase, moreover with a low tin content. The presence of the magadiite phase as the dominating one, even after syntheses with ilerite seeds, and much higher Sn/Si ratios in tin-containing the magadiite and the kenyaite samples indicates that additional, stabilizing silica layer/s has significant influence on the stability of modified structure.

5.2. Scanning Electron Microscopy

The crystals shape and size were studied by scanning electron microscope (SEM). The discussed structures exhibit two characteristic crystals shapes – regular plate-shaped crystals and rosettes-shaped crystals for the ilerite and the magadiite/kenyaite phases, respectively.

5.2.1. Ilerite

SEM pictures (Figure 5.13 - 5.16) made for the samples synthesized according to the procedure I1 and I2 indicate that only the unmodified ilerite samples (Figure 5.13) consisted of regular plate-shaped crystals (see also paragraph 5.1), whereas all the

modified samples consisted of relatively large agglomerates of irregular plate-shape crystals that are not typical for the ilerite nor the magadiite phases (Figure 5.14). Only small amounts of rosettes-shaped crystals, confirming existence of the magadiite phase, were detected. After considering the XRD data, one can assume that in the synthesized samples the magadiite crystals exist as a massive structure, which can be found also in nature [11]. Neither the way of synthesis, nor the heteroatom loading affects significantly the crystals shape (Figure 5.14).
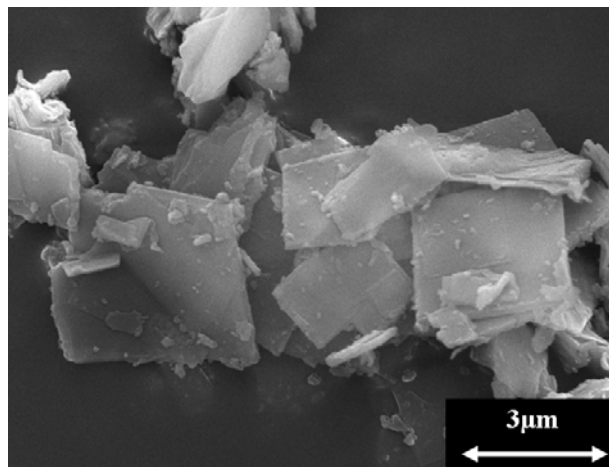
Figure 5.13: SEM picture of non modified Na- ilerite (procedure I2).
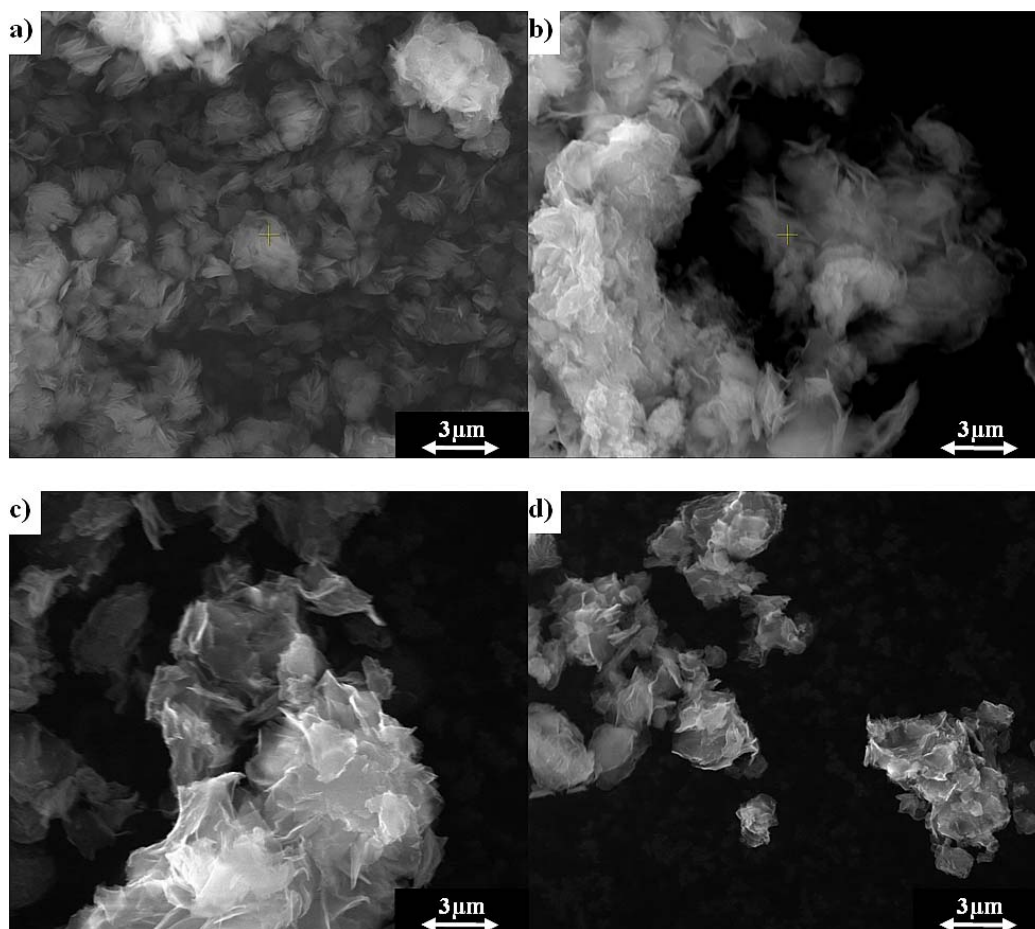
Figure 5.14: SEM pictures of various Na forms of Sn-containing samples (procedure I2 with additional alkali): a) 0.0005 Sn/Si, b) 0.00075 Sn/Si, c) 0.00125 Sn/Si, d) 0.00125 Sn/Si -synthesis in the presence of ilerite seeds.

5.2.2. Magadiite

All the magadiite samples consisted of agglomerates of rosette-shaped crystals (Figure 5.15) with amorphous material present on their surface, what correlates very well with the XRD results (paragraph 5.1). The samples synthesized without Na_2CO_3 have slightly different topography (more flat crystals – Figure 5.15 b) than those synthesized with sodium carbonate. Crystals of the modified samples synthesized without Na_2CO_3 are slightly larger (Figure 5.15 c,d). With increasing tin content, as well as for the samples

synthesized in the presence of magadiite seeds, a decrease in crystal size was observed (Figure 5.15 e). Furthermore, the presence of other crystallographic phases could be excluded because only crystals with topography of magadiite were detected.

5.2.3. Kenyaite

Rosette-like crystals were detected in the case of all non- and modified kenyaite samples (Figure 5.16). Crystal size of the studied material, similar as in the case of the magadiite samples (Figure 5.15), is decreasing with increasing tin content as well as for samples synthesized in the presence of kenyaite seeds. Amount of an amorphous material present on the surface of the crystals is increasing with increasing tin content, which stays in good agreement with the XRD results (see paragraph 5.1). There is no influence of used synthesis procedure on the topology of the crystals. Furthermore, sample contains only crystals with the same topography; therefore, presence of other crystallographic phases could be excluded.
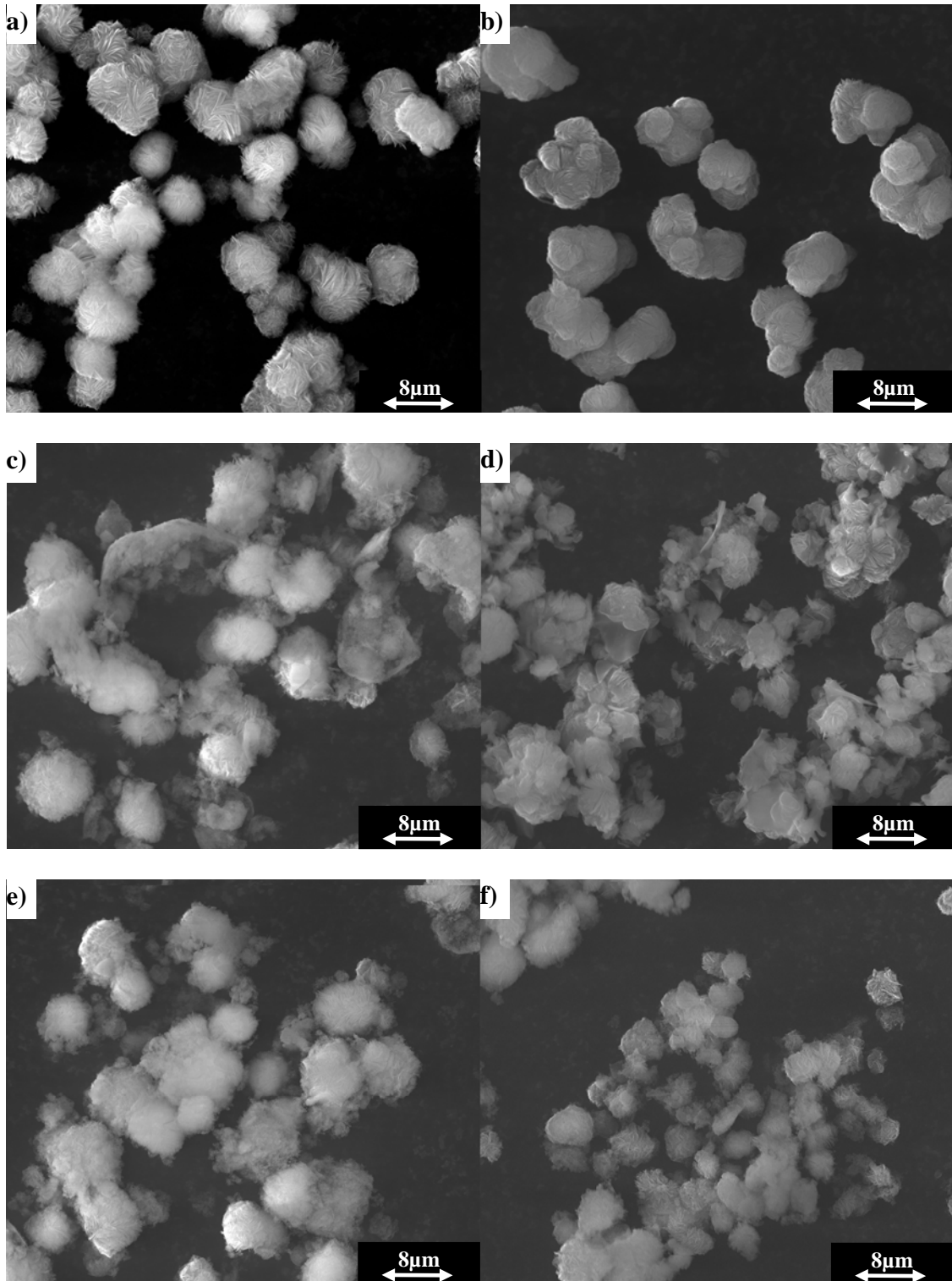
Figure 5.15: SEM pictures of various samples synthesized according to the procedure M1: a) 0.000 Sn/Si – synthesis with Na_2CO_3, b) 0.000 Sn/Si – synthesis without Na_2CO_3, c) 0.015 Sn/Si – synthesis with Na_2CO_3, d) 0.015 Sn/Si – synthesis without Na_2CO_3, e) 0.007 Sn/Si – synthesis with Na_2CO_3, f) 0.015 Sn/Si – synthesis with Na_2CO_3 and magadiite seeds.
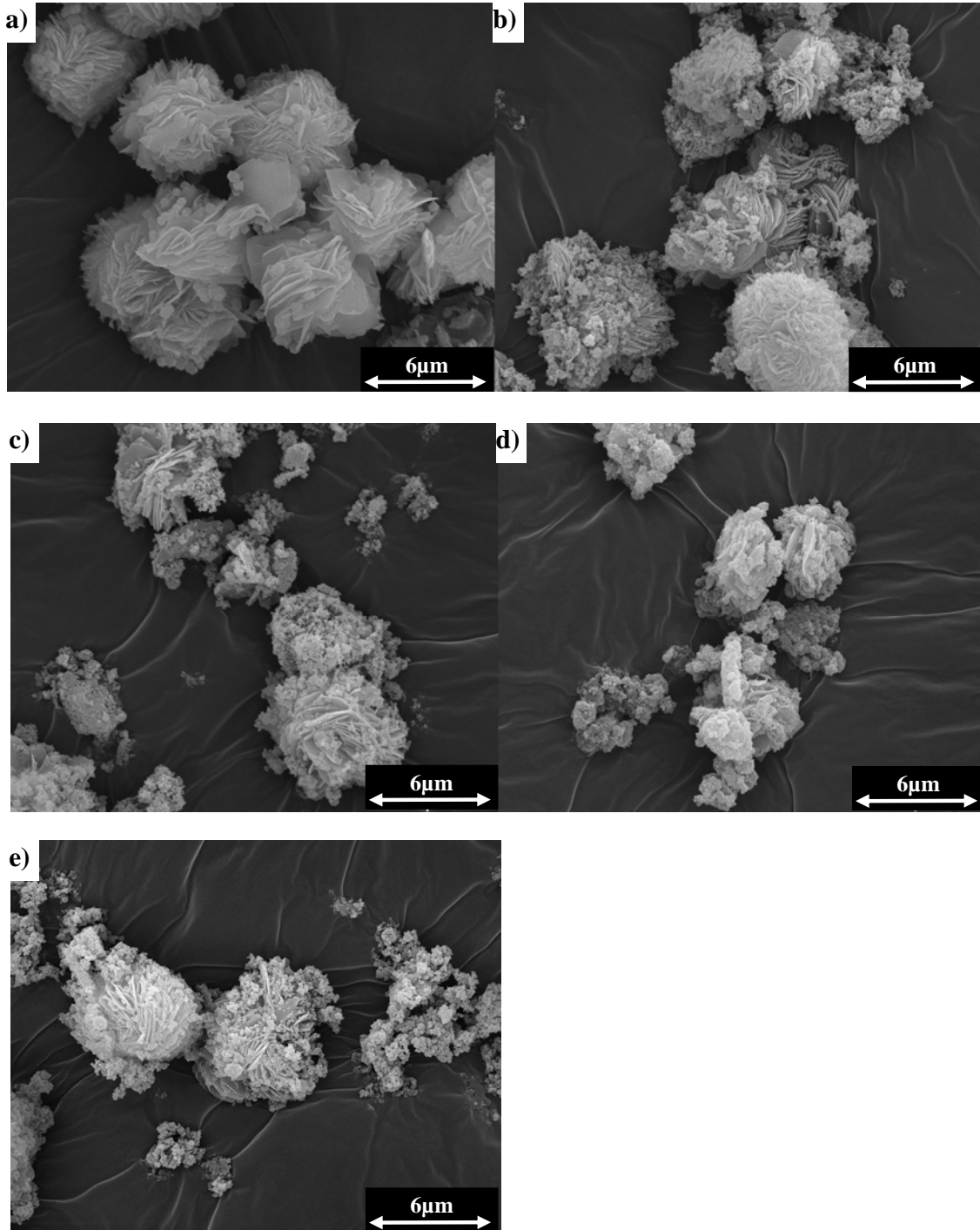
Figure 5.16: SEM pictures of various samples synthesized according to the procedure K1: a) 0.000 Sn/Si, b) 0.015 Sn/Si, c) 0.045 Sn/Si, d) 0.030 Sn/Si – 96 h synthesis, e) 0.045 Sn/Si – synthesis in the presence of kenyaite seeds.

5.3. Nitrogen adsorption

5.3.1. Ilerite

The isotherm of adsorption recorded for all samples synthesized according to the procedure I1 or I2 belong to the type III of IUPAC nomenclature (Figure 5.17). Isotherm shape indicates that there is no micropores adsorption. On the other hand, the adsorption/desorption hysteresis indicates on the presence of mesopores and macropores. As all the discussed layered structures do not exhibit such large basal spacing [4, 22], a condensation of nitrogen should take place on the external surface of the crystals (see also paragraph 5.2). The recorded isotherms are similar to those reported in the literature [4, 86]. The isotherms of other samples are very similar (data not shown).
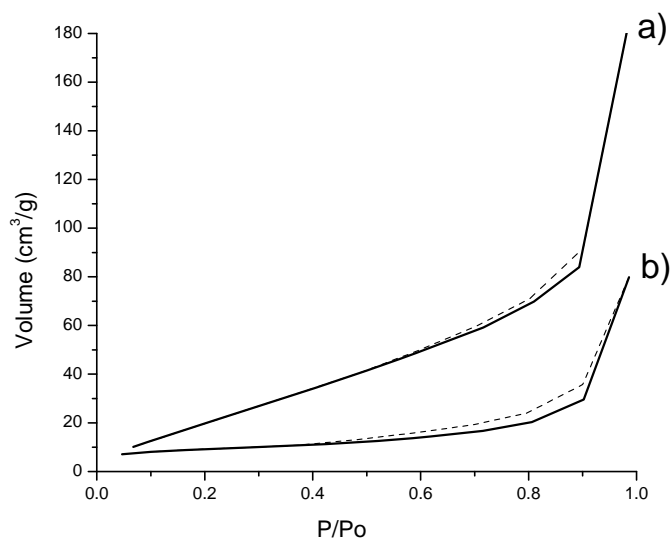
Figure 5.17: *Isotherm of the nitrogen adsorption of a) Na-ilerite – procedure I2 and b) 0.00125 Sn /Si sample - procedure I2.*

The surface areas of the synthesized samples are presented in Table 5.3. There is no significant change of the measured values with increasing tin content in the samples as

the Sn/Si exchange ratio is very low (up to 0.112 wt.%). Only in the case of the sample with the highest tin loading significant decrease of its surface area is observed (Table 5.3). This particular value is similar to that of ilerite impregnated with SnO_2. Thus, the presence of bulky tin oxide as well as amorphous material on the surface of the material (0.0025 Sn/Si) can be concluded. Measured surface areas are higher than those reported in the literature [4, 86, 87], probably due to higher temperature of the sample pretreatment used in the hereby described study.

Table 5.3: *Texture data for various ilerite samples synthesized according to the procedure I2 with additional alkali.*

Sn / Si	Surface area (m^2/g)
0 Sn / 4 Si	100
0.005 Sn / 4 Si	103
0.005 Sn / 4 Si S	107
0.010 Sn/ 4 Si S	32
SnO_2 impregnated on ilerite	30

S –synthesis in the presence of ilerite seeds.

5.3.2 Magadiite

Despite the significantly higher silicon exchange ratio in comparison to the ilerite syntheses, the surface area of the magadiite samples is also not changing meaningly with increasing tin content (Table 5.4). Also for the magadiite samples, the isotherm of adsorption clearly confirms lack of micropores and the presence of the meso- and macropores (Figure 5.18). As the synthesized magadiite does not exhibit such large pores, the mentioned ones can be present between the crystals in the agglomerates (which are confirmed by the SEM pictures – see paragraph 5.2). Thus, lack of significant changes of the samples surface areas as well as no indication of presence of micropores, similar as in the case of samples described in paragraph 5.3.1, can suggest absence of the

interlayer pillars (particularly those build by tin oxide species). The isotherms of other magadiite samples are very similar (data not shown). Acquired data correlates well with those reported in the literature [4, 29, 47]. However, some authors reporting smaller surface areas [86, 88]. Differences could be explained similar as in the case of the ilerite samples.
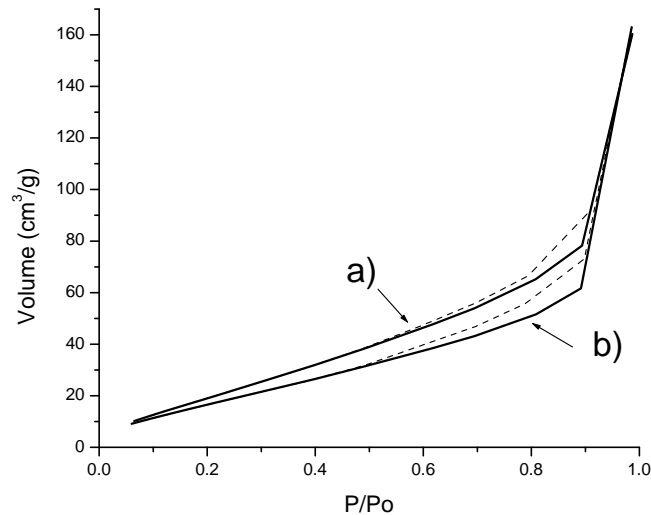
Figure 5.18: *Adsorption isotherms of a) 0.007 Sn/Si magadiite synthesized in the presence of Na$_2$CO$_3$ and b) Na-magadiite synthesized in the presence of Na$_2$CO$_3$.*

Table 5.4: *Texture data for various magadiite samples synthesized with Na$_2$CO$_3$.*

Sn / Si	Surface area (m^2/g)
0.000 Sn / Si	97
0.007 Sn / Si	88
0.015 Sn / Si	79
0.015 Sn / Si *	80
0.015 Sn / Si S	83
SnO$_2$ / Na-magadiite	75

* - 72 h synthesis   S – synthesis in the presence of magadiite seeds

5.3.3. Kenyaite

The surface areas of examined kenyaite samples are similar to the previously described material. (Table 5.5). Also in this case the isotherm of adsorption (type III according to IUPAC classification) clearly indicates on the presence of meso- and macropores located between the crystals in the crystals agglomerates (Figure 5.19). The measured values are in good agreement with the XRD results (paragraph 5.1), as presence of the pillars between the silica layers would lead to generation of the micro and mesopores bigger than 20 Å; therefore, the higher surface areas. Recorded data are similar to those reported in the literature [80]. The isotherms of all samples are very similar (data not shown).
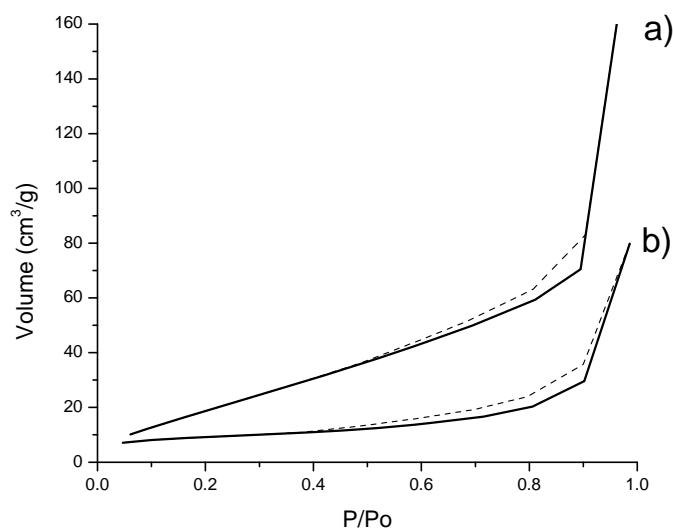
Figure 5.19: *Adsorption isotherms of a) Na-kenyaite and b) 0.015 Sn/Si kenyaite synthesized in 72h.*

Recorded data clearly indicates on absence (or small amount - in the case of the samples made from the ilerite synthesis mixture) of tin between the silica layers.

Table 5.5: *Texture data for various kenyaite samples.*

Sn / Si	Surface area (m^2/g)
0.000 Sn / Si	86
0.030 Sn / Si	89
0.045 Sn / Si	63
0.045 Sn / Si*	55
0.045 Sn / Si S	50
SnO_2 / H-kenyaite	81

* - 4 days synthesis   S – synthesis in the
presence of kenyaite seeds

5.4. Thermal analysis

5.4.1. Sodium forms

The DTA/TG patterns for the Na-forms of the samples are similar (Figure 5.20 and 5.21) despite the different structures and correspond well to those described in the literature [6, 31]. For all the samples two endothermic maxima in temperature between 360 K and 450 K (Figure 5.20 and 5.21) were detected. The first one could be attributed to desorption of the physisorbed water from the surface of the crystals and from the interlayer space. The second one could be attributed to the destruction of the hydration shell of the sodium cations. The slow decrease of weight at temperatures above 500 K (showed on the example of the Na-ilerite sample – Figure 5.20) indicates dehydroxylation of the layered structure [22, 29]. The first thermal effects of the recrystallization of the structure were recorded around 750 K; therefore, the temperature of a pretreatment for all the samples did not exceed this temperature.
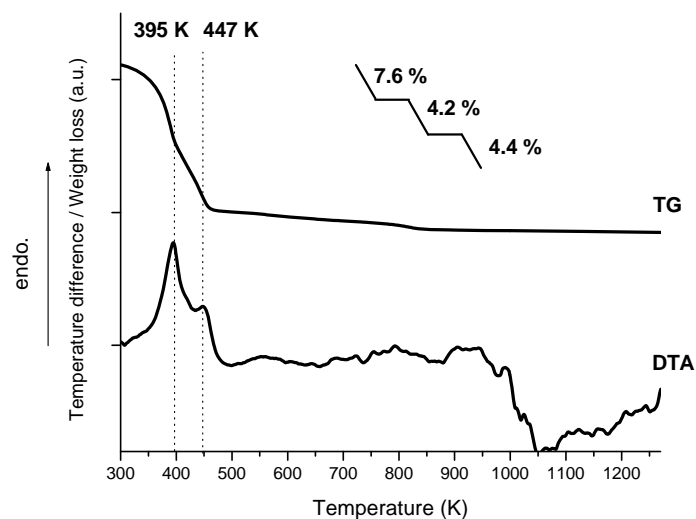
Figure 5.20: *DTA/TG profile of non-modified Na-ilerite. In upper right hand part of the graph the percentage of mass loss is given.*

The amount of desorbed water is not changing meaningly with increasing heteroatom loading most probably due to the absence of tin as free cation between the layers (see also paragraph 5.1 and 5.3). Furthermore, despite the different synthesis procedures and types of the structures, all the shifts of the DTA/TG profiles are in the area of accuracy of the measurement equipment, thus it can be concluded that the incorporation of tin does not change the thermal properties of the resulted materials, which are very much alike those of the unmodified samples (Figure 5.21).

5.4.2. Hydrogen forms

Dissimilar to the sodium forms, only one desorption peak was detected (T=320 K) in the DTA profiles of the H-forms (Figure 5.21 d,e), what can be ascribed to lower basal spacing of such materials [47]. Since the substitution of Na^+ by H^+ was nearly complete (see paragraph 5.1.2 and 5.1.3) the absence of the desorption peaks at 400-450 K (Figure

64

5.21) in the profile of the H-form, allows to assign it to desorption of water from the hydrate shells of the sodium ions
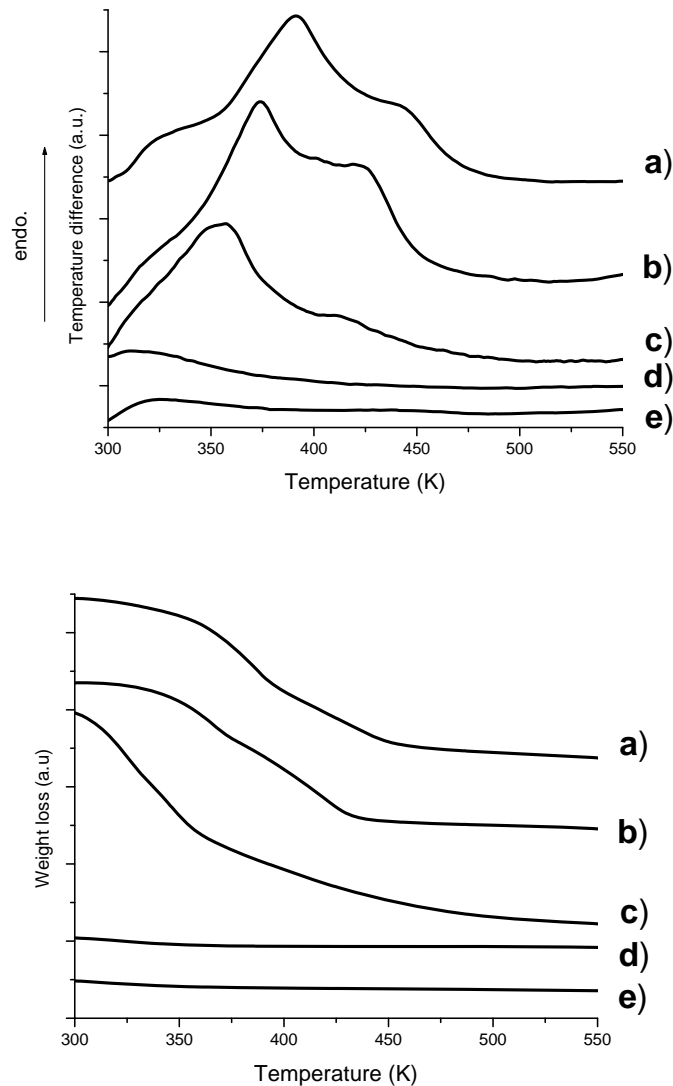
Figure 5.21: The *DTA and TG profiles of various tin-containing samples: a) 0.00125 Sn/Si Na-magadiite synthesized according to the procedure I2, b) 0.007 Sn/Si Na-magadiite synthesized according to procedure the M1, c) 0.03 Sn/Si Na-kenyaite synthesized according to procedure K1, d) 0.00125 Sn/Si H-magadiite synthesized according to procedure I2, e) 0.007 Sn/Si H-magadiite synthesized according to procedure M1.*

The DTA/TG patterns for all H-forms of the samples are similar, which seems to confirm the conclusion that the presence of tin is not affecting the thermal properties of the examined materials.

5.5. Elemental analysis

5.5.1. Ilerite

Presence of tin in the samples was confirmed by an ICP-AES elemental analysis (Table 5.6). Obtained values are closely related to the amount of tin in the synthesis mixture. The largest amount of tin was detected for the sample synthesized in the presence of ilerite seeds. The amount of sodium is not changing meaningly with increasing tin content; however, it is higher for sample synthesized in the presence of ilerite seeds. The above mentioned exception can be explained by the presence of higher amount of an amorphous material and/or by sodium-containing bulky tin compounds in discussed sample. Sn/Si ratios for samples synthesized according to the procedure I2 are significantly smaller than that detected for the magadiite and the kenyaite samples.

Table 5.6: Comparison of *Sn/Si(in ilerite synthesis mixtures - procedure I2), Na/Si, and Sn/Si ratios in the bulk solid, determined by ICP AES.*

Sn/Si in synthesis mixture	Sn/Si in sample	Na/Si in sample
0.00050	0.00027	0.12533
0.00075	0.00064	0.13043
0.00125	0.00090	0.13433
0.00125 S	0.00112 S	0.17385 S

S –synthesis in the presence of ilerite seeds.

5.5.2. Magadiite

In contrast to the samples synthesized from the ilerite synthesis mixture, no influence of the synthesis way modifications (use of magadiite seeds, change of synthesis time etc.) on Sn/Si ratio in the magadiite samples were detected (Table 5.7). For all the samples, the measured Sn/Si ratio is meaningly higher than in the synthesis mixture. This can be explained in term of the assumption that not the whole amount of silicon was involved in building the layered structure during the synthesis. Amount of sodium is changing with increasing tin content, most probably due to changing amount of amorphous material within the mentioned samples (see also paragraph 5.1).

In comparison to the ilerite samples, the maximum Sn/Si ratio for the magadiite structure is increasing along with the increase of the number of the silica layers; therefore, a significant influence of the number of the silica layers on the stability of the modified material can be concluded (see also paragraph 5.1).

Table 5.7: *Sn/Si ratio in magadiite synthesis mixtures (procedure M1), tin and sodium content in the bulk solid, determined by ICP AES*

Sn/Si in synthesis mixture	Synthesis	Sn/Si in sample	Na/Si in sample
0.007	standard	0.0093	0.091
0.015	standard	0.0198	0.128
0.015	without Na_2CO_3	0.0183	0.132
0.015	3 days synthesis	0.0189	0.119
0.015	synthesis in the presence of magadiite seeds	0.0191	0.091

5.5.3. Kenyaite

Similar as in the case of the above mentioned magadiite materials, Sn/Si ratio in the synthesized kenyaite samples was increasing with increasing Sn/Si ratio in the synthesis mixture (Table 5.8). Furthermore, Sn/Si ratios for the synthesized samples are noticeably higher than in the synthesis mixture, which can be explained (similar as in the case of magadiite samples) in term of the assumption that not the whole amount of silicon was used during the synthesis to build the layered structure. There is no significant influence of the applied synthesis procedure on the amount of Sn in the resulting material. Amount of sodium is increasing with increasing tin content, most probably due to higher amount of amorphous material within the samples characterized by higher tin content (see also paragraph 5.1).

The amount of detected tin is significantly higher then that detected in the magadiite or the ilerite samples, which leads to similar conclusion concerning the influence of the number of the silica layers on stability of the resulting material.

Table 5.8: *Sn/Si ratio in kenyaite synthesis mixtures (procedure K1), tin and sodium content in the bulk solid, determined by ICP AES.*

Sn/Si in synthesis mixture	Synthesis	Sn/Si in sample	Na/Si in sample
0.030	72 h synthesis	0.039	0.109
0.045	72 h synthesis	0.067	0.132
0.045	96 h synthesis	0.060	0.123
0.045	synthesis in the presence of kenyaite seeds	0.063	0.134

5.6. Infrared spectroscopy

All recorded spectra exhibit typical bands corresponding to various Si-O-Si vibrations. The above mentioned spectra are somewhat similar to those recorded for silicalite-1 and in fact, usually interpreted through an analogy with them [89, 90]. Therefore, the transmittance band can be assigned as follows: 1250–980 cm^{-1} – to asymmetric stretching of Si-O-Si, 820-780 cm^{-1} to symmetric stretching of Si-O-Si, 600 cm^{-1} to bending vibrations of Si-O-Si [88]. Two additionally bands at 977 cm^{-1} and 920 cm^{-1} were recorded for some H-forms of studied layered silicates. They can be assigned to the presence of OH groups [88, 89].

5.6.1. Ilerite

Recorded spectra of Na-ilerite are similar to those described in the literature [6, 36]. Dissimilar to the spectra of Na-ilerite and samples with Sn/Si ratio lower than 0.00125, material synthesized in the presence of ilerite seeds with Sn/Si = 0.00125 (Figure 5.22 d), exhibits an additional band at 970 cm^{-1}. This band can contribute to Me-O-Si stretching band [6, 36, 91]. It can suggest presence of the heteroatoms in the silica layer or the pillars of tin-containing compounds bound to it. However, such a band is not unique because it can also be ascribed to Si-O-H bonding vibrations [92], which are confirmed by the presence of a band at 977 cm^{-1} in the H-ilerite (Figure 5.22). All H-forms of the tin- or the aluminium-substituted samples shows similar band. Thus, the assignation to T-OH vibration seems to be more likely. Additionally, in the non-modified H-ilerite and in the Al-containing H-ilerite, a band at 920 cm^{-1} was detected, which also can contribute to T-OH vibrations.
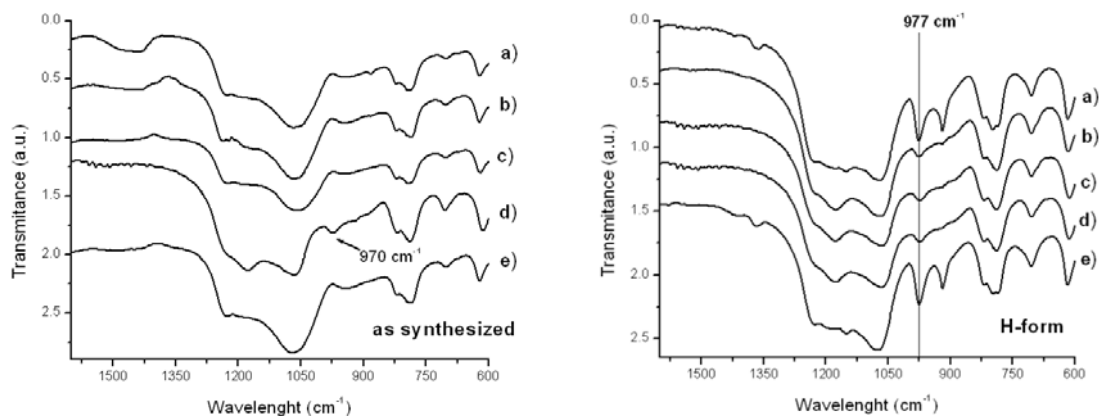
Fig. 5.22: *IR spectra of various Sn- or Al- containing samples synthesized according to the procedure I2: a) non-modified ilerite, b) 0.00075 Sn/Si, c) 0.00125 Sn/Si, d) 0.00125 Sn/Si – synthesis with ilerite seeds, e) 0.00125 Al/Si – 15 days synthesis.*

5.6.2. Magadiite

Recorded spectra of Na-magadiite are similar to those described in the literature [6, 36] and are very much alike those recorded for the ilerite structure. Similar as in the case of samples synthesized from the ilerite synthesis mixture, one can expect the presence of an additional band around 970 cm^{-1} [6, 36] assigned to T-O-Si vibrations. None such separate band was detected (Figure 5.23); however, all the heteroatom-containing magadiite samples exhibit a broadening of the band coming from the asymmetric vibrations of Si-O-Si from 970cm^{-1} to 1100cm^{-1} (Figure 5.23 right), which can indicate the presence of Me-O-Si bond in the layer as well as s bond between an interlayer metallic oxide and the silica layer [93]. Presence of pillars between the silica layers of magadiite samples was excluded (see paragraph 5.1 and 5.3); therefore, one could conclude that the above mentioned band broadening suggest on the presence of incorporated tin. However, such a conclusion appears to be speculative because DRIFT technique is relatively difficult to quantify. There is no clear correlation between the amount of tin in the modified material and the position and the breadth of described band. On the other hand, separate band around ~970 cm^{-1} recorded for sample synthesized

according to the procedure I2 could reflect the presence of interlayer pillars, especially after considering the low crystallinity of the above mentioned material (see paragraph 5.1). However, also in this case such a conclusion is not undisputed because it can also be ascribed to Si-O-H bending vibrations.
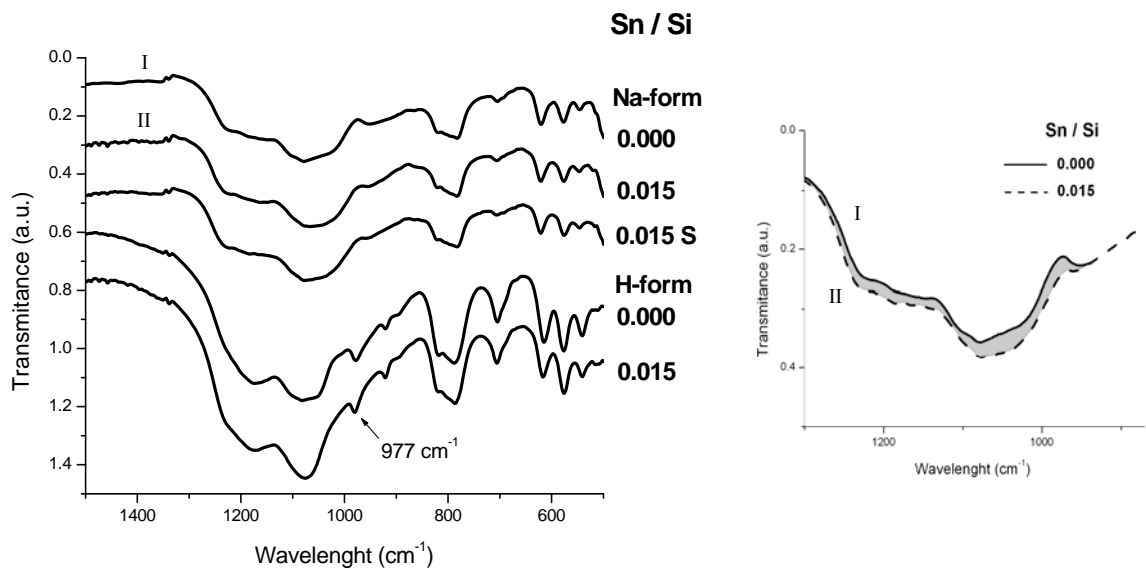
Figure 5.23: *IR spectra of various sodium and hydrogen forms of Sn-containing magadiite samples synthesized according to the procedure M1 with Na$_2$CO$_3$. On the right hand – the difference between the* asymmetric vibrations of Si-O-Si on example of Na-magadiite (I) and 0.015 Sn/Si magadiite (II). *S – synthesis with magadiite seeds.*

5.6.3. Kenyaite

IR spectra of kenyaite samples are similar to those described above (Figure 24-25). Various authors [23, 80] are reporting similar dependence between the presence of a heteroatom in the silica layers and the occurrence of the additional band around ~970 cm^{-1}. Similar as in the case of the magadiite samples no separate band but a broadening between 970-1100 cm^{-1} was recorded. Although the broadening is smaller for samples, which were containing lower amounts of tin (Figure 5.24 d,e), also in this case, the above mentioned correlation can not be treated as direct indication of successful incorporation

of tin into the silica layers (see paragraph 5.6.2).

An additional band at 962 cm^{-1} was detected in spectra of H-forms of all the kenyaite samples (Figure 5.25). Similar as in the case of the ilerite and the magadiite samples it is most probably reflecting the presence of -OH groups. Such a band was also detected in the case of the SnO$_2$ / H-kenyaite sample, which seems to proof that the resulting material is indeed a H-form of kenyaite (see also paragraph 5.1) (Figure 5.25 c).
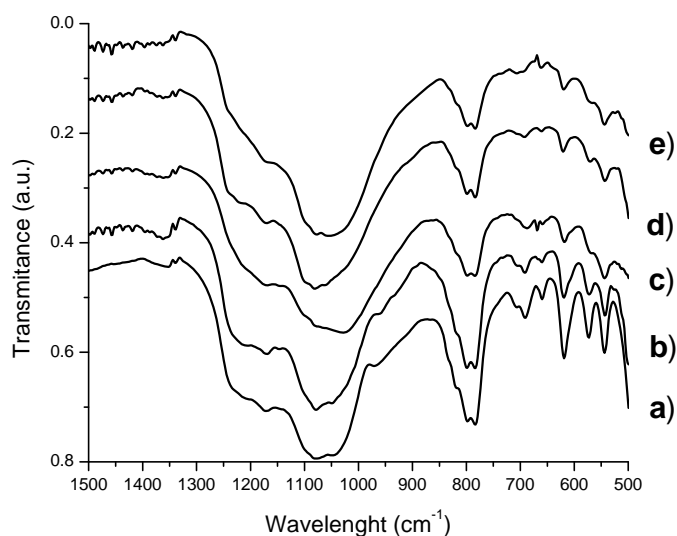
Figure 5.24: *IR spectra of the various Na-forms of the kenyaite samples: a) 0.000 Sn/Si 72h synthesis, b) 0.015 Sn/Si 72h synthesis, c) 0.045 Si/Sn 72h synthesis, d) 0.045 Sn/Si 96h synthesis, e) 0.045 Si/Sn 72h synthesis in the presence of kenyaite seeds.*
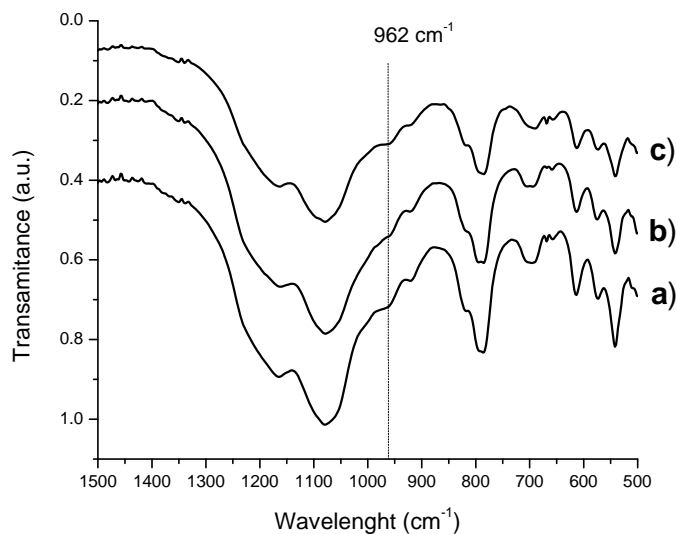
Figure 5.25: *IR spectra of various H-forms of kenyaite samples: a) 0.000 Sn/Si 72h synthesis, b) 0.015 Sn/Si 72h synthesis, c) SnO$_2$ / H-kenyaite.*

5.7. ^{29}Si *magic*-angle spinning nuclear magnetic resonance

Selected magadiite samples were studied by means of ^{29}Si MAS NMR to assess the chemical environment around the Si atoms in the layer. The ^{29}Si MAS NMR spectra of the Na-magadiite sample show three signals at -89; -101 and -104 ppm (Figure 5.26 a). The above mentioned signals can be assigned to Si(OSi)$_3$ silicate species (Q$_3$ signal) and to Si(OSi)$_4$ silicate species (Q$_4$ signal), respectively [47]. Split of the Q$_4$ signal can be explained by difference in average Si-O-Si bond angles [20]. It has been also confirmed by calculations conducted by Smith and Blackwell [94].

As can be seen in the example of the 0.015 Sn/Si magadiite sample synthesized in the presence of carbonate anions (Figure 5.26 b) Q$_3$ signal is much more intense, most probably due to higher amount of amorphous material present in the sample. Additionally, a split of the above mentioned signal was detected. It can be assumed that the split is caused by -OSn linked to Si atoms.
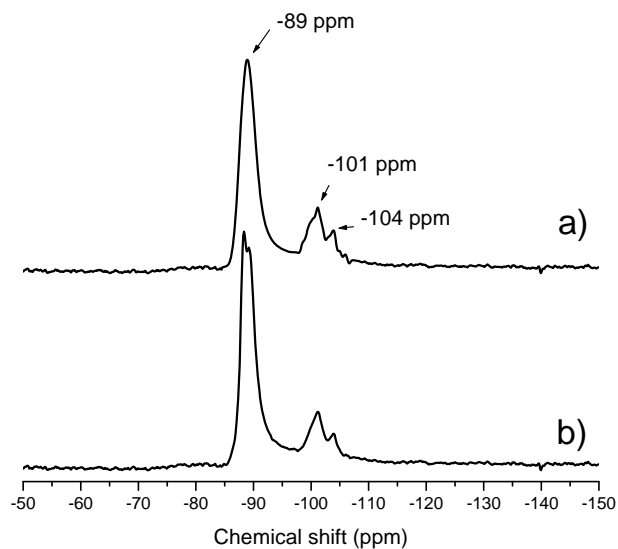
Figure 5.26: ^{29}*Si MAS NMR spectra of a) Na-magadiite and b) 0.015 Sn magadiite synthesized in the presence of Na$_2$CO$_3$.*

5.8. Hydrogen temperature-programmed reduction

To assign various reduction peaks, which could be expected in H$_2$-TPR profiles of tin-modified samples, to different reduction processes additional samples were studied - bulky SnO$_2$ and SnO$_2$ supported on ilerite, magadiite and kenyaite (see also paragraph 4.1).

At the applied conditions, bulky SnO$_2$ (Figure 5.27) is reduced to tin at ~890 K in a one step reduction [95, 96, 97, 98, 99]. On the other hand, reduction of SnO$_2$ supported on various materials, e.g. SiO$_2$, TiO$_2$, MCM-41, Al$_2$O$_3$, zeolites, occurs in a two-step reduction – from Sn^{4+} to Sn^{2+} and from Sn^{2+} to metallic tin [95, 97, 98, 99]. As has been confirmed by Lazar et al. [97], there is a significant influence of the nature of support on the temperature and the reduction steps of SnO$_2$. The above mentioned influence was studied separately for each type of the layer structure.

The amount of the consumed H$_2$ was calculated and found to be corresponding to reduction of approximately 23% of tin in all tin-modified layer materials.

For each recorded data, a deconvolution of reduction profile has been conducted (showed on example of SnO_2 / H-kenyaite sample – Figure 5.31).

.

5.8.1. Ilerite

To study the influence of the support on the reduction of SnO_2, Na-ilerite impregnated with tin oxide was examined. In comparison to Na-lerite (Figure 5.27), two additional peaks were detected at ~675 K and ~820 K. The amount of consumed H_2 was equal for both peaks. This seems to confirm the two-step reduction mechanism of supported SnO_2.
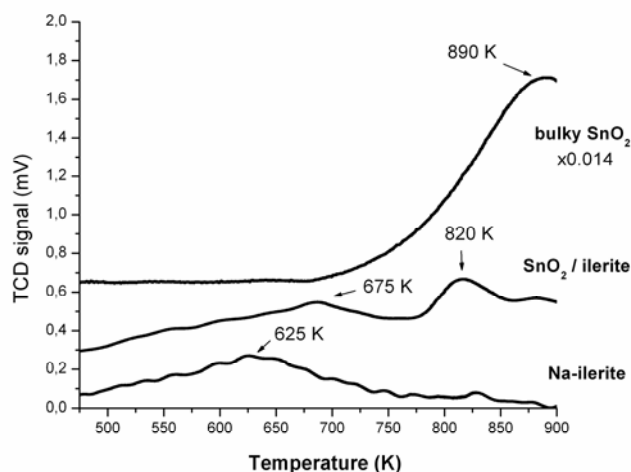
Figure 5.27: *H_2-TPR profiles of various samples synthesized according to procedure I2.*

Note, that due to the low amount of reducible species the profiles are close to the detectable signal to noise ratio. Therefore, the baseline is strongly influenced by a background noise and baking of the bed represented by the peak at ~625 K (Figure 5.27, Na-ilerite). Described effect does not occur for quartz samples.
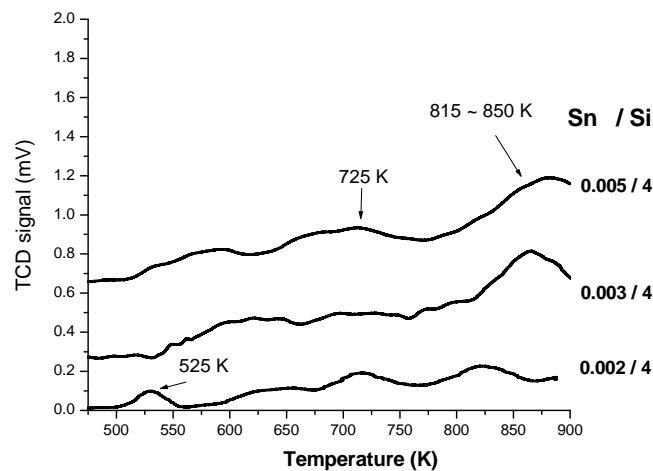
Figure 5.28: *H$_2$-TPR profiles of various Sn-containing samples synthesized according to the procedure I2.*

Tin-containing samples exhibit a peak at ~525 K (Figure 5.28) that can be attributed to the reduction of small tin oxide particles, which are well dispersed on the surface of the crystals. Small additional peaks (Figure 5.28) at ~725 K and 815 ~ 850 K were recorded as well. Due to interactions between tin and silica tetrahedra, higher temperature of tin reduction for tin incorporated into the silica layer can be assumed. Therefore, the above mentioned peaks can be assigned to the reduction of the tin in the silica layers. Since the influence of changed hydrodynamic conditions, which is coming from baking of the bed, could not be separated, a quantitative analysis was impossible.

5.8.2. Magadiite

Similar as in the case of the ilerite material, tin oxide supported on the Na-magadiite samples is reduced in two-step process – from +4 to +2 ~ 630 K and from +2 to 0 ~ 900 K (Figure 5.29). Acquired data fit well to those found in the literature [95, 97, 98, 99], in which two-step reduction of SnO$_2$ supported on porous material (i.e. zeolite, various oxide supports) was reported. In the case of the non-modified magadiite, a small

broad peak with maximum around 600 K can be noticed. It may represent baking of the bed.

For the samples with incorporated Sn^{+4} (Figure 5.29), due to the stabilization of isolated tin ions by the silica layer, one can expect shift of the maxima temperature of the first step of the reduction towards the higher values. Such a shift, from ~ 630 K to ~ 700-720 K, can be observed in all synthesized Sn-magadiite. The second step peak can be noticed at ~ 870 K. Surface beneath the first and the second step of Sn^{+4} reduction were counted and found to be equal, which confirms the two-step reduction process. Additional peak or shoulder in the lower temperature values can be attributed to the reduction of non-bonded, well dispersed tin between the silica layers and/or on the external surface.
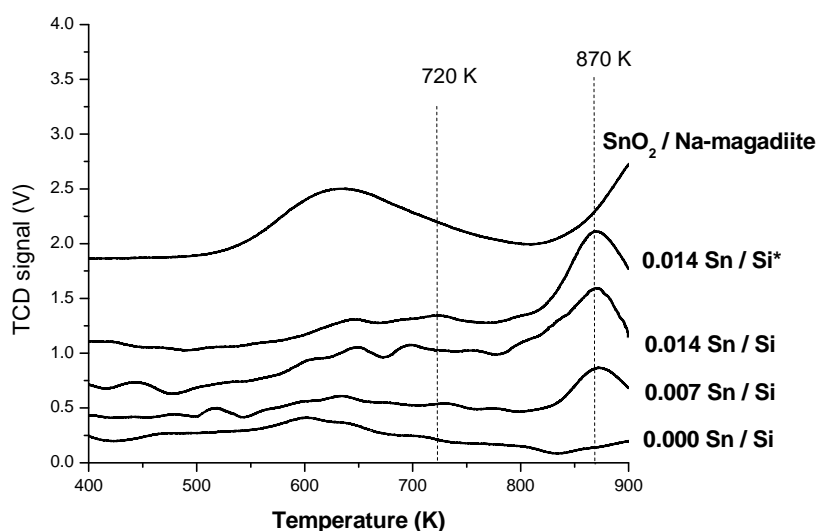
Figure 5.29: *H$_2$-TPR profiles of various samples synthesized according to the procedure M1. * – synthesis without Na$_2$CO$_3$.*

5.8.3. Kenyaite

TPR profile of SnO_2 / H-kenyaite (Figure 5.30) differs significantly from the corresponding profiles of SnO_2 / magadiite and SnO_2 / ilerite. Besides two peaks, which can be find also in the profiles of the above mentioned samples (~600 K and ~845 K), two additional were detected at 507 K and 767 K. The first two are clearly reflecting the same reduction process as in the case of SnO_2 / magadiite – reduction from +4 to +2 and from +2 to 0. A noticeable shift of the reduction temperatures towards the lower values could be caused by difference between SnO_2 particles size on particular material [100].

Because the presence of tin-containing pillars between the layers of SnO_2 / H-kenyaite was already excluded (see paragraph 5.1 and 5.3), the above mentioned peaks are most probably coming from the well dispersed tin bonded to the external surface of the material. After the deconvolution of reduction profile of SnO_2 / H-kenyaite (Figure 5.31), one can see two pairs of peaks representing particular reduction process (A1 and A2 – reduction of tin bonded to the external surface; B1 and B2 –bulky SnO_2 reduction). Each peak have similar surface like the corresponding one. Therefore, it can be concluded that amount of the consumed hydrogen is similar for each step of the reduction of particular form of tin, which seems to confirm the two-step reduction process.

For the samples with Sn^{+4} incorporated into the silica layers, due to the stabilization of the isolated tin ions by the silica layer, a shift of the tin reduction temperature towards higher values can be expected. Such a shift, from 600 K to 650 K, can be observed in all the synthesized Sn-kenyaite samples (Figure 5.30). The second step peak can be observed at 870 K. Surfaces beneath the first and the second step peak were counted and found to be equal, which confirms the two-step reduction process. Reduction profiles of Sn-kenyaite samples are similar to those of Sn-magadiite.
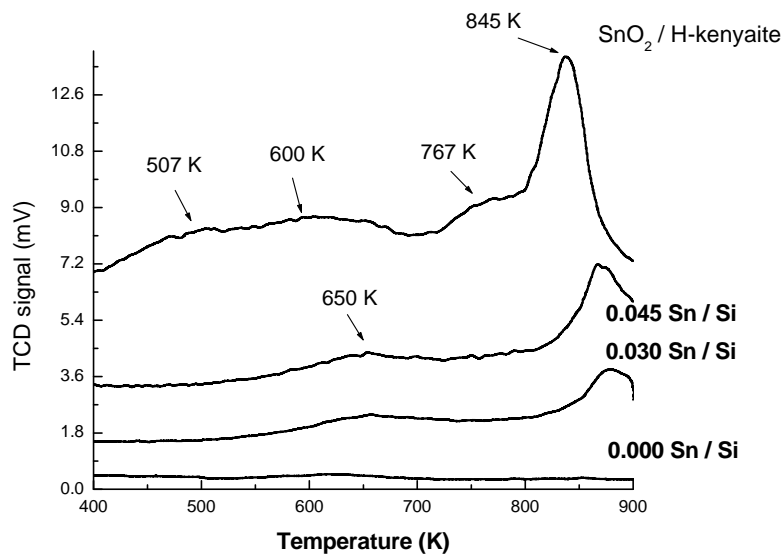
Figure 5.30: *H_2-TPR profiles of various samples synthesized according to the procedure K1- 72h synthesis.*
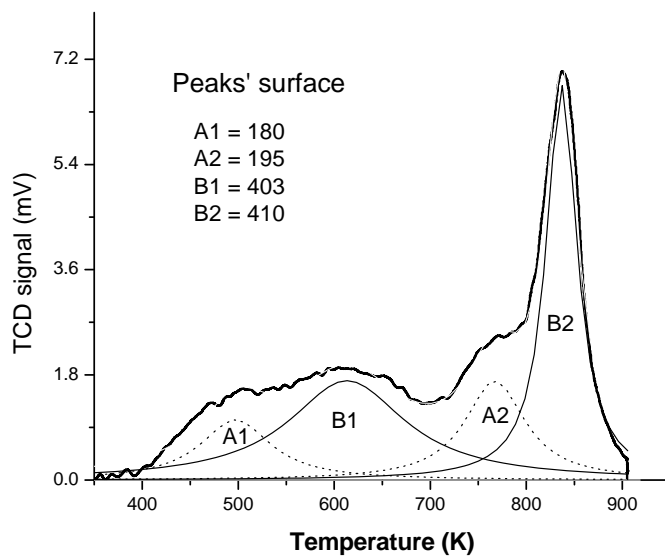
Figure 5.31: Deconvolution of reduction profile showed on example of SnO_2 / H-kenyaite. A1, A2 – peaks coming from the reduction of tin bonded to the external surface. B1, B2 – peaks coming from the reduction of bulky SnO_2.

5.9. Temperature-programmed ammonia desorption

Acidity of the H-forms of synthesized magadiite and kenyaite samples was studied by TPAD. Due to significantly low crystallinity, low silicon exchange ratio and the presence of the magadiite phase as the main one in the samples synthesized according to the procedure I1 and I2, acidity of those samples was determined only by the test reaction of MBOH conversion (see paragraph 5.10).

5.9.1. Magadiite

Besides the desorption peak coming from phisysorbed ammonia ~500 K (Figure 5.32) one additional desorption peak, coming from the desorption of chemisorbed ammonia was recorded. In comparison to the unmodified samples, the temperature of ammonia desorption for all the tin-containing H-forms of magadiite samples is noticeably shifted toward the lower values (from 726 K to 690 K), which seems to suggest that the presence of tin is weakening the acidity of the modified material. Slightly higher temperature of NH_3 desorption for the samples synthesized without Na_2CO_3 indicates higher acidity of those samples. In the case of the Al-samples, additional desorption maximum (~ 770 K) was detected. The above mentioned additional maximum can be assigned to the presence of stronger acid sites, which are generated (similar as in the case of zeolites) most probably by the negative charge of AlO_4^- tetrahedra incorporated into silica layers.
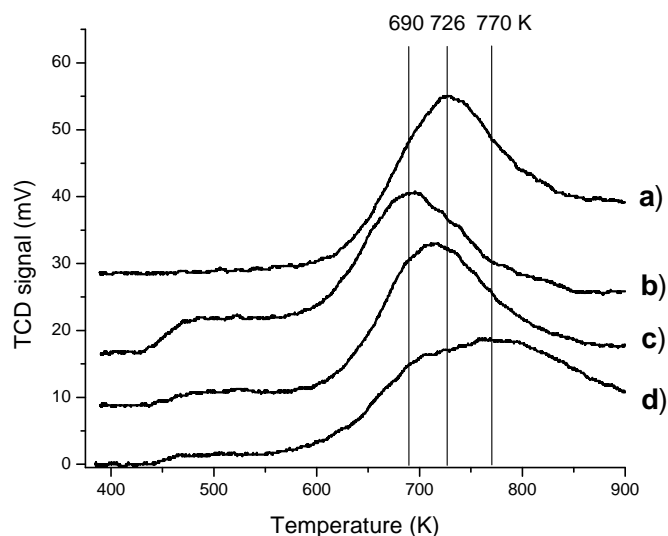
Figure 5.32: *TPAD profiles of H-forms of various magadiite samples: a) 0.000 Sn/Si – synthesis with Na$_2$CO$_3$, b) 0.015 Sn/Si – synthesis with Na$_2$CO$_3$, c) 0.015 Sn/Si – synthesis without Na$_2$CO$_3$, d) 0.003 Al/Si – synthesis with Na$_2$CO$_3$.*

5.9.2. Kenyaite

Similar as in the case of magadiite samples, incorporation of the heteroatom leads to shift of the temperature of ammonia desorption – from 823 K to 700 K (Figure 5.32), which leads to the same conclusion like for the magadiite samples, that the presence of tin is weakening the acidity of the modified material. Additional desorption peak around 500 K for the modified samples could be assigned to the desorption of phisisorbed and/or weakly chemisorbed ammonia on the amorphous part of sample. In the case of the Al-kenyaite samples, additional desorption maximum (~ 857 K) was detected. This indicates the presence of stronger acid sites, generated most probably by the negative charge of AlO$_4$$^-$ tetrahedra. There are no significant differences between samples synthesize in 72h or 96h
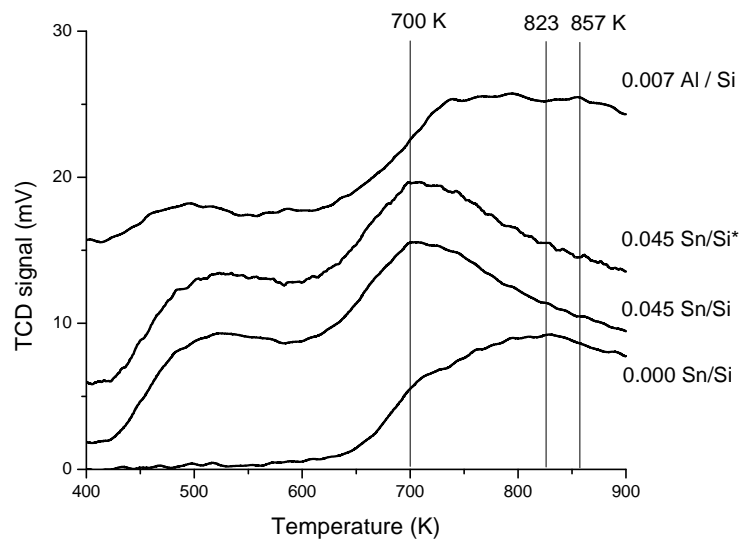
Figure 5.33: *TPAD profiles of H-forms of various kenyaite samples synthesized in 72 h and in *-96 h*

5.10. Conversion of 2-methyl-3-butyn-2-ol

5.10.1. Ilerite

Conversion of MBOH over the Na-forms of the tin-modified samples is increasing with increasing tin content (Figure 5.34). Because the amount of incorporated tin is relatively low, the mentioned difference in the conversion is most probably caused by the increase of amount of amorphous material with increasing tin content in the sample. Similar main products (acetone and acetylene) and similar selectivity have been detected in the case of Na- forms of all non-modified and modified samples synthesized according to the procedure I1 (data not shown) and I2, which indicate the presence of almost only basic active sides (Figure 5.35).

Figure 5.34: *Conversion of MBOH over the Na-forms of different samples synthesized according to the procedure I2 on time on stream:* ◆ *Na-ilerite,* ■ *0.0005 Sn/Si,* ▲ *0.00125 Sn/Si,* ● *0.0005 Al/Si.*

Figure 5.35: *Selectivity of products of MBOH conversion over the Na-forms of different samples synthesized according to the procedure I2 after 66 min. time on stream: a) Na-ilerite, b) 0.0005 Sn/Si, c) 0.00125 Sn/Si, d) 0.0005 Al/Si.*

83

Decrease of the conversion, in comparison to the Na-forms, was observed for the H-forms of all the non- and modified samples (Figure 5.36). The presence of MBYNE as well as acetone and acetylene indicates heterogeneous character of the surface of the tested samples (Figure 5.37). Amount of the acid pathway product is increasing meaningly with increasing tin content, which can be once again explained by significant increase of the amount of amorphous material along with the increase of the tin content in the samples. In contrast, conversion of the H-form of the aluminium-containing samples is increasing in comparison to its Na-form. Moreover, the presence of MBYNE as the main product (Figure 5.37) indicates on mainly acidic character of the surface, which is a result of formation of bridged Al-OH-Si groups, similar like in zeolites [101].
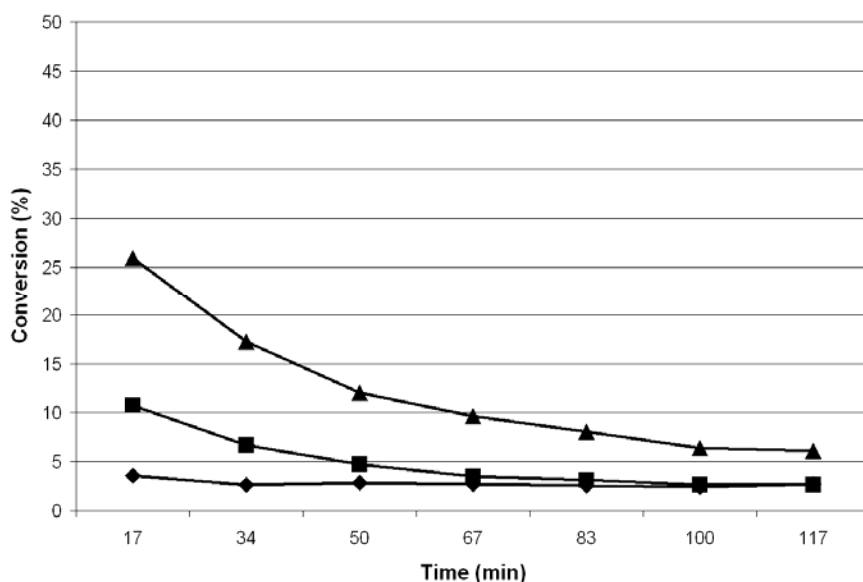
Figure 5.36: *Conversion of MBOH over the H-forms of different samples synthesized according to procedure I2 on time on stream:* ◆ *Na-ilerite,* ■ *0.00125 Sn/Si,* ▲ *0.0005 Al/Si.*

Figure 5.37: *Selectivity of products of MBOH conversion over the H-forms of different samples synthesized according to the procedure I2 after 66 min. time on stream: a) Na-ilerite, b) 0.0005 Sn/Si, c) 0.0005 Al/Si.*

5.10.2. Magadiite

Average conversion of MBOH for all the Na-forms of the samples does not exceed 13% (Figure 5.38). Difference between the conversion of the non- and tin-modified samples do not exceed 6%, which is close to measurement accuracy, whereas in the case of the samples synthesized according to the procedure I2, the mentioned difference was up to 13% despite 10 times smaller tin loading. Therefore, a conclusion could be made that the main influence on changes of the conversion has not the presence of tin in the sample but the amount and the character of the amorphous material in it.

Samples synthesized without the presence of Na_2CO_3 exhibit slightly lower conversion. Similar main products (acetone and acetylene) and similar selectivity were detected in the case of the Na- forms of all the non-modified and modified magadiite samples, which indicate the presence of almost only basic active sides (Figure 5.39).
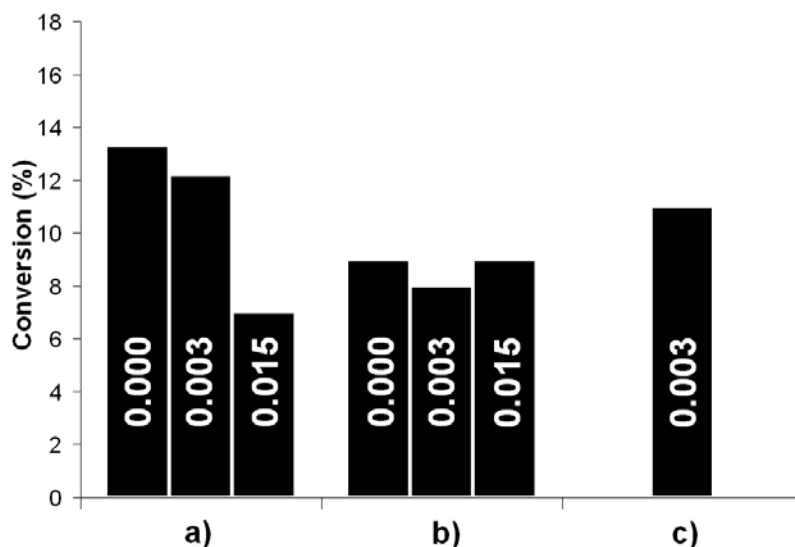
Figure 5.38: *Conversion of MBOH over the Na-forms of different magadiite samples after 66 min. time on stream: a) synthesis with Na_2CO_3 b) synthesis without Na_2CO_3 c) Al-magadiite - synthesis with Na_2CO_3, M/Si ratios are given in the columns.*
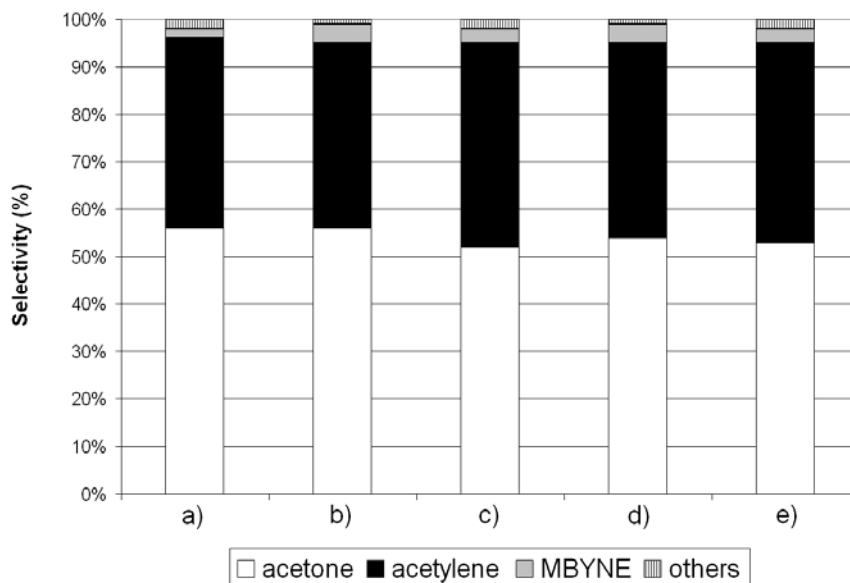
Figure 5.39: *Selectivity of products of MBOH conversion over the Na-forms of different magadiite samples synthesized according to the procedure M1 after 66 min. time on stream: a) Na-magadiite - synthesis with Na_2CO_3, b) Na-magadiite - synthesis without Na_2CO_3, c) 0.003 synthesis with Na_2CO_3, d) 0.003 Sn/Si synthesis without Na_2CO_3, e) 0.003 Al/Si synthesis with Na_2CO_3.*

Conversion of MBOH over the H-forms of all the non-modified and Sn-magadiite was significantly lower than that over the Na-forms of the above mentioned samples (Figure 5.40). The presence of MBYNE as well as acetone and acetylene indicates heterogeneous character of the surface of the samples. No meaningful differences have been found between the tin-containing and non-modified samples, which indicate absence of the additional negative charges on the sample surface. Therefore, it could lead to a conclusion that tin is incorporated into the silica layers in SnO_4 tetrahedra. Dissimilar to the tin-containing samples, conversions of the H-form and the Na-form of the aluminium-containing samples are similar. Moreover, the presence of MBYNE as the main product (Figure 5.41) indicates acidic character of the surface generated most probably by formation of bridged Al-OH-Si groups.
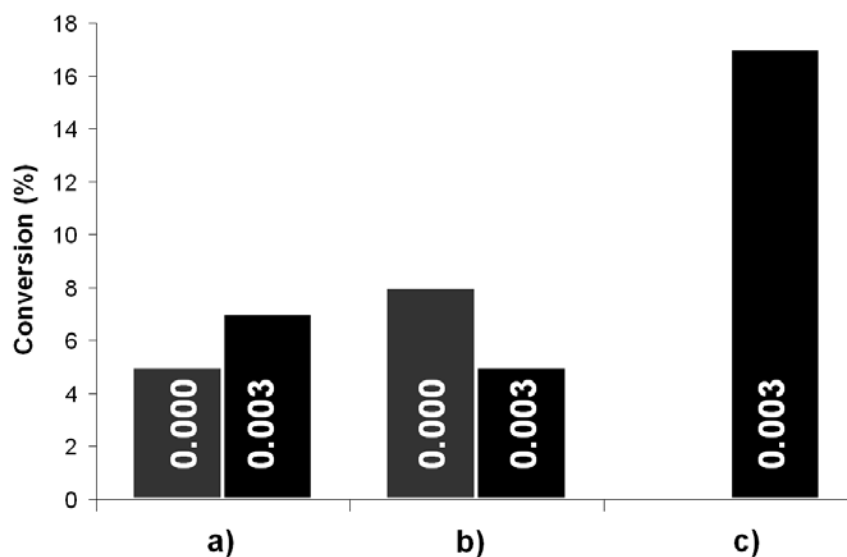
Figure 5.40: *Conversion of MBOH over the H-forms of different magadiite samples after 66 min. time on stream: a) synthesis with Na_2CO_3 b) synthesis without Na_2CO_3 c) Al-magadiite - synthesis with Na_2CO_3, M/Si ratios are given in the columns.*
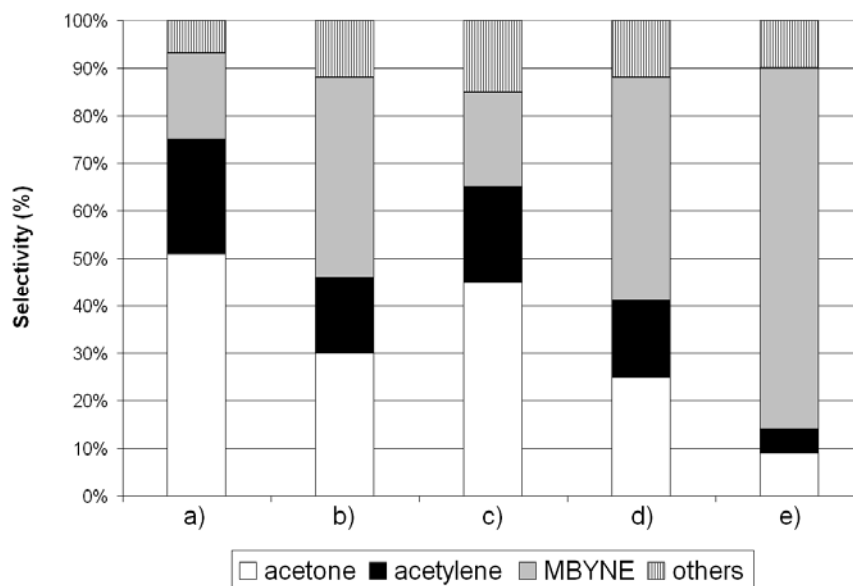
Figure 5.41: *Selectivity of products of MBOH conversion over the H-forms of different magadiite samples synthesized according to the procedure M1 after 66 min. time on stream: a) Na-magadiite - synthesis with Na_2CO_3, b) Na-magadiite - synthesis without Na_2CO_3, c) 0.003 synthesis with Na_2CO_3, d) 0.003 Sn/Si synthesis without Na_2CO_3, e) 0.003 Al/Si synthesis with Na_2CO_3.*

5.10.3. Kenyaite

Conversion values for the Na-forms of all the samples are relatively constant during the test (Figure 5.42). Only exception is the aluminium-containing sample. Conversion for this sample is significantly decreasing with time. Moreover, it is much higher than those of Na-kenyaite and Sn-kenyaite. The above mentioned conversion difference is most probably caused by the presence of additional negative charge coming form AlO_4^- tetrahedral; therefore, higher amounts of sodium in the sample that is generating basic active sides. Lauron-Pernot et al. [102] was observing similar conversion decrease in the case of the SiO_2-Al_2O_3 material, due to strong product adsorption on the catalyst surface.
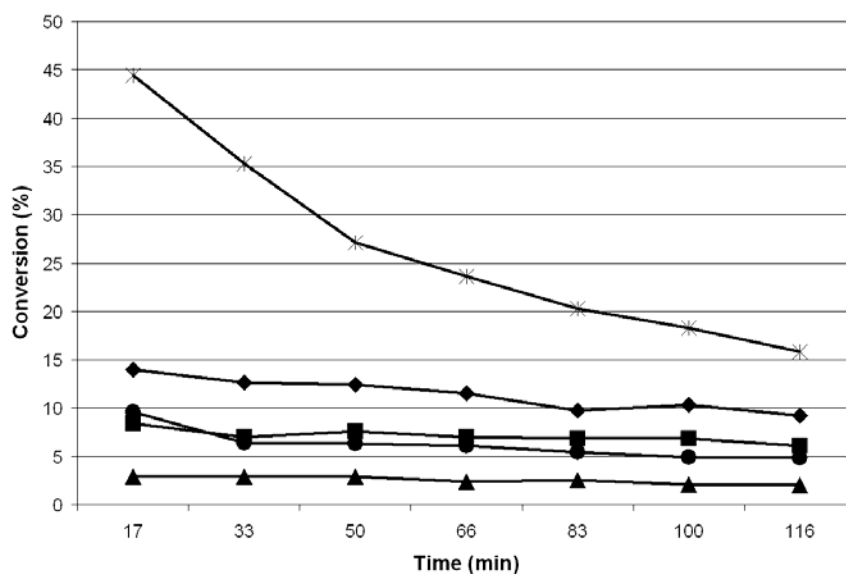
Figure 5.42: *Conversion of MBOH over the Na-forms of different kenyaite samples synthesized according to the procedure K1 on time on stream:* ◆ *Na-kenyaite,* ■ *0.015 Sn/Si,* ▲ *0.045 Sn/Si,* ● *0.045 Sn/Si – 96 h synthesis,* × *0.007 Al/Si.*
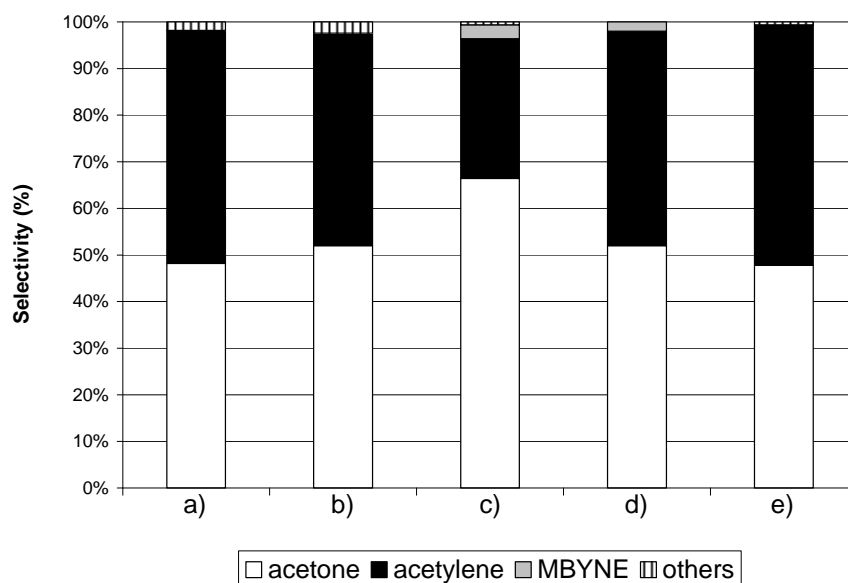
Figure 5.43: Selectivity of products of MBOH conversion over the Na-forms of different samples synthesized according to the procedure K1 after 66 min. time on stream: a) Na-kenyaite, b) 0.015 Sn/Si, c) 0.045 Sn/Si, d) 0.045 Sn/Si – 96 h synthesis, e) 0.007 Al/Si.

In comparison to Na-kenyaite, conversion for Sn-kenyaite is noticeably lower apparently due to lower crystallinity of those samples. Similar main products (acetone and acetylene) and similar selectivity were detected in the case of the Na- forms of all the non-modified and modified kenyaite samples, which indicate the presence of almost only basic active sides (Figure 5.43).

Decrease of conversion, in comparison to the Na-forms, was observed for the H-forms of all the kenyaite samples (Figure 5.44). Also in this case, the H-form of Al-kenyaite is significant different than others samples most probably due to the presence of stronger acid sites.

MBYNE, as well as acetone and acetylene, were detected as main products of MBOH conversion over the H-forms of the kenyaite samples. Therefore, the above mentioned samples surface have heterogeneous character, similar like in the case of the ilerite and magadiite samples. No meaningful differences have been found between the tin-containing and non-modified samples, which indicate absence of additional negative charges on the sample surface. In contrast, the presence of MBYNE as the main product (Figure 5.45) indicates mostly acidic character of the surface generated by the presence of negative charge form AlO_4^- tetrahedra. Conversion of MBOH over the SnO_2 / H-kenyaite sample was very much alike that of H-kenyaite, which seems to confirm that during treatment by $SnCl_4 * 5H_2O$ sodium ions were exchanged with hydrogen cations.
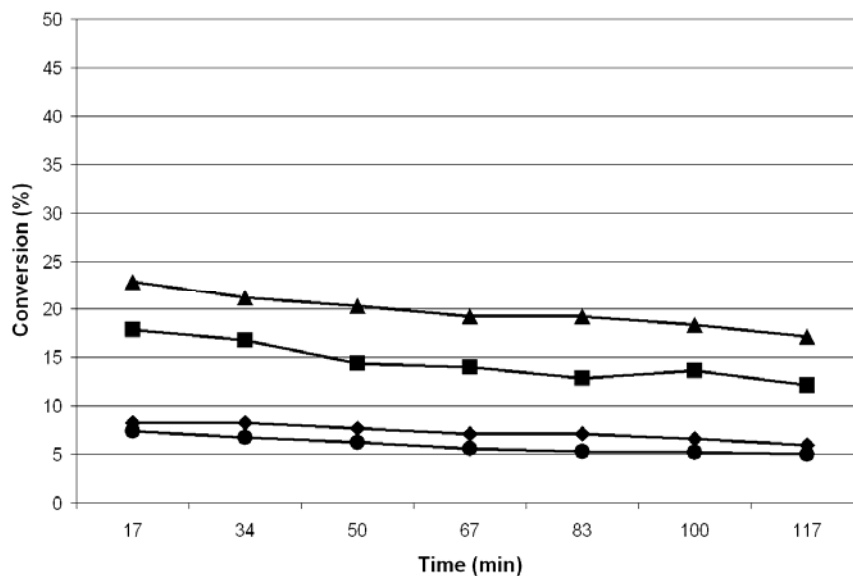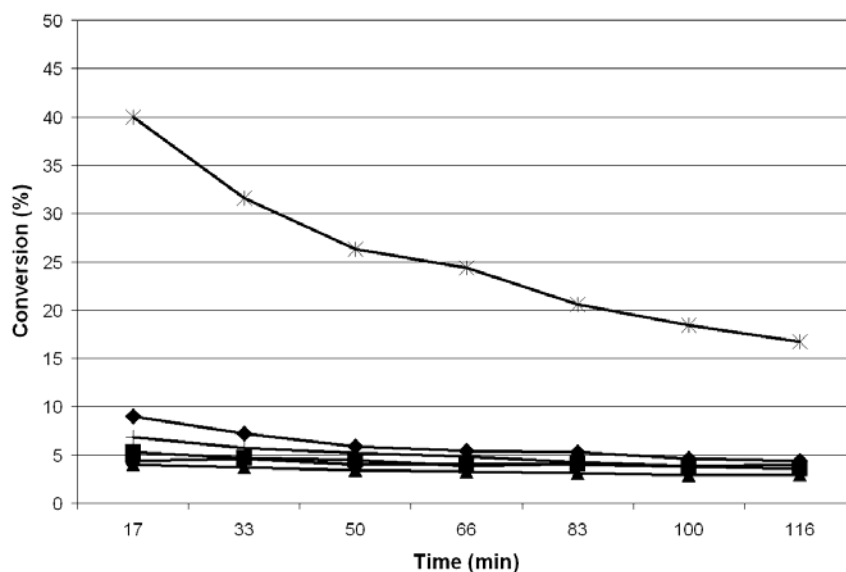
Figure 5.44: *Conversion of MBOH over the H-forms of different kenyaite samples synthesized according to the procedure K1 on time on stream: ◆ Na-kenyaite, ■ 0.015 Sn/Si, ▲ 0.045 Sn/Si, ● 0.045 Sn/Si – 96 h synthesis, × 0.007 Al/Si.*
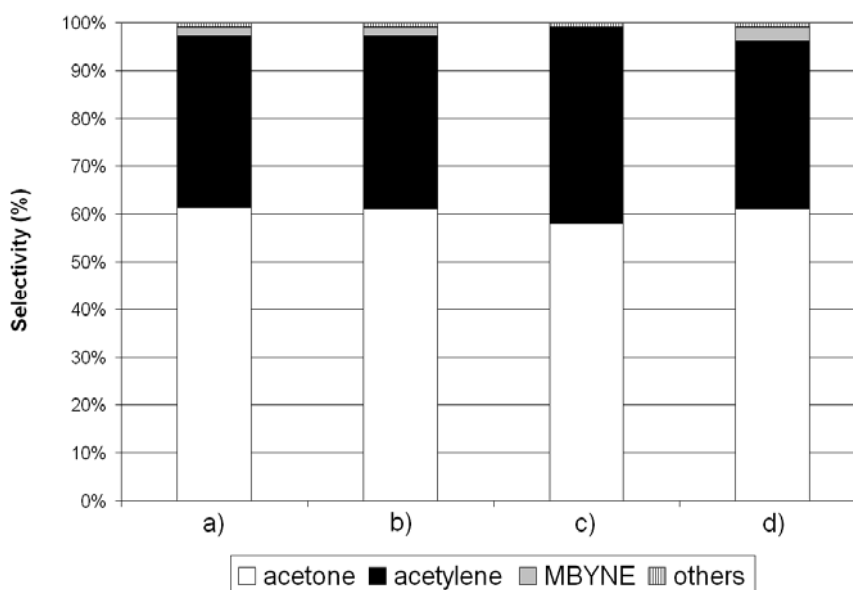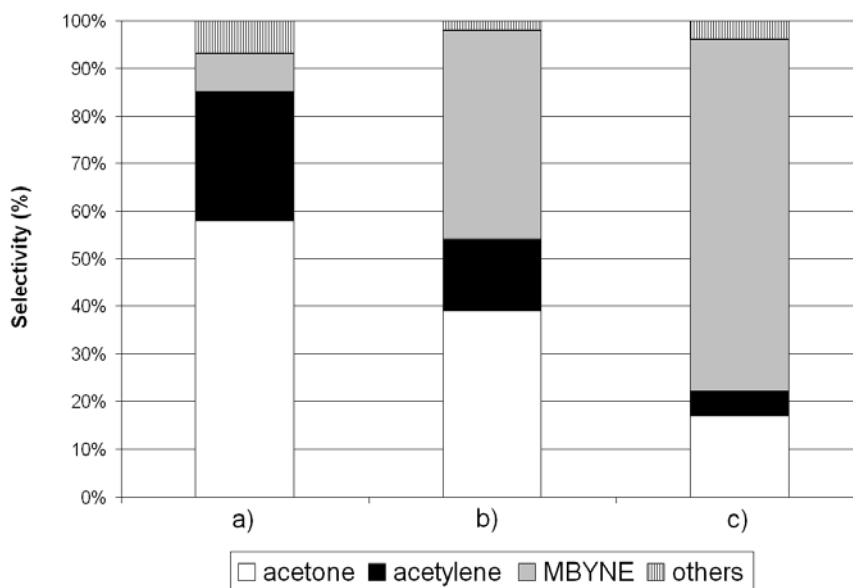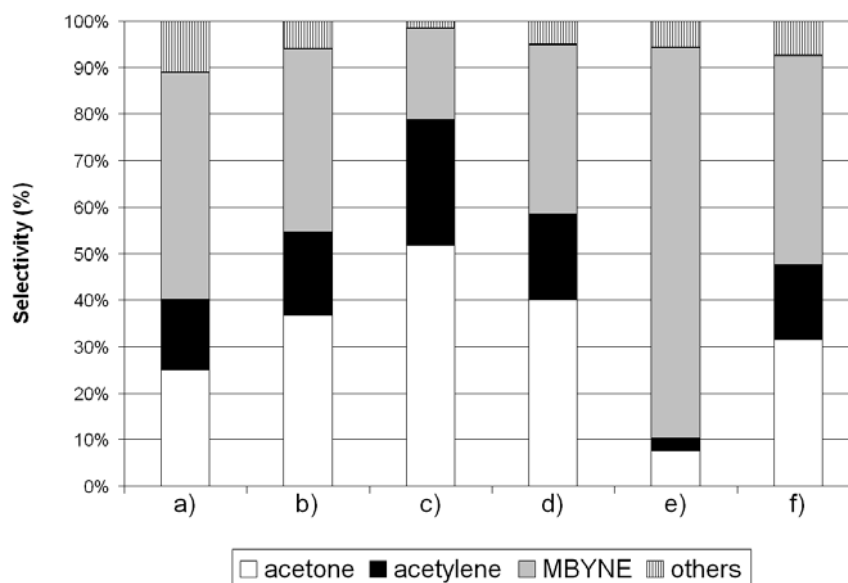

Figure 5.45: *Selectivity of products of MBOH conversion over the H-forms of different kenyaite samples synthesized according to the procedure K1 after 66 min. time on stream: a) Na-kenyaite, b) 0.015 Sn/Si, c) 0.045 Sn/Si, d) 0.045 Sn/Si – 96 h synthesis, e) 0.007 Al/Si, f) SnO$_2$ / H-kenyaite.*

5.10.4. Catalytic tests summary

Conversion of MBOH over all the Na-forms of various samples is similar. Furthermore, it is comparable with the one reported for zeolite NaX [101, 102, 103]. Therefore, it can be concluded that basic activity of the Na-forms of the studied samples is coming from the interlayer sodium cations. Higher conversion values were detected for the Na-forms of the ilerite samples, which contain high amounts of amorphous material. Therefore, a conclusion can be made that incorporation of tin does not have any significant influence on amount and character of the material active sides, whereas amount of amorphous material in the sample has a relatively significant influence on the conversion. One can see similar correlation in the case of selectivity over the studied samples.

Acetone to acetylene ratios were lover than 1 for all samples. Furthermore, the above mentioned ratio is decreasing with decreasing crystallinity of the samples. Some authors are reporting adsorption of acetone on basic active sides [102, 103]; however, there are only few reports in the literature confirming adsorption of acetylene. Handa et al. describes MBOH conversion over $NaNH_2/Al_2O_3$, KNH_2/Al_2O_3, and $RbNH_2/Al_2O_3$. All the studied catalysts were basic and gave acetylene and acetone as main products. Ratio of the above mentioned product was slightly different than one and the difference could be explained by adsorption of acetylene. Unfortunately, the authors do not focus on the above mentioned phenomena. Zadrozna et al. [104] suggest that acetylene could be consumed in a polymerization process on strong acid centres. However, this does not explain the above mentioned phenomena observed for basic samples. Moreover, believe that acetylene/acetone ratio always equals 1 is so strong, that most of the authors refer only to concentrations of acetone or even do not measure those of acetylene [101, 105-107]. Therefore, explaining of the acetone/acetylene ratios fluctuations is impossible on this stage of study.

Because incorporation of tin does not have any significant influence on the catalytic properties of the sample, no clear correlation can be driven between the methods of the synthesis and the catalytic properties of the samples.

The presence of bridged Al-OH-Si groups is well reflected in the selectivity of products of MBOH conversion over thw Al-modified samples. Lack of significant changes between the selectivity over the Na-forms and over the H-forms of the Sn-modified samples can lead to a conclusion that tin was incorporated in form of SnO_4 tetrahedra.

6. Conclusions

Tin-modified layered silicates were successfully synthesized under hydrothermal conditions. It has been shown that crystallization process, particularly in the procedure I1 and the I2 (differing from each other by crystallization time and temperature), is strongly influenced by the pH of synthesis mixture. Without an additional sodium hydroxide (needed for an in-situ formation of sodium hexahydroxo stannate(IV) from tin(IV) chloride pentahydrate during the synthesis) the resulting samples were amorphous. The dominating phase found in the samples synthesized according to the procedure M1 and K1 is magadiite and kenyaite, respectively. Contrary to the above mentioned syntheses, the addition of even small amount of aluminium isopropoxide or tin(IV) chloride pentahydrate to the ilerite synthesis mixture (procedure I1 and I2) directs the synthesis towards the magadiite structure.

Amount of the incorporated tin is increasing along with the increasing number of the silica layers in the examined material. Moreover, despite much smaller Sn/Si ratios for samples synthesized according to the procedure I1/I2 than those used in the procedure M1 or K1, the samples coming from the procedure I1/I2 are much less crystalline than the magadiite or kenyaite samples. Thus, a conclusion can be made that the presence of only one silica layer has significant influence on the stability of the layered silicate. Therefore, modified materials, synthesized according to the procedure I1/I2, have the magadiite structure, which is the more stable one. Stabilization effect can be seen especially on the example of the maximum Sn/Si ratio in the kenyaite samples, which is 36 times larger than that in the ilerite samples. The use of ilerite seeds enhances both the yield of crystallites and the tin loading in the material synthesized according to the procedure I1 and I2. However, even then, despite the presence of ilerite seeds, synthesis leads to the more stable structure - magadiite.

The crystallinity and the crystal size of all synthesized samples are decreasing considerably with increasing tin content. Amorphous material is present also on the surface of the crystals.

Adding Na_2CO_3 to the synthesis mixture enhance slightly the basicity of resulting sample. Furthermore, the crystals of samples synthesized without Na_2CO_3 have slightly different morphology (more flat crystals) than those synthesized with (more round crystals). There are no differences between the reduction profiles of the samples synthesized with or without Na_2CO_3; therefore, a conclusion can be made that influence of carbonate ions on incorporation of tin is negligible.

There is no straight evidence on influence of the applied synthesis method on the amount and the character of incorporated tin.

The synthesis method applied to the tin-modified samples is not suitable for incorporation of aluminium. Silicon exchange ratio is considerably lower for the aluminium-modified samples. It can be explained in term of the assumption that the presence of negative charge coming from the AlO_4 tetrahedra has negative influence on the stability of the resulting material.

There is no straight evidence on existence of the pillars or impurities between the layers. Therefore, the presence of tin between the silica layers in the magadiite and kenyaite samples can be excluded. Moreover, H_2-TPR profiles of the above mentioned samples seem to indicate the presence of only insignificant amounts of bulky tin oxide on the surface of the examined materials crystals. An exception to this are the samples synthesized according to the procedure I1 and I2, in which tin is suspected to be present between the silica layers as well as on the surface of the crystals.

The presence of tin in the layers is not clearly reflected in IR. Although broadening of the Si-O-Si asymmetric vibration band seems to indicate the existence of Sn-O-Si bands in the examined samples (particularly magadiite and kenyaite ones), lack of clear correlation between amount of incorporated tin as well as difficulties in quantifying of the results of the DRIFT technique seems to make such interpretation speculative. However, split of the Q_3 signal in ^{29}Si MAS NMR made for tin-modified magadiite might indicate the presence of –OSn bonded to SiO_2 tetrahedra.

Red-ox properties of the tin-modified samples were proven by H_2-TPR. Amount of reduced tin is increasing with increasing tin content in the samples. Moreover, shifts of the reduction steps temperature seems to confirm the presence of SnO_4 tetrahedra incorporated into the framework positions.

After considering the IR, ^{29}Si MAS NMR and H_2-TPR results, as well as absence of straight evidence on the existence of tin between the silica layers (particularly for magadiite and kenyaite samples) it can be concluded that tin was successfully incorporated into the silica layers.

Opposite to the morphology, the nature of the tin-modified sample active sites is changed meaningly after incorporation of the heteroatom. Due to formation of bridged Al-OH-Si groups, the H-forms of the aluminium-containing samples poses stronger acid sites than the non-modified material, whereas incorporation of tin leads to formation of weaker acid sites.

Despite different synthesis method and structure types, there is no meaningful difference between the selectivity of products of MBOH conversion over the Na-forms of the Sn-modified and non-modified samples. Moreover, the conversion of MBOH was depending more from amount of amorphous material in the studied sample than amount of incorporated tin. Contrary to the Sn-containing samples, the presence of bridged Al-OH-Si groups was significantly reflected in the conversion and the selectivity of the reaction. Therefore, it can be assumed that Sn^{+4} was incorporated in form of SnO_4 tetrahedra.

Possibility of isomorphous exchange of silicon atoms in the silica layer confirms the assumption that the silica layers exhibit similar properties like zeolites, where silicon can be exchanged with variety of atoms. Successful incorporation of tin seems to indicate that incorporation of other active species could be possible as well.

Zusammenfassung

Zinn-modifizierte Schichtsilikate sind erfolgreich unter hydrothermalen Bedingungen synthetisiert worden. Es konnte gezeigt werden, dass der Kristallisations Prozess, insbesondere bei den Verfahren I1 und I2 (unterschiedliche Kristallisationszeit und -temperatur), stark durch den pH-Wert der Synthesemischung beeinflusst wird. Ohne zusätzliches Natriumhydroxid (zur In-situ-Bildung von Natrium hexahydroxo Stannat (IV) aus Zinn (IV)-chlorid-Pentahydrat während der Synthese) waren die erhaltenen Proben amorph. Die dominierenden Phasen, welche in den Proben nach den Verfahren M1 und K1 hergestellt wurden, sind Magadiit beziehungsweise Kenyait. Im Gegensatz zu den genannten Synthesen, bewirkt schon die Zugabe von kleinen Mengen Aluminiumisopropoxid oder Zinn (IV)-chlorid-Pentahydrat zur Ilerite-Synthesemischung (Verfahren I1 und I2) eine Verschiebung in Richtung der Magadiit-Struktur.

Die Menge an eingebautem Zinn nimmt zusammen mit der Anzahl von Kieselsäureschichten in den untersuchten Materialen zu. Des Weiteren sind die Proben aus dem Verfahren I1/I2, trotz kleinerer Sn/Si-Verhältnisse, viel weniger kristallin als die Magadiit- oder Kenyait-Proben. Es kann gesagt werden, dass die Anwesenheit von nur einer Kieselsäureschicht einen signifikanten Einfluss auf die Stabilität des Schichtsilikats hat. Aus diesem Grund haben die Materialien, die nach dem Verfahren I1/I2 synthetisiert worden sind, eine Magadiit-Struktur. Dieser Stabilisierungseffekt ist sehr gut an dem Beispiel mit dem größten Sn / Si-Verhältnis für die Kenyait-Proben zu erkennen, das 36 Mal größer ist als für die Ilerite-Proben. Die Verwendung von Ilerite-Impfkristallen erhöht sowohl die Ausbeute der Kristallite als auch die Zinn-Beladung in dem nach Variante I1 und I2 hergestellten Material. Aber trotz der Anwesenheit von Ilerite-Impfkristallen, resultiert die Synthese in einer stabilen Struktur - Magadiit.

Die Kristallinität und die Kristallgröße aller synthetisierten Proben nehmen deutlich mit zunehmendem Zinngehalt ab und amorphes Material ist ebenfalls auf der Kristalloberfläche vorhanden.

Der Zusatz von Na_2CO_3 zu der Synthesemischung erhöht leicht die Basizität des resultierenden Probe. Darüber hinaus haben Kristalle der Proben ohne den Zusatz von

Na_2CO_3 eine leicht unterschiedliche Morphologie (flache Kristalle), als solche mit Na_2CO_3 als Zusatz (runde Kristalle). Es ist kein Unterschied im Reduktionsverhalten zwischen den Proben, die mit und ohne Na_2CO_3 synthetisiert worden sind, zu erkennen. Aus diesem Grund kann ein Einfluss von Carbonat-Ionen bei der Einarbeitung von Zinn vernachlässigt werden.

Es gibt keinen Nachweis über den Einfluss der angewandten Syntheseverfahren auf die Menge und die Art des eingebauten Zinn.

Die verwendete Synthesemethode für die Herstellung der Zinn-Proben ist nicht geeignet für den Einbau von Aluminium und das Austauschverhältnis für Silizium ist wesentlich niedriger, als für die mit Aluminium modifizierten Proben. Es kann gesagt werden, dass die Anwesenheit negativer Ladung aus dem AlO_4 Tetraeder einen negativen Einfluss auf die Stabilität des entstandenen Materials hat.

Es gibt keinen direkten Hinweis für die Existenz von Säulen oder Verunreinigungen zwischen den Schichten, daher kann die Gegenwart von Zinn zwischen den Kieselsäureschichten im Magadiit und Kenyait Proben ausgeschlossen werden. Darüber hinaus scheinen die TPR-Profile der erwähnten Proben auf das Vorhandensein von nur unbedeutende Mengen von sperrigem Zinnoxid auf der Oberfläche der untersuchten Kristalle hinzudeuten. Eine Ausnahme sind die nach dem Verfahren I1 und I2 hergestellten Proben, in denen Zinn vermutet wird, dass sich zwischen den Kieselsäureschichten sowie auf der Oberfläche der Kristalle eingelagert hat.

Die Anwesenheit von Zinn in den Schichten kann nicht eindeutig mittels IR nachgewiesen werden. Obwohl eine Verbreiterung der asymmetrischen Si-O-Si Schwingungsbande zu erkennen ist, scheint die Existenz von Sn-O-Si Banden in den untersuchten Proben (insbesondere Magadiit und Kenyait), keine klaren Zusammenhang zu der eingebauten Menge an Zinn zu geben. Weitere Schwierigkeiten bei der Auswertung der Ergebnisse aus den DRIFT-Experimenten machen also eine Deutung spekulativ. Allerdings könnte die Spaltung des Q_3-Signals in dem ^{29}Si-MAS-NMR des mit Zinn modifizierten Magadiits die Anwesenheit von -OSn-gebundenem SiO_2-Tetraedern zeigen.

Die Red-ox-Eigenschaften der Zinn-modifizierten Proben sind mittels H_2-TPR nachgewiesen worden. Die Menge an reduziertem Zinn nimmt mit steigendem Zinngehalt in den Proben zu. Temperaturverschiebungen in den Reduktionsprofilen scheinen zu zeigen dass das Zinn in der Form von SnO_4-Tetraedern eingebaut worden ist.

IR, ^{29}Si MAS NMR und H_2-TPR Ergebnisse sowie Fehlen von geraden Beweise für die Existenz von Zinn zwischen den Kieselgelschichten (insbesondere für Magadiit und Kenyait Proben) zeigen, dass Zinn erfolgreich in die Kieselgelschichten aufzunehmen wurde.

Gegenüber der Morphologie sind die aktiven Zentren der mit Zinn modifizierten Proben durch die Einführung eines Heteroatoms geändert worden. Durch Bildung von verbrückenden Al-OH-Si-Gruppen, stellt die H-Form der Aluminium-haltigen Proben die stärkere Säure dar, als die des nicht veränderten Materials. Der Einbau von Zinn führt nur zur Ausbildung von schwächeren Säuren.

Trotz unterschiedlicher Syntheseverfahren und Struktur-Typen gibt es keinen großen Unterschied zwischen der Selektivität der Produkte aus den MBOH-Experimenten an der Na-Form der Sn-modifizierten und nicht modifizierten Proben. Darüber hinaus ist der Umsatz der MBOH-Reaktion hauptsächlich von der Menge an amorphem Material in den untersuchten Proben abhängig, als von der Menge an eingebautem Zinn. Im Gegensatz zu den Sn-haltigen Proben, hat die Anwesenheit von verbrückenden Al-OH-Si-Gruppen einen großen Einfluss auf den Umsatz und die Selektivität der Reaktion. Daher kann davon ausgegangen werden, dass das Zinn in der Form von SnO_4-Tetraedern eingebaut worden ist.

Die Möglichkeit der isomorphen Substitution von Silizium-Atomen in der Kieselsäureschichte bestätigt die Annahme, dass die Kieselsäureschichten ähnliche Eigenschaften wie Zeolithe (wo Silizium mit verschiedenen Atome ausgetauscht werden kann) besitzen. Der erfolgreiche Einbau von Zinn scheint zu bestätigen, dass die Substitution von anderen aktiven Spezies ebenso möglich sein kann.

7.Literature

[1] Davis, M.E.; Lobo, R.F. *Chem. Mater.* 4, **1992**, 156.

[2] Pelster, S.A.; Weimann, B.; Schaack, B.B.; Schrader, W.; Schueth, F. *Angew. Chem. Int. Ed.* 46, **2007**, 6674.

[3] Schaack, B.B.; Schrader, W.; Schueth, F. *Angew. Chem. Int. Ed.* 47, **2008,** 9092.

[4] Schwieger, W.; Lagaly, G. *Alkali Silicates and Crystalline Silicic Acids* in *Handbook of Layered Materials*, New York, **2004**, ISBN: 0-8247-5349-6.

[5] Superti, G. B.; Oliveira, E. C.; Pastore, H. O.; Bordo, A.; Bisio, C.; Marchese, L. *Chem. Mater.* 19 (17), **2007**, 4300.

[6] Borbely, G. ; Beyer, H.K.; Karge, H.G.; Schwieger, W.; Brandt, A.; Bergk, K.H. Clays Clay Miner. 39, **1991**, 490.

[7] Schwieger, W.; Brunner, E. *Colloid Polym. Sci.* 270, **1992**, 935.

[8] Lee, J.D. *Concise Inorganic Chemistry*, 5th edition, London, **1995,** ISBN: 978-0-632-05293-6.

[9] Wiggleswort, C.F. *The constitution of the natural silicates*, Washington, Govt. print. Off **1914**.

[10] Eugster, H.P. *Science* 157, **1967**, 1177.

[11] Sebag, D.; Verrecchia, E.P.; Lee, S.-J.; Durand, A. *Sedimentary Geology* 139, **2001**, 15.

[12] Wang, Y.-R.; Wang, S.-F.; Chang, L.-C. *Appl. Clay Sci.* 33, **2006**, 73.

[13] Borowski, M.; Kovalev, O.; Gies, F. *Microporous Mesoporous Mater.* 107, **2008**, 71.

[14] Vortmann, S.; Rius, J.; Siegmann, S.; Gies, H. *J. Phys. Chem. B* 101, **1997**, 1292.

[15] Schwieger, W.; Heidemann, D.; Bergk, K.-H. *Rev. Chim. Min.* 22, **1985**, 639.

[16] Heidemann, D.; Schwieger, W.; Bergk, K.-H. *Z. anorg. Allg. Chem.*, 555, **1987**, 129.

[17] Brandt, A.; Schwieger, W.; Bergk, K.-H. *Cryst. Res. Technol.* 23, **1988**, 1201.

[18] Brandt, A.; Schwieger, W.; Bergk, K.-H.; Grabner, P.; Porsch, M. *Cryst. Res. Technol.* 24, **1989**, 47.

[19] Schwieger, W.; Brenn, U.; Grabner, P.; Utschick, H. *J. Therm. Anal.* 52, **1998**, 21-32.

[20] Almond, G. G.; Harris, R. K.; Franklin, K. R. *J. Mater. Chem.* 7(4), **1997**, 681.

[21] Garces, J. M.; Rocke, S. C.; Crowder, C. E.; Hasha, D. L.; *Clays and Clay Miner.* 36, **1988,** 409.

[22] Lagaly, G.; Beneke, K. *Am. Mineral.* 60, **1975**, 642.

[23] Kalvachev, Y.; Kostov-Kytin, V.; Todorova, S.; Tenchev, K.; Kadinov, G. *Appl. Catal. B: Environmental* 66, **2006**, 192.

[24] Beneke, K.; Lagaly, G. *Am. Mineral.* 68, **1983**, 818.

[25] Iwasaki, T.; Kuroda, T.; Ichio, S.; Satoh, M. *Chem. Eng. Comm.* 193, **2006**, 69.

[26] Iler, R.K. *J. Colloid Sci.* 60, **1964**, 648.

[27] Wolf, F.; Schwieger, W. *Z. Anorg. Allg. Chem.* 457, **1979**, 224.

[28] Ikeda, T.; Oumi, Y.; Takeoka, T.; Yokoyama, T.; Sano, T.; Hanaoka, T. *Microporous Mesoporous Mater.* 110, **2008**, 488.

[29] Lagaly, G.; Beneke, K. *Am. Mineral.* 60, **1975**, 650.

[30] Yu, J.; Yang, Q.-X. *Appl. Clay Sci.* 48, **2010**, 185.

[31] Schwieger, W.; Gravenhorst, O.; Selvam, T.; Roessner, F.; Schloegl, R.; Su, D.; Mabande, G. T. P. *Colloid Polym. Sci.* 281, **2003**, 584.

[32] Schwieger, W.; Heyer, W.; Bergk, K.-H. *Z. anorg. allg. Chem.* 559, **1988**, 191.

[33] Feng, F.; Balkus Jr., K.J. *J. Porous Mater.* 10, **2003**, 5.

[34] Fletcher, R. A.; Bibby, D. M. *Clays Clay Miner.* 35(4), **1987**, 318.

[35] Brenn, U.; Ernst, H.; Freude, D.; Herrmann, R.; Jaehnig, R.; Karge, H.G.; Kaerger, J.; Koenig, T.; Maedler, B.; Pingel, U.-T.; Prochnow, D.; Schwieger, W. *Microporous Mesoporous Mater.* 40, **2000**, 43.

[36] Kim, S.J.; Jung, K.-D.; Joo, O.-S.; Kim, E. J.; Kang, T. B. *Appl. Catal., A* 266, **2004**, 173.

[37] Crone, L.A.; Franklin, K.R.; Graham, P. *J. Mater. Chem.* 5, **1995**, 7.

[38] Alberti, G.; Bein, T. *Comprehensive Supramolecular Chemistry*, vol. 7, Oxford, Pergamon, 1996.

[39] Kwon, O.-Y.; Jeong, S.-Y.; Suh, J.-K.; Lee, J.-M. *Bull. Korean Chem. Soc.* 16, **1995**, 737.

[40] Schwieger, W.; Heyer, W.; Wolf, F.; Bergk, K.-H. *Z. anorg. allg. Chem.* 548, **1987**, 204.

[41] Ahn, S.-H.; Kim, S.-H; Hahm, H.-S. *Res. Chem. Intermed.* 34, **2008**, 793.

[42] Kuhlmann, A.; Roessner, F.; Schwieger, W.; Gravenhorst, O.; Selvam, T. *Catal. Today* 97, **2004**, 303.

[43] Schwieger, W.; Selvam, T.; Gravenhorst, O.; Pfaender, N.; Schloegl, R.; Mabande, G.T.P. *J. Phys. Chem. Solids* 65, **2004**, 413.

[44] Ozawa, K.; Nakao, Y.; Cheng, Z.; Wang, D.; Osada, M.; Okada, R. *Mater. Lett.* 63, **2009**, 366.

[45] Ozawa, K.; Iso, F.; Nakao, Y.; Cheng, Z.; Fujii, H.; Yamaguchi, H. *J. Eur. Ceram. Soc.* 27, **2007**, 2665.

[45] Selvam, T.; Bandarapu, B.; Mabande, G. T. P.; Toufar, H.; Schwieger, W. *Microporous Mesoporous Mater.* 64, **2003**, 41.

[46] Feng, F.; Balkus Jr., K.J. *Microporous Mesoporous Mater.* 69, **2004**, 85.

[47] Macedo, T.R.; Airoldi, C. *Microporous Mesoporous Mater.* 94, **2006**, 81.

[48] Ishii, R.; Ikeda, T.; Mizukami, F. *J. Colloid Interface Sci.* 331, **2009**, 417.

[49] Wang, S.-F.; Lin, M.-L.; Shieh, Y.-N.; Wang, Y.-R.; Wang, S.-J. *Ceram. Int.* 33, **2007**, 681.

[50] Park, K.-W.; Jung, J. H.; Kim, S. -K,; Kwon, Oh.-Y. *Appl. Clay Sci..* 46, **2009**, 251.

[51] Park, K.-W.; Jeong, S. Y.; Kwon, Oh.-Y. *Appl. Clay Sci..* 27, **2004**, 21.

[52] Guo, Y.; Wang, Y.; Yang, Q.-X.; Li, G. –D.; Wang, C.-S.; Cui, Z.-C.; Chen, J.-S. *Solid State Sci..* 6, **2004**, 1001.

[53] Royer, B.; Cardoso, N.F.; Lima, E.C.; Macedo, T.R.; Airoldi, C. *J. Hazard. Mater.* 181, **2010**, 366.

[54] Toriya, S.; Takei, T.; Fuji, M.; Chikazawa, M. *J. Colloid Interface Sci* 268, **2003**, 435.

[55] H. Kessler, in: J.L. Atwood et al. (Eds.), *Comprehensive Supramolecular Chemistry*, vol. 7, Pergamon, **1996**.

[56] Arends, I.V.C.E.; Sheldon, R.A.; Wallau, V.; Schuchardt, V. *Angew. Chem. Int. Ed. Engl.* 36, **1997,** 1144.

[57] Ione, K.G.; Vostrikova, L.A.; Mastikhin, V.M. *J. Mol. Catal. A: Chem.* 31, **1985**, 355.

[58] Cejka, J.; in: J. Cejka et al. (Eds.), *Zeolites and Ordered Mesoporous Materials: Progress and Prospects, Studies in Surface Science and Catalysis*, vol. 157, Elsevier, Amsterdam, **2005**.

[59] E.M. Flanigen, in: H. Van Bekkum et al. (Eds.), Introduction to Zeolite Science and Practice, *Studies in Surface Science and Catalysis*, vol. 137, Elsevier, Amsterdam, **2001**.

[60] Kosslick, H.; Tuan, V.A.; Fricke, R.; Peuker, Ch.; Pilz, W.; Storek, W. *J. Phys. Chem.* 97, **1997**, 5678.

[61] Conradsson, T.; Dadachov, M.S.; Zou, X.D. *Micropor. Mesopor. Mater.* 41, **2000,** 183.

[62] Cheng, M.; Tan, D.; Liu, X.; Han, X.; Bao, X.; Lin, L; *Microporous Mesoporous Mater.* 42, **2001**, 307.

[63] Pal-Borbely, G.; Beyer, H.K.; Kiyozumi, Y.; Mizukami, F. *Microporous Mesoporous Mater.* 22, **1998**, 57.

[64] Pal-Borbely, G.; Beyer, H.K.; Kiyozumi, Y.; Mizukami, F. *Microporous Mater.* 11, **1997**, 45.

[65] Mihalyi, R.M.; Pal-Borbely, G.; Beyer, H.K.; Szegedi, A.; Koranyi, T.I. *Microporous Mesoporous Mater.* 98, **2007**, 132.

[66] Fudala, A.; Konya, Z.; Kiyozumi, V.; Niwa, S.-I.; Toba, M.; Mizukami, V. *Microporous Mesoporous Mater.* 35-36, **2000**, 631.

[67] Fudala, A.; Kiyozumi, V.; Mizukami, V. Niwa, S.-I.; Toba, M.; Kiricsi, I. *J. Mol. Struct.* 482-483, **1999**, 43-47.

[68] Fudala, A.; Kiricsi, I. *React. Kinet. Catal. Lett*. 65, **1998**, 47.

[69] Mal, N. K.; Ramaswamy, V.; Ganapathy, S.; Ramaswamy, A. V. *J. Chem. Soc. Chem. Commun.* 17, **1994**, 1933.

[70] Mal, N.K.; Ramaswamy, A.V. *J. Mol. Catal. A: Chem.* 105, **1996**, 149.

[71] Mal, N.K.; Ramaswamy, V.; Rakshe, B.; Ramaswamy, A.V.; *Stud. Surf. Sci. Catal.* 105, **1997**, 357.

[72] Boronat, M.; Corma, A.; Renz, M.; *J. Phys. Chem. B* 110, **2006**, 21168.

[73] Corma, A.; Domine, M. E.; Valencia, S. *J. Catal.* 215, **2003**, 294.

[74] Boronat, M.; Concepcion, P.; Corma, A.; Renz, M. *Catal. Today*, 121, **2007**, 39.

[75] Chaudhari, K., Das, T.K.; Rajmohanan, P.R.; Lazar, K.; Silvasanker, S.; Chandwadker, A.J. J. Catal. 183, 1999, 281-291,

[76] Taralkar, U.S.; Kalita, P.; Kumar, R.; Joshi, P.N. Appl. Catal. A 358, 2009, 88-94.

[77] Ramaswamy, V.; Shah, P.; Lazar, K.; Ramawamy, A.V. *Catal. Surv. Asia* 12, **2008**, 283.

[78] Abdel-Fattah, T.M.; Pinnavaia, T. *J. Chem. Commun.* **1996**, 665.

[79] Candu, N.; Coman, S.; Pervulescu, V.I.; Haskouri, J.E.; Amoros, P.; Beltran, D. *Top. Catal.* 52, **2009**, 1182.

[80] Alarcón, E.; Villa de P., A. L.; Montes de C., C. *Catal. Today.* 107–108, **2005**, 942.

[81] Wroblewska, A.; Lawro, E.; Milchert, E. *Ind. Eng. Chem. Res.* 45, **2006**, 7365.

[83] Swainson, I. P.; Dove, M. T.; Harris, M. J. *J. Phys. Condens. Matter.* 7, **1995**, 4395.

[84] Chandwadkar, A.; Bhat, R.; Ratnasamy, P. *Zeolites* 11, **1991**, 42.

[85] Meier, W.M. *Z. Kristallogr.* 115, **1961**, 439.

[86] Eypert-Blaison, C.; Villieras, F.; Michot, L . J.; Pelletier, M. *Clay Miner.* 37, **2002**, 531.

[87] Kim, S. J., ; Kang, T. B.; Jung, K.-D.; Joo, O.-S.; Shin, C.-H. *J. Porous Mater.* 13, **2006**, 27.

[88] Steudel, A. *Selection strategy and modification of layer silicates for technical applications*, Universität Karlsruhe (TH), Fakultät für Bauingenieur-, Geo- und Umweltwissenschaften, **2008**, ISBN: 978-3-86644-352-5.

[89] Miecznikowski, A.; Hanuza, J. *Zeolites*, 7, **1987**, 249.

[90] Tao, D.; Fangxia, F.; Yongzhuang, X.; Jinghui, C. *Reaet.Kinet.Catal.Lett.* 61, **1997**, 97.

[91] Khouw, C.B.; Davis, M.E. *J. Catal.* 151, **1995**, 77.

[92] Camblor, M. A.; Corma, A.; Perez-Pariente, *J. J. Chem. Soc., Chem. Commun.* **1993**, 557.

[93] Szostak, R.; Nair, V.; Thomas, T. L. *J. Chem. Soc., Faraday Trans.* 83, **1987**, 487.

[94] Smith, J.V.; Blackwell, C.S. *Nature*, 303, **1983**, 223.

[95] Rodriguez, R.; Pfaff, C.; Melo, L.; Betancourt, P. *Catal. Today* 107-108, **2005**, 100.

[96] Haneda, M.; Ohzu, S.; Kintaichi, Y.; Shimizu, K.; Shibata, J.; Yoshida, H.; Hamada, H. *Bull. Chem. Soc. Jpn.* 74, **2001**, 2075.

[97] Lazar, K.; Chandwadkar, A. J.; Fejes, P.; Cejka, J.; Ramaswamy, A.V.; J. *Radioanal. Nucl. Chem.* 246, **2000**, 143.

[98] Auroux, A.; Sprinceana, D.; Gervasini, A. *J. Catal.* 195, **2000**, 140.

[99] Janiszewska, E.; Kowalak, S.; Supronowicz, W.; Roessner, F. *Microporous Mesoporous Mater.* 117, **2009**, 423.

[100] Burch, V.; Caps, V.; Gleeson, V.; Nishiyama, S.; Tsang, S.C. *Appl. Catal. A: General* 194 –195, **2000**, 297.

[101] Meyer, U.; Hoelderich, W.F. *J. Mol. Catal. A: Chem.* 142, **1999**, 213.

[102] Lauron-Pernot, H.; Luck, F.; Popa, J.M. *Appl. Catal.* 78, **1991**, 213.

[103] Lauron-Pernot, H. Catal. Rev., 48, **2006**, 315,

[104] Zadrozna, G.; Souvage,E.; Kornatowski, J. *J. of Catal.* 208, **2002**, 270.

[105] Chebout, R.; Tichit, D.; Layrac, G.; Barama, A.; Coq, B.; Cota, I.; Rangel, E.R.; Medina, F. *Solid State Sci.* 12, **2010**, 1013.

[106] Conesa, T.D.; Hidalgo, J.M.; Luque, R.; Campelo, J.M.; Romero, A.A. *Appl. Catal. A: General* 299, **2006**, 224.

[107] Handa, H.; Fu, Y.; Baba, T.; Ono, Y. *Catal. Lett.* 59, **1999**, 195.

8. Appendix

Summary results for the decomposition of MBOH over various samples.

- Na-ilerite synthesized according to the procedure I2.

Time on stream	MBOH	Acetylene		Acetone		MBYNE		Others	
Min	conversion	yield	selectivity	yield	selectivity	yield	selectivity	yield	selectivity
0	8,4	3,0%	35,5%	5,1%	60,3%	0,2%	2,9%	0,1%	1,4%
17	8,3	2,9%	35,6%	5,1%	61,2%	0,2%	2,0%	0,1%	1,1%
34	8,3	2,8%	33,9%	5,2%	62,4%	0,2%	1,9%	0,1%	1,8%
50	7,7	2,7%	34,8%	4,7%	60,9%	0,1%	1,9%	0,2%	2,4%
67	7,1	2,5%	35,7%	4,3%	61,3%	0,1%	1,8%	0,1%	1,2%
83	7,1	2,4%	34,5%	4,4%	62,1%	0,1%	1,8%	0,1%	1,6%
100	6,6	2,2%	33,7%	4,1%	62,1%	0,1%	1,9%	0,2%	2,3%
117	5,9	2,1%	35,4%	3,6%	60,9%	0,1%	2,0%	0,1%	1,7%
134	5,6	2,0%	35,2%	3,4%	60,6%	0,1%	2,1%	0,1%	2,2%

- 0.0005 Sn/Si Na-ilerite synthesized according to the procedure I2.

Time on stream	MBOH	Acetylene		Acetone		MBYNE		Others	
min	conversion	yield	selectivity	yield	selectivity	yield	selectivity	yield	selectivity
0	17,5	5,2%	29,8%	11,6%	66,3%	0,5%	2,6%	0,2%	1,2%
17	17,9	6,5%	36,4%	10,9%	61,1%	0,3%	1,6%	0,2%	0,8%
34	16,8	5,8%	34,6%	10,5%	62,4%	0,3%	1,6%	0,2%	1,5%
50	14,4	5,4%	37,5%	8,6%	59,7%	0,3%	1,7%	0,2%	1,0%
67	14,0	5,1%	36,4%	8,5%	60,5%	0,2%	1,6%	0,2%	1,4%
83	12,9	2,2%	20,3%	8,4%	77,3%	0,2%	2,2%	0,0%	0,2%
100	13,6	4,7%	34,4%	8,4%	61,7%	0,2%	1,7%	0,3%	2,3%
117	12,1	4,5%	37,3%	7,1%	58,1%	0,3%	2,1%	0,3%	2,6%
134	12,1	4,3%	35,8%	7,4%	61,5%	0,2%	1,5%	0,1%	1,2%

- 0.00125 Sn/Si Na-ilerite synthesized according to the procedure I2.

Time on stream	MBOH	Acetylene		Acetone		MBYNE		Others	
min	conversion	yield	selectivity	yield	selectivity	yield	selectivity	yield	selectivity
0	25,3	10,4%	41,0%	14,6%	57,6%	0,2%	0,9%	0,1%	0,4%
17	22,9	9,7%	42,5%	12,8%	56,0%	0,2%	0,8%	0,1%	0,6%
34	21,2	9,0%	42,5%	11,9%	56,3%	0,2%	0,8%	0,1%	0,5%
50	20,3	8,4%	41,1%	11,5%	56,5%	0,2%	0,8%	0,3%	1,5%
67	19,3	7,8%	40,5%	11,2%	58,0%	0,2%	0,8%	0,1%	0,7%
83	19,2	9,2%	45,5%	11,0%	54,2%	0,1%	0,3%	0,0%	0,1%
100	18,3	7,2%	39,4%	10,7%	58,4%	0,1%	0,7%	0,3%	1,4%
117	17,1	6,8%	39,9%	10,0%	58,5%	0,1%	0,8%	0,1%	0,7%
134	16,4	6,7%	40,7%	9,3%	56,7%	0,1%	0,8%	0,3%	1,7%

- 0.00125 Al/Si Na-ilerite synthesized according to the procedure I2.

Time on stream	MBOH	Acetylene		Acetone		MBYNE		Others	
min	conversion	yield	selectivity	yield	selectivity	yield	selectivity	yield	selectivity
0	7,4	2,6%	34,9%	4,4%	59,9%	0,2%	3,3%	0,1%	1,9%
17	7,4	2,5%	34,4%	4,5%	61,0%	0,2%	2,7%	0,1%	1,9%
34	6,8	2,3%	34,2%	4,0%	58,8%	0,2%	2,6%	0,3%	4,3%
50	6,2	2,2%	35,1%	3,8%	60,6%	0,2%	2,7%	0,1%	1,6%
67	5,6	2,0%	35,4%	3,4%	60,7%	0,2%	2,8%	0,1%	1,2%
83	5,3	1,9%	36,0%	3,2%	61,2%	0,1%	1,9%	0,0%	0,9%
100	5,2	1,8%	35,1%	3,1%	59,3%	0,1%	2,7%	0,1%	2,8%
117	5,0	1,7%	34,1%	3,1%	61,7%	0,1%	2,6%	0,1%	1,6%
134	4,8	1,6%	33,9%	2,8%	59,6%	0,1%	2,6%	0,2%	3,8%

- H-ilerite synthesized according to the procedure I2.

Time on stream	MBOH	Acetylene		Acetone		MBYNE		Others	
min	conversion	yield	selectivity	yield	selectivity	yield	selectivity	yield	selectivity
0	3,7	1,1%	28,6%	2,2%	58,9%	0,3%	9,1%	0,1%	3,4%
17	3,5	1,0%	27,4%	2,1%	58,7%	0,3%	7,8%	0,2%	6,1%
34	2,6	0,8%	29,6%	1,6%	61,1%	0,2%	8,1%	0,0%	1,1%
50	2,8	0,8%	27,1%	1,7%	59,0%	0,2%	7,6%	0,2%	6,3%
67	2,7	0,7%	26,7%	1,6%	58,1%	0,2%	7,0%	0,2%	8,2%
83	2,5	0,7%	27,2%	1,5%	59,6%	0,2%	7,0%	0,2%	6,1%
100	2,4	0,7%	28,0%	1,5%	60,5%	0,2%	7,2%	0,1%	4,3%
117	2,7	0,7%	27,8%	1,6%	60,6%	0,2%	7,7%	0,1%	3,9%
134	2,6	0,7%	27,5%	1,5%	58,1%	0,2%	7,2%	0,2%	7,2%

- 0.0005 Sn/Si Na-ilerite synthesized according to the procedure I2.

Time on stream	MBOH	Acetylene		Acetone		MBYNE		Others	
min	conversion	yield	selectivity	yield	selectivity	yield	selectivity	yield	selectivity
0	21,7	0,7%	3,1%	2,3%	10,6%	18,3%	84,1%	0,5%	2,2%
17	10,8	0,6%	5,8%	1,8%	17,2%	7,9%	73,2%	0,4%	3,8%
34	6,7	0,6%	8,7%	1,6%	23,9%	4,4%	65,7%	0,1%	1,7%
50	4,7	0,5%	11,4%	1,4%	30,5%	2,6%	54,1%	0,2%	4,0%
67	3,4	0,5%	15,4%	1,3%	38,4%	1,5%	44,1%	0,1%	2,1%
83	3,1	0,5%	17,0%	1,4%	45,3%	0,9%	29,7%	0,2%	7,9%
100	2,6	0,5%	20,1%	1,3%	49,6%	0,6%	23,3%	0,2%	7,0%
117	2,6	0,5%	19,6%	1,3%	51,6%	0,5%	20,8%	0,2%	7,9%
134	2,6	0,5%	20,3%	1,4%	51,8%	0,5%	19,4%	0,2%	8,6%

- 0.0005 Al/Si Na-ilerite synthesized according to the procedure I2.

Time on stream	MBOH	Acetylene		Acetone		MBYNE		Others	
min	conversion	yield	selectivity	yield	selectivity	yield	selectivity	yield	selectivity
0	55,2	0,8%	1,4%	3,3%	6,0%	50,2%	91,0%	0,9%	1,6%
17	25,9	0,6%	2,5%	2,2%	8,4%	22,6%	87,1%	0,5%	2,0%
34	17,3	0,6%	3,7%	1,9%	11,0%	14,3%	82,7%	0,5%	2,7%
50	12,0	0,5%	4,4%	1,6%	13,3%	9,4%	78,6%	0,4%	3,7%
67	9,7	0,5%	5,5%	1,6%	16,8%	7,1%	74,1%	0,4%	3,6%
83	8,1	0,6%	7,1%	1,5%	18,7%	5,6%	69,8%	0,4%	4,4%
100	6,4	0,5%	8,3%	1,3%	19,7%	4,3%	67,3%	0,3%	4,8%
117	6,1	0,6%	9,6%	1,5%	25,4%	3,5%	57,9%	0,4%	7,1%
134	5,2	0,5%	9,9%	1,4%	27,3%	2,8%	54,2%	0,5%	8,7%

- Na-magadiite synthesized according to the procedure M1 without Na_2CO_3.

Time on stream	MBOH	Acetylene		Acetone		MBYNE		Others	
min	conversion	yield	selectivity	yield	selectivity	yield	selectivity	yield	selectivity
0	10,4%	4,2%	40,0%	5,7%	54,4%	0,5%	5,3%	0,0%	0,3%
17	10,5%	4,2%	39,7%	5,6%	53,8%	0,4%	4,1%	0,3%	2,5%
34	9,8%	4,0%	40,3%	5,4%	54,7%	0,4%	3,8%	0,1%	1,3%
50	8,8%	3,6%	41,3%	4,7%	53,7%	0,3%	3,6%	0,1%	1,3%
67	8,6%	3,4%	39,6%	4,8%	55,5%	0,3%	3,7%	0,1%	1,3%
83	8,3%	3,2%	38,3%	4,6%	54,9%	0,3%	3,6%	0,3%	3,2%
100	7,8%	3,0%	39,0%	4,4%	55,8%	0,3%	3,6%	0,1%	1,6%
117	7,8%	2,9%	37,6%	4,3%	55,3%	0,3%	3,6%	0,3%	3,5%
134	7,0%	2,8%	40,0%	3,9%	55,3%	0,2%	3,3%	0,1%	1,4%

- Na-magadiite synthesized according to the procedure M1 with Na_2CO_3.

Time on stream	MBOH	Acetylene		Acetone		MBYNE		Others	
min	conversion	yield	selectivity	yield	selectivity	yield	selectivity	yield	selectivity
0	15,4%	6,3%	41,1%	8,5%	55,6%	0,5%	3,1%	0,0%	0,2%
17	17,8%	7,5%	42,0%	9,8%	54,9%	0,4%	2,3%	0,1%	0,8%
34	15,8%	6,3%	40,1%	8,8%	56,1%	0,4%	2,2%	0,2%	1,5%
50	13,4%	5,5%	40,8%	7,5%	56,2%	0,3%	2,2%	0,1%	0,8%
67	13,3%	5,4%	40,4%	7,5%	56,6%	0,3%	2,2%	0,1%	0,9%
83	12,9%	5,2%	40,5%	7,3%	56,6%	0,3%	2,1%	0,1%	0,8%
100	12,3%	4,9%	39,8%	7,0%	57,0%	0,3%	2,2%	0,1%	1,0%
117	12,8%	5,1%	39,9%	7,3%	57,1%	0,3%	2,2%	0,1%	0,8%
134	13,4%	5,3%	39,4%	7,7%	57,3%	0,3%	2,0%	0,2%	1,2%

- 0.003 Sn/Si Na-magadiite synthesized according to the procedure M1 without Na$_2$CO$_3$.

Time on stream	MBOH	Acetylene		Acetone		MBYNE		Others	
min	conversion	yield	selectivity	yield	selectivity	yield	selectivity	yield	selectivity
0	8,5%	3,4%	40,7%	4,6%	53,9%	0,4%	5,1%	0,0%	0,3%
17	8,9%	3,7%	41,6%	4,8%	53,5%	0,3%	3,4%	0,1%	1,5%
34	8,6%	3,5%	41,4%	4,6%	53,9%	0,3%	3,3%	0,1%	1,4%
50	7,7%	3,2%	41,7%	4,1%	53,7%	0,2%	3,1%	0,1%	1,5%
67	7,2%	3,0%	41,1%	3,9%	54,3%	0,2%	3,2%	0,1%	1,3%
83	6,8%	2,7%	40,2%	3,7%	53,9%	0,2%	3,5%	0,2%	2,5%
100	6,2%	2,5%	40,3%	3,4%	54,8%	0,2%	3,5%	0,1%	1,3%
117	5,4%	2,1%	38,1%	3,1%	56,7%	0,2%	3,4%	0,1%	1,8%
134	5,0%	2,0%	40,3%	2,7%	54,8%	0,2%	3,2%	0,1%	1,6%

- 0.003 Sn/Si Na-magadiite synthesized according to the procedure M1 with Na$_2$CO$_3$.

Time on stream	MBOH	Acetylene		Acetone		MBYNE		Others	
min	conversion	yield	selectivity	yield	selectivity	yield	selectivity	yield	selectivity
0	20,8%	9,2%	44,3%	10,7%	51,7%	0,6%	2,7%	0,3%	1,3%
17	16,5%	7,3%	44,2%	8,6%	52,0%	0,4%	2,7%	0,2%	1,0%
34	14,9%	6,5%	43,5%	7,7%	52,0%	0,4%	2,6%	0,3%	1,8%
50	13,2%	5,6%	42,6%	6,9%	52,7%	0,4%	2,8%	0,3%	1,9%
67	12,2%	5,2%	42,8%	6,4%	52,4%	0,3%	2,8%	0,3%	2,0%
83	10,7%	4,6%	42,8%	5,7%	53,1%	0,3%	2,9%	0,1%	1,1%
100	10,2%	4,3%	42,6%	5,4%	53,3%	0,3%	2,9%	0,1%	1,2%
117	10,3%	4,2%	40,7%	5,6%	54,1%	0,3%	2,8%	0,2%	2,4%
134	9,2%	3,9%	42,1%	5,0%	54,3%	0,2%	2,7%	0,1%	0,9%

- 0.015 Sn/Si Na-magadiite synthesized according to the procedure M1 without Na$_2$CO$_3$.

Time on stream	MBOH	Acetylene		Acetone		MBYNE		Others	
min	conversion	yield	selectivity	yield	selectivity	yield	selectivity	yield	selectivity
0	10,7%	4,8%	45,0%	5,4%	50,1%	0,4%	4,0%	0,1%	1,0%
17	11,3%	5,1%	45,3%	5,7%	50,1%	0,3%	3,0%	0,2%	1,5%
34	10,6%	4,8%	45,8%	5,3%	50,4%	0,3%	2,7%	0,1%	1,1%
50	10,7%	4,8%	44,7%	5,5%	51,7%	0,3%	2,5%	0,1%	1,1%
67	9,9%	4,6%	46,5%	5,0%	50,2%	0,2%	2,4%	0,1%	1,0%
83	9,9%	4,5%	45,6%	5,0%	51,0%	0,2%	2,4%	0,1%	1,0%
100	9,2%	4,1%	44,9%	4,8%	51,8%	0,2%	2,3%	0,1%	1,0%
117	8,7%	3,9%	45,0%	4,5%	51,3%	0,2%	2,4%	0,1%	1,2%
134	8,4%	3,9%	45,9%	4,3%	50,8%	0,2%	2,2%	0,1%	1,2%

- 0.015 Sn/Si Na-magadiite synthesized according to the procedure M1 with Na_2CO_3.

Time on stream	MBOH	Acetylene		Acetone		MBYNE		Others	
min	conversion	yield	selectivity	yield	selectivity	yield	selectivity	yield	selectivity
0	11,7%	4,8%	41,6%	6,0%	51,6%	0,6%	5,5%	0,2%	1,3%
17	9,7%	3,9%	40,0%	5,1%	52,4%	0,5%	4,9%	0,3%	2,8%
34	8,6%	3,4%	39,5%	4,6%	52,8%	0,4%	4,7%	0,3%	3,0%
50	7,5%	3,0%	39,7%	4,1%	54,1%	0,3%	4,6%	0,1%	1,6%
67	7,2%	2,8%	39,4%	3,9%	54,3%	0,3%	4,5%	0,1%	1,9%
83	6,9%	2,7%	39,0%	3,8%	54,9%	0,3%	4,4%	0,1%	1,8%
100	6,6%	2,5%	38,5%	3,6%	55,1%	0,3%	4,4%	0,1%	1,9%
117	6,2%	2,4%	38,8%	3,4%	55,1%	0,3%	4,4%	0,1%	1,7%
134	6,2%	2,4%	38,2%	3,5%	55,8%	0,3%	4,3%	0,1%	1,7%

- 0.003 Al/Si Na-magadiite synthesized according to the procedure M1 with Na_2CO_3.

Time on stream	MBOH	Acetylene		Acetone		MBYNE		Others	
min	conversion	yield	selectivity	yield	selectivity	yield	selectivity	yield	selectivity
0	10,9%	9,2%	44,3%	10,7%	51,7%	0,6%	2,7%	0,3%	1,3%
17	5,3%	7,3%	44,2%	8,6%	52,0%	0,4%	2,7%	0,2%	1,0%
34	4,7%	6,5%	43,5%	7,7%	52,0%	0,4%	2,6%	0,3%	1,8%
50	3,4%	5,6%	42,6%	6,9%	52,7%	0,4%	2,8%	0,3%	1,9%
67	5,0%	5,2%	42,8%	6,4%	52,4%	0,3%	2,8%	0,3%	2,0%
83	1,8%	4,6%	42,8%	5,7%	53,1%	0,3%	2,9%	0,1%	1,1%
100	1,9%	4,3%	42,6%	5,4%	53,3%	0,3%	2,9%	0,1%	1,2%
117	5,0%	4,2%	40,7%	5,6%	54,1%	0,3%	2,8%	0,2%	2,4%
134	2,7%	3,9%	42,1%	5,0%	54,3%	0,2%	2,7%	0,1%	0,9%

- H-magadiite synthesized according to the procedure M1 without Na_2CO_3.

Time on stream	MBOH	Acetylene		Acetone		MBYNE		Others	
min	conversion	yield	selectivity	yield	selectivity	yield	selectivity	yield	selectivity
0	16,0%	1,7%	10,6%	2,9%	18,3%	8,2%	51,5%	3,1%	19,6%
17	11,2%	1,5%	13,7%	2,6%	23,6%	5,4%	48,2%	1,6%	14,4%
34	9,9%	1,4%	14,6%	2,6%	26,4%	4,4%	44,5%	1,4%	14,5%
50	8,5%	1,4%	15,9%	2,4%	28,3%	3,7%	43,8%	1,0%	12,1%
67	8,0%	1,3%	16,1%	2,4%	30,2%	3,3%	41,7%	1,0%	12,0%
83	7,4%	1,2%	16,7%	2,4%	32,3%	3,0%	39,8%	0,8%	11,3%
100	5,5%	0,9%	16,1%	1,9%	34,5%	2,0%	35,9%	0,7%	13,5%
117	5,5%	1,0%	17,5%	2,0%	36,0%	2,0%	36,5%	0,6%	10,0%
134	5,8%	1,0%	17,0%	2,1%	35,3%	1,9%	33,0%	0,9%	14,7%

- H-magadiite synthesized according to the procedure M1 with Na$_2$CO$_3$.

Time on stream	MBOH	Acetylene		Acetone		MBYNE		Others	
min	conversion	yield	selectivity	yield	selectivity	yield	selectivity	yield	selectivity
0	5,7%	1,4%	24,4%	2,6%	45,5%	1,6%	28,7%	0,1%	1,4%
17	5,2%	1,3%	24,3%	2,5%	47,4%	1,2%	22,4%	0,3%	5,9%
34	4,8%	1,2%	24,6%	2,3%	49,2%	1,0%	20,7%	0,3%	5,5%
50	4,8%	1,1%	23,9%	2,4%	50,0%	0,9%	18,7%	0,4%	7,5%
67	4,7%	1,1%	24,4%	2,4%	51,2%	0,8%	17,8%	0,3%	6,7%
83	4,5%	1,1%	24,6%	2,3%	51,3%	0,8%	17,5%	0,3%	6,6%
100	4,2%	1,1%	25,6%	2,2%	52,7%	0,7%	17,3%	0,2%	4,4%
117	4,3%	1,0%	24,1%	2,3%	52,1%	0,7%	16,3%	0,3%	7,5%
134	4,0%	1,0%	25,5%	2,2%	53,8%	0,7%	16,4%	0,2%	4,3%

- 0.003 Sn/Si H-magadiite synthesized according to the procedure M1 without Na$_2$CO$_3$.

Time on stream	MBOH	Acetylene		Acetone		MBYNE		Others	
min	conversion	yield	selectivity	yield	selectivity	yield	selectivity	yield	selectivity
0	11,0%	1,1%	9,9%	1,7%	15,1%	6,3%	57,0%	2,0%	17,9%
17	7,7%	1,0%	12,8%	1,5%	19,1%	4,1%	53,0%	1,2%	15,1%
34	6,7%	1,0%	14,3%	1,5%	21,7%	3,4%	50,8%	0,9%	13,1%
50	6,1%	0,9%	15,2%	1,4%	23,6%	2,9%	48,5%	0,8%	12,7%
67	5,5%	0,9%	16,1%	1,4%	24,9%	2,6%	47,2%	0,6%	11,8%
83	5,2%	0,9%	16,4%	1,3%	25,4%	2,3%	45,0%	0,7%	13,1%
100	4,9%	0,8%	17,3%	1,3%	27,1%	2,2%	44,8%	0,5%	10,9%
117	4,7%	0,8%	17,9%	1,3%	27,7%	2,1%	44,0%	0,5%	10,4%
134	4,4%	0,8%	18,3%	1,2%	27,7%	1,9%	43,3%	0,5%	10,8%

- 0.003 Sn/Si H-magadiite synthesized according to the procedure M1 with Na$_2$CO$_3$.

Time on stream	MBOH	Acetylene		Acetone		MBYNE		Others	
min	conversion	yield	selectivity	yield	selectivity	yield	selectivity	yield	selectivity
0	13,0%	1,1%	16,7%	1,6%	38,1%	6,3%	25,0%	2,0%	20,1%
17	9,7%	1,0%	16,8%	1,5%	38,1%	4,1%	23,0%	1,2%	22,1%
34	8,9%	1,2%	17,3%	1,5%	40,7%	3,4%	22,8%	0,9%	18,1%
50	8,3%	0,9%	19,2%	1,4%	41,6%	2,9%	22,5%	0,8%	16,7%
67	7,3%	0,9%	20,1%	1,3%	43,9%	2,6%	21,0%	0,6%	15,0%
83	6,1%	1,1%	21,4%	1,0%	44,4%	2,3%	20,0%	0,7%	14,1%
100	5,4%	0,8%	22,3%	1,3%	47,1%	2,2%	19,8%	0,5%	10,9%
117	5,3%	0,9%	21,9%	0,9%	45,7%	2,1%	19,0%	0,5%	10,4%
134	4,9%	0,9%	23,3%	1,2%	47,7%	1,9%	19,3%	0,5%	10,8%

- 0.003 Al/Si H-magadiite synthesized according to the procedure M1 with Na_2CO_3

Time on stream	MBOH	Acetylene		Acetone		MBYNE		Others	
min	conversion	yield	selectivity	yield	selectivity	yield	selectivity	yield	selectivity
0	32,9%	1,1%	3,0%	2,1%	5,8%	27,9%	77,8%	4,8%	13,3%
17	23,8%	1,0%	3,8%	1,7%	6,4%	21,3%	78,1%	3,2%	11,7%
34	21,1%	1,0%	4,2%	1,8%	7,7%	18,1%	77,1%	2,6%	11,0%
50	17,9%	0,9%	4,6%	1,5%	7,4%	15,6%	77,4%	2,1%	10,6%
67	17,6%	0,9%	4,8%	1,7%	8,9%	14,1%	75,6%	2,0%	10,7%
83	16,1%	0,9%	5,2%	1,4%	8,2%	13,1%	76,4%	1,7%	10,2%
100	15,3%	0,9%	5,3%	1,6%	9,8%	12,0%	74,6%	1,7%	10,3%
117	12,4%	0,8%	5,6%	1,5%	9,9%	11,2%	74,8%	1,4%	9,7%
134	12,5%	0,8%	5,8%	1,4%	10,2%	10,5%	74,2%	1,4%	9,8%

- Na-kenyaite synthesized according to the procedure K1.

Time on stream	MBOH	Acetylene		Acetone		MBYNE		Others	
min	conversion	yield	selectivity	yield	selectivity	yield	selectivity	yield	selectivity
0	17,2%	9,2%	53,3%	7,6%	44,1%	0,4%	2,5%	0,0%	0,2%
17	14,0%	7,2%	51,2%	6,6%	47,3%	0,2%	1,5%	0,0%	0,0%
34	12,6%	6,5%	51,3%	6,0%	47,3%	0,2%	1,4%	0,0%	0,0%
50	12,4%	6,3%	50,7%	5,9%	48,0%	0,2%	1,3%	0,0%	0,0%
67	11,5%	5,8%	50,5%	5,5%	48,2%	0,1%	1,3%	0,0%	0,0%
83	9,7%	5,0%	51,3%	4,6%	47,4%	0,1%	1,3%	0,0%	0,0%
100	10,3%	5,2%	50,1%	5,0%	48,6%	0,1%	1,3%	0,0%	0,0%
117	9,2%	4,6%	49,8%	4,5%	48,8%	0,1%	1,3%	0,0%	0,0%
134	9,1%	4,6%	50,0%	4,5%	48,7%	0,1%	1,3%	0,0%	0,0%

- H-kenyaite synthesized according to the procedure K1.

Time on stream	MBOH	Acetylene		Acetone		MBYNE		Others	
min	conversion	yield	selectivity	yield	selectivity	yield	selectivity	yield	selectivity
0	16,0%	1,2%	7,4%	1,7%	10,4%	9,6%	60,0%	3,5%	22,1%
17	9,0%	1,0%	11,0%	1,6%	17,3%	5,0%	55,9%	1,4%	15,9%
34	7,2%	0,9%	12,8%	1,5%	20,9%	3,8%	52,9%	1,0%	13,3%
50	5,9%	0,8%	14,3%	1,3%	22,4%	3,0%	51,1%	0,7%	12,2%
67	5,4%	0,8%	15,1%	1,4%	25,1%	2,6%	48,7%	0,6%	11,1%
83	5,3%	0,8%	15,7%	1,4%	27,0%	2,5%	47,1%	0,5%	10,2%
100	4,6%	0,8%	16,9%	1,2%	27,2%	2,1%	45,8%	0,5%	10,1%
117	4,4%	0,8%	17,4%	1,3%	29,3%	1,9%	43,7%	0,4%	9,5%
134	4,2%	0,7%	17,2%	1,4%	32,9%	1,7%	41,2%	0,4%	8,8%

- 0.015 Sn/Si Na-kenyaite synthesized according to the procedure K1.

Time on stream	MBOH	Acetylene		Acetone		MBYNE		Others	
min	conversion	yield	selectivity	yield	selectivity	yield	selectivity	yield	selectivity
0	10,2%	**4,8%**	46,8%	5,2%	50,7%	0,2%	2,3%	0,0%	0,2%
17	8,4%	3,9%	46,5%	4,3%	51,5%	0,1%	1,6%	0,0%	0,4%
34	7,0%	3,2%	45,2%	3,7%	52,0%	0,1%	1,6%	0,1%	1,3%
50	7,6%	3,5%	45,7%	3,9%	51,9%	0,1%	1,4%	0,1%	1,1%
67	7,0%	3,2%	45,6%	3,6%	51,9%	0,1%	1,4%	0,1%	1,1%
83	6,8%	3,1%	45,2%	3,6%	52,2%	0,1%	1,4%	0,1%	1,2%
100	6,8%	3,1%	45,4%	3,5%	52,2%	0,1%	1,4%	0,1%	1,1%
117	6,1%	2,7%	45,3%	3,1%	51,9%	0,1%	1,4%	0,1%	1,3%
134	6,0%	2,7%	44,5%	3,2%	52,3%	0,1%	1,4%	0,1%	1,7%

- 0.015 Sn/Si H-kenyaite synthesized according to the procedure K1.

Time on stream	MBOH	Acetylene		Acetone		MBYNE		Others	
min	conversion	yield	selectivity	yield	selectivity	yield	selectivity	yield	selectivity
0	5,9%	1,1%	19,0%	2,0%	34,6%	2,4%	41,2%	0,3%	5,2%
17	5,3%	0,9%	17,3%	1,8%	35,0%	2,2%	41,1%	0,3%	6,6%
34	4,7%	0,8%	17,3%	1,7%	36,2%	1,9%	40,3%	0,3%	6,2%
50	4,4%	0,8%	17,3%	1,6%	37,0%	1,8%	39,9%	0,3%	5,8%
67	3,9%	0,7%	17,7%	1,4%	36,8%	1,5%	39,5%	0,2%	5,9%
83	4,1%	0,7%	17,4%	1,6%	39,2%	1,6%	37,9%	0,2%	5,4%
100	3,8%	0,7%	17,4%	1,5%	39,5%	1,5%	37,9%	0,2%	5,1%
117	3,6%	0,6%	17,5%	1,5%	41,2%	1,3%	36,4%	0,2%	4,9%
134	3,6%	0,7%	18,3%	1,4%	39,6%	1,4%	37,3%	0,2%	4,7%

- 0.045 Sn/Si Na-kenyaite synthesized according to the procedure K1.

Time on stream	MBOH	Acetylene		Acetone		MBYNE		Others	
min	conversion	yield	selectivity	yield	selectivity	yield	selectivity	yield	selectivity
0	3,7%	1,3%	35,1%	2,2%	58,8%	0,1%	3,9%	0,1%	2,2%
17	2,9%	1,0%	33,6%	1,8%	62,0%	0,1%	3,5%	0,0%	0,9%
34	2,9%	0,9%	32,4%	1,8%	63,2%	0,1%	3,6%	0,0%	0,7%
50	2,9%	0,9%	32,2%	1,8%	63,9%	0,1%	3,3%	0,0%	0,6%
67	2,4%	0,7%	30,7%	1,6%	66,4%	0,1%	3,0%	0,0%	0,0%
83	2,5%	0,7%	28,2%	1,7%	67,4%	0,1%	3,6%	0,0%	0,8%
100	2,1%	0,6%	28,7%	1,4%	67,7%	0,1%	3,1%	0,0%	0,5%
117	2,0%	0,5%	26,2%	1,4%	69,7%	0,1%	3,6%	0,0%	0,5%
134	1,7%	0,4%	24,2%	1,2%	72,3%	0,1%	3,6%	0,0%	0,0%

- 0.045 Sn/Si H-kenyaite synthesized according to the procedure K1.

Time on stream	MBOH	Acetylene		Acetone		MBYNE		Others	
min	conversion	yield	selectivity	yield	selectivity	yield	selectivity	yield	selectivity
0	4,9%	1,5%	29,9%	2,4%	48,8%	1,0%	19,7%	0,1%	1,6%
17	4,0%	1,2%	29,5%	1,9%	49,2%	0,8%	19,5%	0,1%	1,8%
34	3,7%	1,1%	28,4%	1,9%	50,0%	0,7%	19,5%	0,1%	2,1%
50	3,4%	0,9%	27,8%	1,7%	50,6%	0,7%	19,7%	0,1%	2,0%
67	3,3%	0,9%	26,8%	1,7%	51,0%	0,6%	19,8%	0,1%	2,4%
83	3,1%	0,8%	27,1%	1,6%	50,6%	0,6%	20,2%	0,1%	2,1%
100	2,9%	0,8%	26,5%	1,5%	50,8%	0,6%	20,1%	0,1%	2,6%
117	3,0%	0,8%	26,4%	1,5%	51,2%	0,6%	20,4%	0,1%	2,0%
134	2,8%	0,7%	25,7%	1,5%	52,3%	0,6%	19,9%	0,1%	2,1%

- 0.045 Sn/Si Na-kenyaite synthesized according to the procedure K1, 96h synthesis.

Time on stream	MBOH	Acetylene		Acetone		MBYNE		Others	
min	conversion	yield	selectivity	yield	selectivity	yield	selectivity	yield	selectivity
0	17,2%	8,6%	49,9%	8,3%	48,1%	0,3%	1,8%	0,0%	0,3%
17	9,6%	4,7%	48,6%	4,8%	49,8%	0,2%	1,6%	0,0%	0,0%
34	6,4%	3,0%	46,5%	3,3%	51,7%	0,1%	1,8%	0,0%	0,0%
50	6,3%	2,9%	46,8%	3,2%	51,4%	0,1%	1,8%	0,0%	0,0%
67	6,1%	2,8%	46,2%	3,2%	51,8%	0,1%	2,0%	0,0%	0,0%
83	5,4%	2,5%	45,9%	2,8%	52,3%	0,1%	1,9%	0,0%	0,0%
100	4,9%	2,2%	45,6%	2,6%	52,4%	0,1%	2,0%	0,0%	0,0%
117	4,8%	2,2%	45,5%	2,5%	52,4%	0,1%	2,1%	0,0%	0,0%
134	4,5%	2,0%	44,7%	2,4%	53,3%	0,1%	2,0%	0,0%	0,0%

- 0.045 Sn/Si H-kenyaite synthesized according to the procedure K1, 96h synthesis.

Time on stream	MBOH	Acetylene		Acetone		MBYNE		Others	
min	conversion	yield	selectivity	yield	selectivity	yield	selectivity	yield	selectivity
0	5,0%	1,0%	20,9%	2,1%	41,8%	1,7%	34,0%	0,2%	3,4%
17	4,4%	0,9%	20,2%	1,8%	40,7%	1,5%	35,1%	0,2%	4,0%
34	4,6%	0,9%	19,3%	1,8%	40,1%	1,7%	36,1%	0,2%	4,4%
50	4,0%	0,7%	18,3%	1,6%	40,1%	1,5%	37,1%	0,2%	4,5%
67	4,1%	0,7%	18,3%	1,6%	40,1%	1,5%	36,5%	0,2%	5,1%
83	4,0%	0,7%	17,6%	1,7%	41,7%	1,5%	36,0%	0,2%	4,6%
100	3,8%	0,7%	18,2%	1,6%	41,3%	1,4%	35,9%	0,2%	4,7%
117	3,6%	0,6%	17,0%	1,5%	42,8%	1,3%	35,0%	0,2%	5,2%
134	3,4%	0,6%	17,4%	1,5%	43,9%	1,2%	34,1%	0,2%	4,6%

- 0.007 Al/Si Na-kenyaite synthesized according to the procedure K1.

Time on stream	MBOH	Acetylene		Acetone		MBYNE		Others	
min	conversion	yield	selectivity	yield	selectivity	yield	selectivity	yield	selectivity
0	55,8%	29,9%	53,6%	25,7%	46,1%	0,1%	0,2%	0,1%	0,1%
17	44,4%	23,7%	53,4%	20,6%	46,2%	0,1%	0,2%	0,1%	0,1%
34	35,3%	18,3%	51,9%	16,8%	47,6%	0,1%	0,3%	0,1%	0,2%
50	27,1%	14,0%	51,8%	12,9%	47,7%	0,1%	0,3%	0,1%	0,2%
67	23,6%	12,2%	51,6%	11,3%	47,8%	0,1%	0,4%	0,1%	0,3%
83	20,3%	10,4%	50,9%	9,8%	48,3%	0,1%	0,4%	0,1%	0,3%
100	18,3%	9,3%	50,7%	8,9%	48,4%	0,1%	0,5%	0,1%	0,3%
117	15,8%	8,0%	50,7%	7,7%	48,4%	0,1%	0,5%	0,1%	0,4%
134	13,3%	6,6%	49,6%	6,6%	49,4%	0,1%	0,5%	0,1%	0,5%

- 0.007 Al/Si H-kenyaite synthesized according to the procedure K1.

Time on stream	MBOH	Acetylene		Acetone		MBYNE		Others	
min	conversion	yield	selectivity	yield	selectivity	yield	selectivity	yield	selectivity
0	59,1%	1,2%	2,0%	2,5%	4,3%	48,6%	82,3%	6,8%	11,4%
17	40,4%	0,9%	2,3%	2,0%	5,0%	33,6%	83,1%	3,9%	9,6%
34	31,6%	0,9%	2,7%	1,9%	5,9%	26,0%	82,1%	2,9%	9,3%
50	26,3%	0,8%	2,9%	1,8%	6,8%	21,4%	81,4%	2,4%	8,9%
67	24,4%	0,6%	2,7%	1,8%	7,5%	20,5%	84,1%	1,4%	5,7%
83	20,6%	0,7%	3,3%	1,7%	8,1%	16,5%	80,2%	1,7%	8,4%
100	18,4%	0,7%	3,6%	1,6%	8,7%	14,6%	79,1%	1,6%	8,6%
117	16,7%	0,6%	3,7%	1,5%	8,9%	13,2%	79,1%	1,4%	8,3%
134	15,6%	0,6%	3,8%	1,5%	9,8%	12,3%	78,7%	1,2%	7,7%

- SiO$_2$ / H-kenyaite

Time on stream	MBOH	Acetylene		Acetone		MBYNE		Others	
min	conversion	yield	selectivity	yield	selectivity	yield	selectivity	yield	selectivity
0	9,4%	1,1%	12,0%	2,1%	22,8%	5,6%	59,8%	0,5%	5,4%
17	6,8%	0,9%	13,4%	1,8%	27,1%	3,6%	53,6%	0,4%	5,9%
34	5,7%	0,8%	14,5%	1,7%	30,2%	2,8%	49,1%	0,4%	6,2%
50	5,2%	0,8%	15,2%	1,6%	31,4%	2,5%	47,0%	0,3%	6,4%
67	4,8%	0,8%	15,8%	1,5%	31,5%	2,1%	45,1%	0,4%	7,5%
83	4,2%	0,7%	15,7%	1,5%	34,2%	1,9%	44,5%	0,2%	5,6%
100	3,9%	0,6%	16,1%	1,4%	35,5%	1,7%	42,8%	0,2%	5,6%
117	4,0%	0,7%	16,7%	1,4%	35,9%	1,7%	42,1%	0,2%	5,4%
134	4,0%	0,7%	16,5%	1,6%	39,0%	1,6%	39,0%	0,2%	5,5%

Selbständigkeitserklärung

Hiermit erkläre ich, dass ich diese Arbeit selbständig und ohne unerlaubte fremde Hilfe verfasst und keine anderen als die angegeben Quellen und Hilfsmittel benutzt habe.

Oldenburg, den 8. März 2011   Wojciech Supronowicz

Lebenslauf

PERSÖNLICHE DATEN

Name: Wojciech Supronowicz

Nationalität: Polnisch

Geburstdatum: 22. Mai 1983

WERDEGANG

12.2010 - …	**Postdoc Position an der Max Planck Institute in Mülheim an der Ruhr**
10.2007 – 12.2010	**Promotionsstudium an der Carl von Ossietzky Universität in Oldenburg, Deutschland -** Fachrichtung Technische Chemie (DAAD Stipendium)
2002 – 2007	**Studium am Institut für Chemie an der Adam Mickiewicz Universität Poznan, Polen –** mit der Fachrichtung Technische Chemie, abgeschlossen als Master of Science
02.2006 – 08.2006	**Socrates/Erasmus Stipendium für sechs Monate Forschung an der Carl von Ossietzky Universität in Oldenburg, Deutschland** – Forschung in angewandter Katalyse
2005 – 2006	**Teilnahme an einem „English CAE language course" - Poznan, Polen –** erfolgreich abgeschlossen mit einem *Certificate in Advanced English*
1998 – 2002	**Oberschule in Pila/Polen**
1990 – 1998	**Grundschule in Pila/Polen**

Oldenburg, den 8. März 2011   Wojciech Supronowicz